SEE FOLLOWING NOTE

VOIR NOTE CI-APRÈS

PARTS OF THE ORIGINAL DOCUMENT ARE OF POOR REPRODUCTIVE QUALITY.

MICROMEDIA LIMITED HAS ATTEMPTED TO PRODUCE THE BEST POSSIBLE COPY.

CERTAINES PARTIES DU DOCUMENT ORIGINAL SONT DE PIÈTRE QUALITÈ DE REPRODUCTION.

MICROMEDIA LTEE A ESSAYEE DE PROCURER LE MEILLEUR EXEMPLAIRE POSSIBLE.

ENERGY, MINES AND RESOURCES CANADA

ROCK MECHANICS ASSESSMENTS OF SLOPE DEFORMATION AND SLOPE INSTABILITY IN THE CASSIAR OPEN PIT

prepared by

Cassiar Mining Corporation

and

Piteau Associates Engineering Ltd.

June 15,1990

Work on the project was conducted under the auspices of Canada Centre for Mineral and Energy Technology, Energy, Mines and Resources Canada.

DSS File No. 009SQ.23440-9-9227

DSS Contract Serial No. 23440-9-9227/01-SQ

CANMET Project No. 9-9227

CANMET Scientific Authority: Y.S. Yu

171 pp & figs.

MICROMEDIA

91-00369/

ACKNOWLEDGEMENT AND DISCLAIMER

The research project, for which this report is submitted, was funded by the Government of Canada and administered by Supply and Services Canada and the CANMET Mining Research Laboratory in Ottawa.

This report and its contents, the research project in respect of which it is submitted and the technology produced or demonstrated in the research project, do not necessarily reflect the view of the Government of Canada, its officers, employees or agents. Neither the Government of Canada nor its officers, employees or agents makes any warranty, express or implied, representation or otherwise, in respect of this report or its contents.

The Government of Canada, its officers, employees and agents are exempted, excluded and absolved from all liability for damage or injury, howsoever caused, to any person in connection with or arising out of the use by that person for any purpose of this report or its contents.

EXECUTIVE SUMMARY

INTRODUCTION

Cassiar Mine is located in steep mountainous terrain in northern British Columbia approximately 1200 km north of Vancouver. During development of the final phase of the open pit, instability developed in the approximately 1100 foot hanging wall (east wall) slope. This report describes the unique failure mechanism that was identified, the results of back analyses of the failure and the measures undertaken by the mine to enable continued mining and recovery of the available ore.

ENGINEERING GEOLOGY

The engineering geology and structural geology of the open pit is given in plan on Fig. 2 and on sections in Appendix A. The Cassiar orebody occurs in a sill of serpentinized peridotite of the McDame Intrusions, which intrudes the west limb of a syncline of Paleozoic argillites, dolomites, quartzites and associated rocks of the Sylvester Group. The orebody occurs in the central portion of the sill. The hanging wall slope consists of an upper 240 metre (800 ft) section of argillite and volcanic rocks overlying an approximately 120 metre (400 ft) section of barren serpentinite and ore.

STRUCTURAL GEOLOGY

The rock mass has been offset by several major faults and shear zones with displacement of up to several hundred metres. Fault zones vary from 100mm to 20m in width and have a major influence on hydrogeology, strength and slope stability.

In addition to bedding, argillite and volcanics of the Sylvester Group contain three well developed sets of discontinuities. Joints and faults of Set A are continuous whereas bedding and other discontinuity sets are less continuous. Discontinuity populations are more complex in the serpentinite which contains up to six sets of discontinuities, most of which have associated veins and shear zones.

ROCK STRENGTH AND COMPETENCY

Argillites and volcanic rocks of the Sylvester Group in the hanging wall are competent having an unconfined compressive strength of about 76 MPa (11,000 psi) and an RQD of 73 to 96%. Strength and competency of serpentinite varies. Serpentinite has an unconfined compressive strength of about 34 to 48 MPa (5,000 to 7,000 psi) and an RQD of 53 to 81%. Rock in shear zones is even less competent having an estimated unconfined compressive strength of <8 MPa (<1,200 psi) and an RQD of <50%. Estimates of strength properties of the intact rock, discontinuities and the rock mass has been based on laboratory testing, back analysis of previous failures in the pit and assessment of accepted failure criteria. These assessments generally indicate the following material properties for the main rock types in the hanging wall.

ROCK MASS	DISCONTINUITY STRENGTH		ROCK MASS STRENGTH	
	Friction Angle, ø (°)	Cohesion kPa	Friction Angle, ø (°)	Cohesion kPa
Argillite	30 to 35	0	32	690
Barren Serpentinite	26.5	0	26	345
Serpentinite Ore	26.5	0	26	207
Shear Zones	26.5	0 to 70	26.5	69

The relative deformability of the rock mass was not considered prior to the development of the large failure on the east wall.

HYDROGEOLOGY

Annual precipitation at the site is 305mm of rain and 3,950mm of snowfall. Considerable recharge occurs on McDame Ridge with the result that natural groundwater levels are high. Serpentinite has an estimated hydraulic conductivity of 10^{-8}m/sec. The argillite rock mass is considered to be approximately 10 to 100 times as permeable as the serpentinite. Hence, high groundwater pressures develop because the serpentinite in the toe of the slope does not provide adequate drainage of the rock mass. Significant groundwater pressure fluctuation occurs between the spring and summer (high recharge) and winter months (low recharge).

SLOPE STABILITY ANALYSES AND SLOPE DESIGNS

Slope stability analyses for the final pit consisted of statistical assessment of kinematically possible failure modes, involving discontinuities, assessment of major structural discontinuities and rotational shear failure analyses for the high slopes with weak serpentinite in the toe. The results of these analyses indicated that there were no kinematically possible failures involving major faults on the east wall. Adequate bench design was provided by the following slope angles:

Argillite	54.5°
Barren Serpentinite	43.0°
Ore and Shear Zones	40.5°

Rotational failure analyses indicated that these slope designs would have only marginal stability, particularly if slopes were not depressurized.

The mining approach adopted was to mine the slopes at the angles indicated above and provide a comprehensive system of movement monitoring prisms to

provide adequate warning in the event that instability developed in the late stages of mining. Slope depressurization was to be conducted as necessary.

SLOPE PERFORMANCE

The east wall of the open pit was mined in a series of phases involving stripping of waste to expose ore. The final phase of stripping was begun in the early 1980's and completed in June 1989. The bulk of the final slope in serpentinite was completed between June 1987 and June 1989. The final slope involved a 3° increase in the final slope angle from 39° to 42° in the northeast corner of the pit. Instability of the northeast wall first developed in June 1988. Additional prisms and surface wire extensometers were placed on the slope and monitored regularly to assess the failure mechanisms and failure rate. By August 1988, it was apparent that more than three million tonnes were unstable. Slope flattening or regrading was not economically feasible. Hence, a program of accelerated mining was adopted to complete the pit before spring break up of 1989. A total of 2.5 million tonnes of ore was mined between September 1988 and June 1989, of which 1.68 million tonnes were stockpiled outside the open pit. Slope monitoring was conducted daily until mid-June, when slope acceleration and movements in excess of 75 to 125mm/day (3.0 to 5.0 in/day) and increased rockfall activity forced closure of the open pit. Movement rates greater than 125mm/day (5 in/day) were recorded during July and August 1989 by which time the size of the failure had reached an estimated 17.8 million tonnes.

Movement rates slowed to less than 40mm/day (1.5 in/day) in late January 1990, and the pit was reopened to recover the remaining mineable ore in the bottom of the pit and on the haulroad. By early May 1990, movement rates were again beginning to increase as spring thaw advanced.

MONITORING CRITERIA

Monitoring was conducted weekly when mining was not active in the pit. During periods of mining activity, monitoring frequency varied from once a week to

twice per day depending on monitored movement rates. Daily monitoring was conducted when movement rates exceeded 12mm/day (0.5 in/day). Movements in excess of 50mm/day (2.0 in/day) required visual inspection by sentries and continuous monitoring of prisms and surface extensometers.

FAILURE MECHANISM

Detailed examination of geological mapping data, movement monitoring records and visual observations indicate that the failure occurred by a deep seated graben toppling mechanism exacerbated by high groundwater pressures in the slope and the presence of soft deformable rocks in the toe. Failure in the upper section of the slope involved planar shear sliding of a large graben at an oblique angle to the slope. The rock mass in the middle portion of the slope failed by the toppling of large blocks formed by a combination of tensile failure and shearing through the rock mass. The lower section of the slope is failing by a combination of squeezing of the soft, sheared serpentinite rocks and sliding/toppling of a deep seated block as shown on Fig. 12. Photos 8 to 13 illustrate the salient features of the unstable area.

BACK ANALYSES

Three dimensional limit equilibrium back analyses of the failure summarized in Figs. 12 and 13 indicate that the rock mass strengths and shear strengths are appropriate for the failure mechanism identified. In addition, the slope is extremely sensitive to fluctuation in the groundwater pressures which confirms the observed variation in slope movements depending on the climate conditions.

Numerical modelling using the Universal Distinct Element Code (UDEC), as summarized in Fig. 14 and Table IX, confirms the observed behaviour and extreme sensitivity to groundwater levels. The numerical modelling further indicates that the failure mechanism requires the deformation of sheared, weak serpentinite in the toe to provide sufficient room for the graben toppling to develop. The numerical model also indicates that stability is relatively

insensitive to rock mass cohesion, but is extremely sensitive to the friction angle.

CONCLUSIONS

The results of the limit equilibrium back analyses and numerical modelling indicate that instability of high rock slopes may develop, even if major discontinuities are not present, or the slopes are designed so that kinematically possible failures involving discontinuties are controlled. In the case of the Cassiar failure, the major discontinuities were not daylighted by the slope. However, the deformation of the weak serpentinite in the lower section of the slope appears to have led to tensile failure and development of irregular discontinuities in the fractured rock mass which are unfavourably oriented for the development of a deep seated graben toppling failure. Numerical modelling of the failure using the observed discontinuities indicates that shear failure occurs along the discontinuities, even when the cohesion along the discontinuities approximates the rock mass cohesion. Numerical modelling also indicated that as the rock mass strength was decreased, additional tensile failures were induced in the graben at orientations subparallel to the observed discontinuities.

High groundwater pressures and low rock mass strength and friction angles contributed to the failure. Both numerical modelling and limit equilibrium back analyses have proved very useful in understanding the slope deformation mechanism and sensitivity of movement to material properties and groundwater.

Even though displacements in excess of 30 metres (100 ft) have been documented, the nature of this failure and the understanding of the failure mechanisms have enabled mining to take place under controlled conditions with careful monitoring and regular assessment of slope conditions.

CONTENTS

1. INTRODUCTION 1

1.1 BACKGROUND 1
1.2 PURPOSE AND SCOPE 2
1.3 ACKNOWLEDGEMENTS 3

2. ENGINEERING GEOLOGY 4

2.1 SITE LOCATION, PHYSIOGRAPHIC SETTING AND CLIMATE 4
2.2 REGIONAL AND LOCAL GEOLOGY 4
2.3 LITHOLOGY OF THE OPEN PIT 6
2.3.1 Sylvester Group Rocks 6
2.3.2 McDame Serpentinite Intrusion 7
2.3.3 Argillite/Serpentinite Contact Zones 7

2.4 MAJOR FAULTS 8
2.4.1 45° Shear 9
2.4.2 South Fault 9
2.4.3 70° Shear 9
2.4.4 Footwall Fault 10
2.4.5 North Fault 10

2.5 ANALYSIS OF DISCONTINUITY POPULATIONS 11
2.5.1 Sylvester Group Rocks in the East Wall 12
2.5.2 McDame Intrusions (Serpentinite) 14

2.6 ROCK STRENGTH AND COMPETENCY 15
2.6.1 Strength Properties of Intact Rock 15
2.6.2 Shear Strength of Discontinuities 16
2.6.3 Rock Competency and Core Quality 17
2.6.4 Assessment of Rock Mass Strength 19
2.6.5 Verification of Rock Mass Strength from Back Analysis of Slope Failures 20

2.7 HYDROGEOLOGY 22

3. SLOPE STABILITY ANALYSES AND SLOPE DESIGN 24

3.1 SLOPE STABILITY ANALYSES BASED ON STRUCTURAL ANALYSIS RESULTS 24
3.2 DEEP SEATED FAILURES INVOLVING MAJOR DISCONTINUITIES 26
3.3 DEEP SEATED ROTATIONAL FAILURE OF THE OVERALL SLOPE 26
3.4 ROTATIONAL FAILURE OF SLOPES IN SERPENTINITE AND SHEAR ZONES 27
3.5 SLOPE DESIGN PHILOSOPHY 28

CONTENTS (cont'd.)

4. MINING HISTORY AND SLOPE PERFORMANCE 30

4.1 MOVEMENT MONITORING SYSTEMS 31
4.2 ASSESSMENT OF PRISM MONITORING DATA 32
4.2.1 Prisms on East and South Walls 33
4.2.2 Prisms in Main Area of Instability 34

4.3 ASSESSMENT OF FAILURE GEOMETRY 38
4.3.1 Volume of Failure 37
4.3.2 Failure Mechanism 37

5. LIMIT EQUILIBRIUM BACK ANALYSIS 40

6. NUMERICAL MODELLING OF SLOPE FAILURE 44

6.1 DESCRIPTION OF THE PROGRAM 44
6.2 DESCRIPTION OF THE MODEL 45
6.3 ANALYSIS RESULTS FOR MODEL WITHOUT CRACKS 46
6.4 ASSESSMENT OF MODEL WITH ONE ROCK TYPE WITH CRACKS 47
6.5 ASSESSMENT OF MODEL WITH TWO ROCK TYPES WITH CRACKS 48
6.6 VARIATION OF GROUNDWATER CONDITIONS FOR THE SLOPE MODEL 49
6.7 VARIATION OF DISCONTINUITY STRENGTH FOR HIGH GROUNDWATER CONDITIONS 49
6.8 COMPARISON OF PREDICTED DISPLACEMENT FOR THE VARIOUS MODELS AND DOCUMENTED DISPLACEMENT OF THE SLOPE 50
6.9 SUMMARY OF NUMERICAL MODELLING 51

7. CONCLUSIONS 52

8. REFERENCES 54

APPENDIX A Representative Geotechnical Sections Showing Engineering Geology and Movement Summaries

APPENDIX B Summary of Prism Movements for Selected Representative Prisms

APPENDIX C Analysis Method and Results for the Three Dimensional Limit Equilibrium Back Analysis

APPENDIX D Results of Two Dimensional Numerical Modelling Using the Universal Distinct Element Code (UDEC)

FIGURES

Figure 1 Location Map

Figure 2 Engineering Geology and Structural Geology of the Cassiar Open Pit

Figure 3 Lower Hemisphere Equal Area Projections of Discontinuity Populations on the East Wall of the Open Pit

Figure 4 Estimated Strength of Intact Rock, Discontinuities and Rock Mass Strength for Argillite, Volcanics and Alteration on the Hanging Wall

Figure 5 Estimated Strength of Intact Rock, Discontinuities and Rock Mass Strength for Serpentinite Waste and Ore

Figure 6 Estimated Strength of Intact Material, Discontinuities and the Rock Mass Strength for Shear Zones

Figure 7 Back Analyses Results for Slopes in Sheared Serpentinite

Figure 8 Details of South Wall Failure

Figure 9 Ultimate Pit Plan

Figure 10 Summary of Prism Movements from June 1988 to June 1989

Figure 11 Summary of Prism Movements from June 1989 to April 1990

Figure 12 Failure Geometry and Failure Mechanism

Figure 13 Limit Equilibrium Analysis Results

Figure 14 Slope Model Used for Numerical Modelling

TABLES

Table I Summary of Discontinuity Populations on the East Wall

Table II Summary of Strength Testing of Intact Rock Samples

Table III Direct Shear Strength of Discontinuities

Table IV Summary of Geotechnical Parameters Logged in Diamond Drill Core

Table V Rock Mass Strengths Estimated from Laboratory Testing and Core Logging

Table VI Deep Seated Rotational Failure Analysis Results

Table VII Summary of Prism Monitoring

Table VIII Material Properties used for Numerical Modelling with the UDEC Program

Table IX Summary of Numerical Modelling Results

PHOTOS

Photo 1	Panoramic view of the open pit in August 1983 during the early stage of the final mining phase
Photo 2	Hard, indurated argillite and volcanic rocks of the Sylvester Group on the hanging wall. Note well developed discontinuities of Set A
Photo 3	Fractured and block serpentinite of the McDame Intrusion in the open pit
Photo 4	Sheared and fractured serpentinite in the ore zone
Photo 5	Footwall contact, 70° Shear and Footwall Fault on the footwall (west) side of the open pit
Photo 6	45° Shear and North Fault on the 5360 Bench
Photo 7	South wall failure which occurred in May 1988 involving the 45° Shear and footwall contact of the serpentinite
Photo 8	Panoramic view of the east wall on May 18, 1989
Photo 9	Panoramic view of the east wall on August 1, 1989 showing advanced development of the graben toppling failure
Photo 10	Panoramic view of the east wall on May 14, 1990 showing advanced development of the graben toppling failure
Photo 11	View looking south along the Serpentinite Dyke showing displacement of graben block. Surface extensometer is shown to the right of the pick-up truck
Photo 12	View looking north showing approximately 12 metres of displacement along the Serpentinite Dyke by mid-September 1989
Photo 13	Oblique view of northeast wall showing development of cracks in the main (initial) area of instability on September 11, 1989

1. INTRODUCTION

1.1 BACKGROUND

This report documents the engineering geology and rock mechanics assessments conducted for the slope deformations and slope failure on the northeast wall of the Cassiar Open Pit between 1988 and 1990.

The Cassiar open pit commenced operation in 1958 and the open pit was completed in May 1990. During the mine life, a total of 39 million tonnes of ore and 68 million tonnes of waste was mined at an overall average strip ratio of 1.74:1. Slope instability, which was experienced during mine life was accommodated by the phased nature of the mining operation which permitted development of interim highwall slopes until the final mining phase (i.e. Phase 10) which was excavated between 1983 and 1990. Between 1987 and 1990, the full height of the 1100 foot hanging wall slope was developed through the weaker ore bearing rocks in the lower sections of the pit. In mid 1988, a major slope failure involving an estimated 3.2 million tonnes developed at the northeast end of the highwall in response to the onset of spring thaw and an increase in slope angle from 39° to 42° for the final mining phase. The failure subsequently increased in size to approximately 17.8 million tonnes during the completion of mining. A program of accelerated mining was initiated and approximately 1.68 million tonnes of ore was stockpiled outside the open pit before slope movements and rockfalls in June 1989 forced closure of the open pit for the summer season. Mining recommenced between February 1990 and May 1990 when slope movements were sufficiently reduced to enable the remaining 144,000 tonnes of available ore to be safely removed from the pit. Total slope deformation in excess of 30 metres (100 feet) have been experienced without catastrophic failure during this period.

Because the behaviour of a steep high slope is not well known, a comprehensive program of monitoring and slope documentation using prisms and surface wire extensometers was used to assess slope movements from June 1988 until May 1990. This program was comprehensive enough to detect and assess any slope movements in any area of the pit and provide adequate warning of potential failure to ensure safety of operating personnel and equipment. The detailed deformation information from the monitoring program also provides valuable information concerning the deformation behaviour of high rock slopes as well as the feasibility and constraints to be considered when mining in the vicinity of a failing slope.

In late 1989, the Mining Research Centre at CANMET and Supply and Services Canada were approached to provide funding for a research project to document the slope behaviour, assess the slope monitoring data, conduct a back analysis and provide criteria concerning the operational constraints associated with mining near the failure. The project was approved in late February 1990 and a contract was received by Cassiar Mining Division in mid March 1990. Analysis and preparation of this report was completed between late March and June 1990.

1.2 PURPOSE AND SCOPE

The purpose of the research project is to document the engineering geology, structural geology, hydrogeology and rock mechanics conditions in the Cassiar open pit as they relate to the major instability on the northeast wall.

This information is combined with documented deformation information from the monitoring program to define the failure mechanism and conduct a back analysis using limit equilibrium and numerical modelling techniques.

The documentation of slope deformations and back analyses are used to determine the controls on slope stability and establish criteria for mine

operations concerning the feasibility and constraints to be considered when mining in the vicinity of failing slopes.

1.3 ACKNOWLEDGEMENTS

The research project for which this report is submitted was administered by Supply and Services Canada and supported by the CANMET Mining Research Laboratory in Ottawa. Review and comments by Mr. Y. Yu of the Mining Research Laboratory are acknowledged with thanks.

The encouragement, cooperation and assistance of management and staff at Cassiar Mining Division and Piteau Associates Engineering Ltd. is acknowledged with thanks. The project was coordinated and directed by E.F. Mehr, Chief Engineer of Cassiar Mining Division. Management and personnel at Cassiar who participated in the project include W. Zemenchik, T. Carew, R. Tyne, J. Jakubec, and C. Garducci. Geotechnical aspects of the project were conducted by D. Martin of Piteau Associates Engineering Ltd. Personnel from Piteau Associates who participated in the project include E. Foster, M. Hawley, M. Leir, B. Lindstrom, L. Stevens, A. Stewart, and J. Tod. Professor W. Savigny and K. Everard of the Department of Geological Sciences at the University of British Columbia conducted the numerical modelling.

2. ENGINEERING GEOLOGY

2.1 SITE LOCATION, PHYSIOGRAPHIC SETTING AND CLIMATE

Cassiar is located in northern British Columbia approximately 700 km north of Prince Rupert, B.C., and 150 km southwest of Watson Lake in the Yukon Territory (see Fig. 1). The mine is located approximately in the middle of a belt of deformed and undeformed sedimentary, volcanic and igneous rocks which form the Cassiar Mountains. This belt is approximately 80 km wide, being bounded on the east by the Liard Plain and on the west by the Stikine Plateau.

The area has been extensively glaciated, resulting in broad U-shaped valleys with steep flanks, razor backed serrated ridges, cirques and other typical glacial features. Valleys are covered with thick deposits of glacial moraines and glaciofluvial material. The flanks and crests of ridges consist of bare rock with variable thicknesses of colluvium and transported soils. The highest point in the McDame Range is 2,150 metres (7,000 feet) above sea level. Average relief is of the order of 1000 to 1500m.

Climate is typical of North American cold regions having a mean daily temperature of -3.2°C and an average total precipitation of 700mm. Precipitation comprises an average of 305mm of rain and 3950mm of snow. Mean daily temperatures is less than 0°C from early October until late April. Snow remains on north facing slopes in the open pit until late August or September.

2.2 REGIONAL AND LOCAL GEOLOGY

The Cassiar orebody lies in a thick sequence of Precambrian and Paleozoic sedimentary and volcanic rocks on the northeast flank of the northwesterly trending granitic Cassiar Batholith. This sequence has been folded into a broad northwest trending syncline adjacent to the batholith.

The basic lithological units in the area, as detailed by Plumb (1968), Gabrielse (1963), Nelson et al (1989) and O'Hanley (1990), are given in the following:

i) Good Hope Group (Proterozoic): a thick sequence of limestone, dolomite, slate and argillite.
ii) Atan Group (Lower Cambrian): buff limestone and pink quartzite.
iii) Ketchika Group (Cambrian-Ordivician): thin bedded graptolitic limy shales, slates and phyllites.
iv) Sandpile Group (Silurian): distinctive marker horizon of massive white-weathering sandy dolomite.
v) McDame Group (Devonian): black fetid dolomite.
vi) Sylvester Group (Devonian-Mississippian): thick eugeosynclinal assemblage of quartzites, argillites and interbedded volcanic flows, tuffs, greenstones and associated rocks.

The McDame Intrusions consist of a series of late Paleozoic or early Mesozoic ultramafic bodies which intrude the Sylvester Group intermittently for some 110 kilometres along the axis of the syncline adjacent to the Cassiar Batholith.

Cassiar Mine is located on the western flank of McDame Mountain. The orebody occurs in a sill of serpentinized peridotite which intrudes the west limb of a syncline formed in argillite and associated rocks of the Sylvester and Sandpile Groups.

The orebody strikes north-south and dips moderately east. It is roughly tabular, although changes in thickness and dip are evident along strike and dip, due possibly to the deformed nature of the enclosing sediments and presence of several major faults and shear zones which offset the serpentinite sill and orebody. The contact between the serpentinite intrusion and the enclosing sediments is demarcated on the footwall side of the pit by a

pronounced zone of sheared soft graphitic argillite. On the hanging wall, the contact appears indurated, consisting of a tough hard alteration zone up to 6 metres wide. Argillites on the hanging wall are more competent than those on the footwall, probably due to the more deformed and faulted nature of the footwall materials.

2.3 LITHOLOGY OF THE OPEN PIT

Distribution of the main rock types, location of geological contacts and major structural information obtained from geological mapping in the open pit are given in Fig. 2. Typical sections showing the engineering geology and structural geology in the pit area are included in Appendix A. Photo 1 is a panoramic view of the open pit during the early stages of the final mining phase. The main rock types in the pit area are described in the following.

2.3.1 Sylvester Group Rocks

The Sylvester Group is Devonian-Mississippian in age and consists of a thick eugeosynclinal assemblage of quartzite, argillite, interbedded volcanic flows, tuff, greenstone and associated rocks (Plumb, 1968). The Sylvester Group rocks in the hanging wall consist mainly of blocky, competent, black and greenish argillite, which is interbedded at irregular intervals with greenstone or similar rocks derived from volcanic flows (Plumb, 1968).

The argillite is generally fine grained or aphanitic and laminae are well indurated. The volcanic rocks may be fine or coarse grained and form tight contacts with the sediments with which they are deposited. Both the argillite and volcanic rocks are generally hard and competent, except in close proximity to fault or shear zones where less competent material is encountered. Photo 2 is a typical exposure of Sylvester Group rocks on the hanging wall.

Sylvester Group rocks in the footwall consist of dark, aphanitic argillite, cherty argillite and graphitic schist. These rocks are generally weak and fractured due to shearing and contortion of rock in the footwall.

2.3.2 McDame Serpentinite Intrusion

The McDame intrusion consists of mottled, light-to-dark green serpentinite which has a greasy lustre. Mineralogical studies indicate that the serpentinite is an alteration product of an olivine, orthopyroxene and clinopyroxene cumulate rock. Asbestos fibre occurs as fracture filling developed primarily within open joints. Photos 3 and 4 show typical exposures of fractured serpentinite in the open pit.

As a consequence of considerable faulting and shearing in the intrusive body, the serpentinite is well fractured and blocky, and most fractures show evidence of shearing. Many major shears or zones of sheared rock were noted in the serpentinites (Photos 5 and 6). Strength and competency of the serpentinite varies depending on the degree of fracturing and the infilling along fractures or veins and proximity to shear zones. Waste serpentinite is considered to be generally more competent than the ore serpentinite.

2.3.3 Argillite/Serpentinite Contact Zones

i) Footwall

The contact between the McDame intrusion and the Sylvester Group on the footwall (west) side of the pit consists of a 0.5 to 2 metre wide zone of weak, sheared graphitic argillite, clay gouge and alteration (Photo 5). In the vicinity of the 45° Shear on the south wall, a 6 to 27 metre

wide zone of sheared, black, highly contorted, graphitic argillite is developed. This zone varies from moderately to intensely sheared with an estimated unconfined compressive strength less than 700 kPa. Sheared material consists typically of thin, "fishscale" platelets of intact rock with greasy, graphitic infillings. Sympathetic shearing of the immediately adjacent serpentinites is evident.

ii) Hanging Wall

The hanging wall contact between the Sylvester Group rocks and the McDame serpentinite instrusive rock is characterized by a 0.5 to 6 metre thick zone of very hard, highly indurated rock which results from contact metamorphism during the emplacement of the serpentinite sill. The indurated zone consists essentially of a cream coloured tremolite-zoisite hornfels (Plumb, 1968) and some jade. This material is possibly comprised of materials derived both from the Sylvester Group rocks and the serpentinite and is the only extensive evidence of contact metamorphism. The small stratigraphic thickness, however, indicates that the serpentinite may have been at a relatively low temperature during intrusion. The alteration zone appears to be relatively impermeable except where transected by faults or other major discontinuities.

2.4 MAJOR FAULTS

Several major faults have offset the serpentinite sill by a few metres to several hundred metres. These faults are important features for understanding the structural geology of the rock mass as well as for slope stability. A brief description of each fault is given in the following:

2.4.1 45° Shear

The 45° Shear has an average orientation of 090/45 (dip direction/dip) and runs through the centre of the open pit. The shear zone varies from 3 to 30 metres wide and consists of extremely sheared and broken rock and gouge as shown in Photo 6. Core logging indicates that zones of more competent rock may occasionally occur within the 45° Shear. Geological interpretations indicate that the 45° Shear has offset the serpentinite by several hundred metres and may have also resulted in thickening of the sill in the vicinity of the orebody (O'Hanley, 1990).

2.4.2 South Fault

The South Fault has an average orientation of 350/78. A smaller, sympathetic fault, which occurs on the south wall, has an average orientation of 175/73. These faults occur in the southeast corner of the pit (Photo 1). They have been identified in the argillite on the hanging wall and serpentinite. However, it has not been possible to trace these features across the 45° Shear. There is a possibility that the 70° Shear on the west side of the pit could form the offset extension of the South Fault; however, this would have to be confirmed by additional assessments. In argillite, the South Fault consists of a 0.5 to 3 metre wide zone of gouge and broken rock. In serpentinite, the fault zone consists of a 3 to 15 metre wide zone of sheared and broken rock and gouge.

2.4.3 70° Shear

The 70° Shear occurs on the southwest wall of the open pit and has an average orientation of 015/70 (Photo 5). The shear zone is about 6 to 15 metres wide and consists of broken and sheared serpentinite and gouge. The 70° Shear has not been traced across the 45° Shear although

the width of both shear zones increases near their intersection. The intersection of the 70° Shear zone and the Footwall Fault has resulted in a wedge failure occurring over several benches on the west wall (Photo 5).

2.4.4 Footwall Fault

The Footwall Fault occurs on the west wall and has an average orientation of 152/52. This fault appears to have offset the footwall contact of serpentinite by a few hundred metres, although it is extremely difficult to trace the fault beyond the area where the argillite serpentinite contact has been offset (Photo 5). The fault zone consists of 0.5 to 1 metre of clay gouge and broken rock. The weak nature of this material has resulted in two areas of instability on the footwall.

2.4.5 North Fault

The North Fault occurs in the northeast corner of the pit and has an average orientation of 124/55. This fault also appears to have offset the serpentinite by more than 200 metres. The fault zone is less distinct than the other major faults and is difficult to trace except at the contact between argillite and serpentinite (Photo 1). The North Fault consists of a 1.5 to 5 metre zone of gouge and breccia. The fault zone appears to form several 0.3 to 1.5 metre wide serpentinite shear zones within the serpentinite orebody and hence is difficult to trace through the serpentinite (Photo 6). The North Fault and Footwall Fault may be the same structure which has been subsequently offset by the 45° Shear.

2.5 ANALYSIS OF DISCONTINUITY POPULATIONS

Detailed line mapping and related techniques were used to collect geologic structural data to assess the orientation and distribution of discontinuity sets in the rock mass at the mine. Rational slope stability analysis and pit slope design requires that the pit be subdivided into areas of approximately similar geologic structural and mechanical characteristics. Extrapolation of stability analysis results and slope design criteria is valid only within parts of the rock mass which have similar physical and mechanical properties. Such areas with similar geological structure are called structural domains (Herget, 1977).

Orientation of geological structures is the most important consideration in determining whether geologic structural populations within a structural domain or between structural domains are similar or dissimilar. Other parameters, such as continuity (joint extent or size), joint infilling, waviness, etc., are also considered in evaluating the engineering properties and nature of joint sets, but are not used for designation of structural domains. Equal area projections were used to define the peak or average orientation and possible range of orientations for the various sets of discontinuities in the individual structural domains.

The rock mass at the mine was initially divided into several structural domains. The boundaries of the structural domains are based on the boundaries of main lithologic units and major faults identified from surface mapping and core logging. Discontinuity populations have significantly different properties in Sylvester Group rocks in the hanging wall, Sylvester Group rocks in the footwall and serpentinite of the McDame intrusions. The following discussion is confined to the analysis of discontinuity populations in the hanging wall and ore zone in the area of the major failure on the east wall.

2.5.1 Sylvester Group Rocks in the East Wall

An extensive analyis of structural populations in the argillite, volcanics, and related rocks of the Sylvester Group in the Hanging wall was presented by Piteau and Martin (1977). These rocks have a uniform structural pattern but show localized variation in orientation and other parameters. The distribution of discontinuity populations in the Sylvester Group rocks on the east wall based on mapping conducted by Cassiar personnel in 1983 are given in Fig. 3. Average orientation of discontinuity populations are summarized in Table I.

i) Bedding

Bedding or compositional layering of the argillite is reasonably uniform across the hanging wall slope. Bedding dips away from the pit, having an average orientation of 080/21 (Fig. 3). Bedding appears to be rotated in the southeast portion of the pit, probably due to the effects of the 45° Shear and South Fault in this area.

Bedding planes are generally well indurated and few fractures or joints occur parallel to bedding.

ii) Joint Sets

Cross joints and joints related to faulting are generally well developed in the Sylvester Group rocks. Many joints are continuous over one or two benches and well defined joints are evident in all areas (Photo 2). Three well developed joint sets related to folding and subsequent relaxation of stresses occur in the Sylvester Group rocks as summarized in Table I and illustrated in Fig. 3 and described briefly below.

Joint Set A: Very well developed joints of considerable continuity which are shear features formed sub-parallel to major transverse faults and other structural features (see Fig. 3). The orientation of Joint Set A undergoes a distinct rotation in strike on the south wall. This variation is thought to be related to disturbance from the South Fault and the 45° Shear.

Joint Set B: Reasonably well developed shear joints which strike sub-parallel to Joint Set A, and dip steeply to the south. Joints of Joint Set B are generally less continuous than joints of Joint Set A.

Joint Set C: Generally less well developed joints which strike north-south and have an average orientation of 266/75 (Fig. 3). Joints of Joint Set C are generally somewhat irregular, dicontinuous and often terminated against joints of Joint Set A and Joint Set B. These joints are approximately normal to the main shear joints and are probably tension joints.

Miscellaneous sets, summarized in Table I, are less well developed except in local areas such as near faults or near the contact with the McDame intrusions.

iii) Fault Sets and Shear Sets

Several major faults, which are continuous over the hanging wall, were mapped in the Sylvester Group rocks. As indicated in Fig. 2, some of these faults have offset the argillite/serpentinite contact by amounts varying from 3 to 60 metres. The location and extent of development of some of the smaller faults into serpentinite is not certain. Major faults of similar orientation are not evident in the footwall, and correlation of fault structures between footwall and hanging wall is difficult.

Major faults and shears mapped on the east wall are subparallel to Joint Set A, having an average orientation of 353/66 (Fig. 3). There is some evidence of a clockwise rotation of orientation of faults and shears on the south wall probably due to the offset and related disturbance associated with the South Fault and 45° Shear.

2.5.2 McDame Intrusions (Serpentinite)

The serpentinite rocks in the open pit are extremely fractured and blocky, so much so that distinct joint and fault sets are difficult to delineate and individual discontinuties are difficult to trace. Most discontinuities show evidence of previous shear movement, such as slickensides and gouge. Discontinuities are generally infilled with serpentine, asbestos fibre, talc or related minerals. The 45° Shear, North Fault, South Fault, 70° Shear and argillite/serpentinite contact were assumed to form the boundaries of structural domains in the serpentinites, as shown in Fig. 2. Examination of lower hemisphere equal area projections of discontinuity populations in serpentinite on the east wall, indicates a variation in the orientations of joint sets and shear sets on either side of the North Fault as shown in Fig. 3.

i) Joints

As summarized in Table I, five sets of joints occur in serpentinite, with degree of development varying between the structural domains. Joint Sets A, B and C have similar orientation to the sets defined in Sylvester Group rocks. Joint Sets D and E are also well developed in the serpentinite rocks. In general, joints tend to be less steeply dipping in the serpentinite than in the argillite. Joint sets in the serpentinite tend to be less consistent between structural domains, and populations tend to be dispersed and less well defined.

ii) Shears

Although sets of joints and shears occasionally have similar orientations, large variations in the orientation of joints and shears are common in the serpentinites. Shears tend to be slickensided and gouge filled with variable orientations and lengths. The peak orientations of shear sets are summarized in Table I and Fig. 3. Correlation between individual shears in serpentinite and faults and shears in argillites is extremely difficult and has not been carried out.

iii) Veins

Veins are generally formed as fracture fillings along joints sub-parallel to the main discontinuity sets or as irregular discontinuous structures in serpentinite. Many veins are healed and have a higher shear strength than joints or shears. Detailed assessments of veins was not carried out for this study.

2.6 ROCK STRENGTH AND COMPETENCY

2.6.1 Strength Properties of Intact Rock

Results of laboratory testing of intact rock specimens carried out in 1981 and point load index testing of rock cores carried out in 1975 are summarized in Table II. Sylvester Group rocks on the hanging wall (argillites, volcanics, alteration and related rocks) are the strongest rocks in the pit area. Mean unconfined compressive strengths of these rocks are greater than 75 MPa (>11,000 psi) and mean tensile strengths are greater than 9 MPa (>1,300 psi). Unsheared serpentinites have mean unconfined compressive strengths ranging from 35 to 50 MPa (5,000 to

7,000 psi) and mean tensile strengths ranging from 3 to 6 MPa (450 to 900 psi). Sheared serpentinites are the weakest rocks tested, having a mean unconfined compressive strength of about 8 MPa (1,200 psi). Sheared graphitic argillites are expected to have similar or lower compressive strengths.

Intact strength envelopes for the various rock types were estimated based on unconfined compressive strength and tensile strength testing results (see Figs. 4, 5 and 6). These envelopes are useful in assessing the relative strengths of intact rock and discontinuities which are used as a basis for estimating the rock mass strength.

2.6.2 Shear Strength of Discontinuities

Results of direct shear tests of discontinuities carried out in 1975 and 1981 are summarized in Table III. These results were based on specimens of various sizes and rock types which were tested at a variety of normal loads. These laboratory tests provided relatively consistent values for the residual friction angle which are about 26.0 to 26.5° for discontinuities in serpentinite and about 32° for discontinuities in Sylvester Group rocks. Residual friction angles generally appeared to be higher for normal loads less than 2 MPa (<250 psi).

Cohesion is difficult to estimate from laboratory test specimens, many of which are disturbed during coring or cutting. Cohesions in excess of 2 MPa (>250 psi) were recorded for healed asbestos veins, whereas most joints had little or no cohesion. Clay gouge samples tested in direct shear indicated a cohesion of about 70 to 140 kPa (10 to 20 psi) If it is assumed that a portion of faults and shears occurs along cohesionless joints, a maximum cohesion of 70 kPa (10 psi) is appropriate for shear zones.

Based on an assessment of these results, design shear strengths for discontinuities, which are recommended for use in stability analyses were chosen and are summarized in Table III. Shear strength envelopes for discontinuities in the various rock types are shown in Figs. 4, 5 and 6.

An assessment of discontinuity stiffness is required for application of some numerical modelling techniques. Shear Stiffness, K_s, of a discontinuity is calculated as the ratio of peak shear strength to shear displacement at the peak. Normal Stiffness, K_n, is calculated as the ratio of peak shear stress to normal dilation of a joint at the peak strength. Direct shear testing data from the 1975 testing program was used to estimate the shear stiffness, and normal stiffness of discontinuities in Sylvester Group rocks and McDame intrusions. Preliminary estimates of the discontinuity stiffness are included in Table III.

2.6.3 Rock Competency and Core Quality

A general assessment of the physical and mechanical characteristics of the rock mass is based largely on susceptibility to mechanical deterioration and chemical alteration, strength, and geologic structural characteristics for each rock type. Various methods have been presented for classifying and assessing rock quality in a general way based on observations of drill core. These methods include measurement of RQD, fracture spacing index, fracture frequency, solid core recovery, Stability Index and Degree of Breakage (Martin, 1986).

In order to assess general rock mass quality at Cassiar, the following geotechnical parameters were recorded by mine personnel for selected rock cores in the pit area:

i) Core recovery
ii) RQD based on natural fractures
iii) RQD based on all fractures
iv) Frequency of natural joints
v) Roughness and condition of natural joints
vi) Degree of breakage
vii) Rock type
viii) Rock hardness

In addition, logging of lithology and significant structures in the core, as well as fibre density (CCRG), was carried out.

In order to appreciate the variability of a rock mass and to aid in the assessment of rock mass strength, the rock mass must be divided into zones or areas within which the behaviour of the mass as a whole is expected to be similar. This process is analogous to the concept of structural domains, however, geotechnical parameters, such as RQD, degree of breakage, and hardness, are of principal interest. At Cassiar, the rock mass has been classified based on rock type, fibre content, and the location of shear zones. Core logging results have been assessed statistically for each general rock type defined. Analyses results are described in the following and summarized in Table IV.

Core recovery in all rock types is generally in excess of 80 percent; however, recovery in shear zones is consistently four to five percent lower than in other areas. Natural RQD is generally highest in argillites and volcanics, decreasing in serpentinites, and lowest in shear zones. As can be seen from natural joint spacing, argillites and volcanics on the hanging wall tend to be more massive than serpentinites or shear zones. Argillites and volcanics are also harder and tend to be less susceptible to breakage than the other rocks.

Based on the assessment of the data in Table IV, the rocks in the hanging wall were divided into four basic rock mass groups as follows:

1) Argillites, volcanics and related rocks.
2) Barren (waste) serpentinites.
3) Unsheared, ore-bearing serpentinites.
4) All shear zones.

The expected strength and behaviour of the rock mass in each of these groups is described in the following section:

2.6.4 Assessment of Rock Mass Strength

The concept that the strength of the rock mass is related to the discontinuities in the mass as well as the intact rock is fundamental to the analyses of high slopes in fractured rock. The rock mass is defined as an anisotropic, discontinuous and heterogeneous medium, made up of intact material partitioned by discontinuities. If the intact rock is sufficiently weak and/or the slope is sufficiently high or steep that failure could occur through some intact material, it is possible that a failure surface could develop from a combination of sliding along discontinuities and failure through intact rock. Thus, rock mass strength may be considered to be a combination of intact rock strength and discontinuity strength. In this case, the rock mass strength would fall somewhere between the values for intact strength and discontinuity strength for each rock mass group (see Figs. 4, 5 and 6).

The strength envelopes for intact rock and discontinuities shown in Figs. 4, 5 and 6 were used as a basis for assessing the rock mass strengths for the four main rock mass groups indicated in Section 2.6.3. The rock mass strength envelopes used by Call Nicolas Inc. (1981) are plotted on these figures for comparison purposes. Rock mass strengths were also estimated using the criteria developed by Hoek and Brown (1980). This method employs a set of empirical equations from which Mohr failure envelopes can be developed over the range of stresses

expected in the slope. Selection of the equation used to model the strength of the rock mass is based principally on assessments of rock mass quality (as reflected by the geotechnical parameters discussed above), rock type and unconfined compressive strength.

The rock mass strengths selected for slope design at Cassiar were estimated based on a critical review of all of the above criteria, as shown on Figs. 4, 5 and 6 and summarized in Table V.

2.6.5 Verification of Rock Mass Strength from Back Analysis of Slope Failures

Prior to development of the large failure on the northeast wall, a number of small failures occurred involving one or more benches in the various rock types. Back analyses of these failures was conducted using available information and combined with slope documentation information to verify the rock mass strength criteria.

i) Failures in Argillite

A back analysis was carried out for a small wedge failure on the 5960 bench in argillite on the east wall. Results of this back analysis indicate that the shear strength values assumed for discontinuities in the argillite are reasonable.

ii) Slopes in Serpentinite

Both failures involving discontinuities and rotational failures have been reported in the serpentinite rocks, although both types were poorly documented. Planar type failures were observed on moderate to steeply dipping joints in serpentinite on the 5600 bench. Because these joints are relatively steep, back analyses would provide only an upper bound to the discontinuity strength.

At least one, and possibly two, large failures occurred in sheared serpentinite on the east wall on a previous mining phase in the mid 1970's. Although there is no documented information on these failures, it appears that they were related to the 45° Shear which occurred on the pit wall at that time.

Back analyses were carried out based on an existing slope in sheared serpentinite on the south wall. This slope was about 95 metres high and had been mined at an angle of about 38° (see Fig. 7). Analyses were carried out assuming the slope was composed of a single material with a friction angle of 26.5°. Various failure surfaces were assessed for cohesions of 0, 70, 138 and 207 kPa (0, 10, 20 and 30 psi) and the minimum Factor of Safety was determined for each. The GEOSLP computer program, developed by Houlding et al (1982) based on the Janbu method of slices, was used for the back analysis. Analysis results are plotted on Fig. 7 in terms of Factor of Safety versus cohesion. If it is assumed that the slope is marginally stable (i.e. Factor of Safety is 1.1 to 1.2) the cohesion of the slope material would be about 70 kPa (10 psi). Because this slope has not failed, these back analyses results provide a lower bound estimate of cohesion of 70 kPa (10 psi) for this material which is considered appropriate for design. It must be noted that the slope in question may contain some percentage of stronger serpentinite which could also contribute to the cohesion of the rock mass in that area.

iii) South Wall Slope Failure

A major failure occurred on the South Wall during the spring thaw in mid May 1988. Figure 8 shows the salient features of this failure which occurred as a large wedge failure involving an estimated 250,000m^3, which slid along a line of intersection formed by the 45° Shear and

several throughgoing discontinuities of Set A (Photo 7). The failure zone subsequently expanded to include the footwall of the serpentinite sill. Failure surfaces consist of graphitic gouge of low strength and low permeability. Water flow in excess of 30 gpm was noted in the toe area of the failure. The line of intersection of the discontinuity is about 20° to 30°. Back analyses have shown that failure occurred due to high water pressures on the shear surfaces involved.

As a remedial measure, the slope was flattened to about 40° to 42° in this area and the slope stabilized sufficiently to complete mining.

2.7 HYDROGEOLOGY

Groundwater flow systems in the open pit are relatively complex due to the variation in hydrogeological properties of the various rock types and faults. Recharge to the groundwater flow system occurs as precipitation on the ridges to the east and west of the pit, and on the new divide created by the intersection of the southwest wall of the pit with the original slope. At higher elevations, infiltration of precipitation to the groundwater flow system is estimated at about 5% of the annual precipitation. The remainder of the precipitation becomes surface water run-off or evapotranspiration. Because groundwater represents a small percentage of the annual precipitation, it is not a major component of the total water inflow to the pit. However, groundwater pressures in the rock could cause slope stability problems.

Reports of observations made during construction of the exploration adit indicate that the argillite is much more permeable than the serpentinite. Small seeps were apparently observed along the section of the adit constructed in argillite, whereas the section of adit constructed in serpentinite was virtually "dry". Some seepage was apparently noted along the first ten metres of the adit beyond the argillite-serpentinite contact, and in the vicinity of the South Fault. Occurrences of seepage in the pit substantiate the

observations of seepage in the adit. Seepage generally can be observed at the hanging wall contact between the argillite and the serpentinite. This suggests that the lower permeability serpentinite is acting as a barrier to movement of water, thereby forcing it to surface around the contact zone. These seepages are most obvious adjacent to faults on the east wall and around the south end of the pit.

Results of falling head tests in sealed standpipe piezometers in serpentinite indicate that the apparent hydraulic conductivity of serpentinite is about 10^{-8}m/sec. Although no permeability testing was conducted, a reasonable estimate of hydraulic conductivity for the Sylvester Group rocks in the hanging wall is about 10^{-7}m/sec based on observed seepage in the open pit and exploration adit. Although bulk permeabilities are relatively low, considerable water flow has been observed from faults in the Sylvester Group rocks. Only limited seepage has been observed from faults in the McDame intrusions, even in underground workings.

A steady-state finite-element computer model was used to simulate existing groundwater flow along a typical section in the pit. This model confirms the hydraulic conductivity of the rock units based on the measured flows from the open pit and exploration adit. Assessment of this model for the final slope is consistent with field observations which confirm that the groundwater flow through the argillite is much greater than the serpentinite can transmit, resulting in a seepage face above the contact and sufficient recharge to the serpentinite to maintain high groundwater pressures in much of the slope.

The hydrogeological monitoring and modelling indicated the requirements for slope depressurization during the final phase of mining. A program of subhorizontal drainholes for slope depressurization was completed in October and November 1988. These drainholes, combined with the flows in the exploration adit below the south and east wall, have helped to depressurize those areas of the final slope.

3. SLOPE STABILITY ANALYSES AND SLOPE DESIGN

Slope stability analyses involved investigating various failure mechanisms with respect to faults, joints and other discontinuities which could lead to shallow failures of individual benches and/or deep seated failure involving large sections of the slope.

Examination of the open pit slopes and assessment of the geological and geotechnical data collected for the slope stability studies indicate that the design of the open pit slopes depends primarily on the design of safe benches. However, the proposed high, steep ultimate slopes could be subject to deep seated rotational failure. This type of failure is particularly important in the fractured serpentinite in the lower section of the slope where two large failures had occurred in sheared serpentinites in the past.

At Cassiar, the approach to slope design was to first prepare a rational design for benches and interramp slopes based on statistical analysis of the various sets of structural discontinuities to assess all kinematically possible failures. The overall slopes developed from the design of benches were then assessed in terms of deep seated failure of the rock mass involving several benches or the entire slope. Results of the back analyses and estimates of rock mass strength discussed in Section 2.6 were used to carry out stability assessments and prepare a design for slopes where fractured and sheared serpentinite is expected to occur in the lower 75 to 100 metres of the slope.

3.1 SLOPE STABILITY ANALYSES BASED ON STRUCTURAL ANALYSIS RESULTS

Stability analyses were carried out to assess the kinematically possible failure modes determined from the geologic structural analysis results. Structural domains were divided into design sectors, within which the final

slope orientation is relatively constant and the behaviour of the rock mass is expected to be uniform (Herget, 1977). Within each design sector, the main kinematically possible modes of failure were determined and appropriate slope stability analyses were carried out. Due to the considerable number of possible wedge failures of various orientations in most design sectors, limit equilibrium analyses results and wedge distribution were tested statistically. A unique statistical analysis technique (Piteau et al, 1985) based on assessing the cumulative percentage frequency of possible unstable wedge failures with respect to the apparent plunge angle and factor of safety was used. Slope angles were determined for the dip or apparent plunge of failures which were assumed to control bench design based on the statistical analysis results as well as an assessment of the possible main failure mode which was considered to control stability. Documented bench face angles in the pit were also considered in the bench design.

Results of kinematic assessments indicated that the following slope designs were feasible:

AREA/DESCRIPTION	BENCH HEIGHT (m)	BERM WIDTH (m)	BENCH FACE ANGLE (°)	SLOPE ANGLE (°)
Sylvester Group rocks on the East Wall	27	9	70	54.5
Barren Serpentinite on the East Wall	18	11	66	43.0
Ore Bearing Serpentinite and Shear Zones	18	13	66	40.5

These general slope designs were implemented in the Phase 10 ultimate pit design shown in Fig. 9. These designs were then examined to assess the potential for deep seated failure involving structural discontinuities or shear failures through the rock mass as discussed in the following.

3.2 DEEP SEATED FAILURES INVOLVING MAJOR DISCONTINUITIES

Deep seated failure, involving several benches or even the whole slope, may involve throughgoing faults or other major discontinuities. All possible combinations of major discontinuities and major discontinuity sets were assessed using equal area projections and carrying out stability analyses using the geometry and discontinuity strength data available. Analyses results indicated that no major possible failures formed by faults would be undercut by the proposed Phase 10 ultimate slope on the east wall. It is noteworthy that the lines of intersection of the North Fault and faults of Fault Set A plunge to the east (into the slope) at about 25° and hence, the combination of these discontinuities was not expected to result in the formation of a kinematically possible failure mode.

3.3 DEEP SEATED ROTATIONAL FAILURE OF THE OVERALL SLOPE

Deep seated failures may develop through a complex interaction of minor and/or major structures to form a large, continuous, if somewhat irregular, failure surface. In some cases, deep seated failure surfaces may develop in part by failure through intact rock bridges between discontinuties. Such failures are often precipitated by small slope readjustments and high stress concentrations at the toe of the slope, which tend to exceed the strength of the rock mass. This type of failure mechanism is possible in highly fractured rock masses such as fractured serpentinite or in rock masses significantly weakened by weathering and/or alteration.

In terms of deep seated rotational failure of the rock mass at Cassiar, separate assessments of stability were carried out for the overall slope as well as slopes in serpentinite and shear zones at the base of the slope. The potential for deep seated rotational failure of overall slopes was investigated based on proposed final slope geometries and geological interpretations for the highest and steepest overall slope in the pit. The toe of the slope occurs in sheared and faulted serpentinite adjacent to the 45° Shear Zone and other faults.

Limit equilibrium analyses were carried out using the Janbu method of slices, the rock mass shear strength criteria summarized in Table V and the anticipated groundwater conditions. Analyses were carried out to determine the location of the possible critical failure surface for a rotational failure for the engineering geology conditions shown on Section 23,400N as well as a typical geotechnical section through the south wall. This latter section was chosen because it represented the highest slope with the greatest amount of sheared serpentinite.

For each case examined, the radius of the slip circle and location of the centre of the slip circle were varied, Factors of Safety determined and contoured, and overall minimum Factors of Safety determined. Analysis results summarized in Table VI indicated that the overall slopes would be marginally stable for the assumed slope geometry, strength and groundwater conditions. Because the slope geometry, rock mass strength and groundwater conditions used in the analyses were generally assumed to be conservative, it was felt that the probability of deep seated rotational failure of the overall slope was low.

3.4 ROTATIONAL FAILURE OF SLOPES IN SERPENTINITE AND SHEAR ZONES

Stability analyses of the overall slope indicated that rotational failure would be more likely to occur within the weaker, more highly broken

serpentinites and shear zone material in the lower section of the slope. This prediction is consistent with rotational failures which had been reported within the serpentinite and shear zones during previous mining phases.

Detailed stability analyses were carried out for rotational failure in the serpentinite and shear zones in the lower section of the slope. These analyses were carried out in a similar manner as described above for the lower portions of slopes on the two typical geotechnical sections using the GEOSLP program (Houlding et al, 1982). Analyses were carried out for a range of rock mass strengths, groundwater conditions and proposed slope geometries. Analysis results are summarized in Table VI. Factors of Safety given in Table VI are calculated values based on assumed rock mass strengths. Results were interpreted in terms of relative slope stability and sensitivity to variations in slope conditions.

Analysis results summarized in Table VI indicated that slopes would be at best marginally stable even if depressurized. More accurate assessments of slope designs were not feasible given the state-of-the-art in assessing deformation behaviour of high rock slopes.

3.5 SLOPE DESIGN PHILOSOPHY

The strategy adopted by Cassiar Mining Corporation was to mine the slopes at the design angles summarized above (54.5°, 43°, 40.5°), depressurize the slope as required and provide a network of monitoring prisms to enable detection of any significant slope deformation. Provision was also made to leave a buttress of intact rock near the toe of the south wall as shown in Fig. 9 and discussed by Martin and Carew (1986). This area was the highest slope with the greatest amount of sheared material in the toe. The buttress was to be mined out in the last stage of mining. If instability developed during mining of the buttress, a relatively small portion of the orebody would be lost.

The actual slope performance and mining sequence adopted for the final slope, after instability began to develop on the east wall, are described in the following sections.

4. MINING HISTORY AND SLOPE PERFORMANCE

Mining of the final phase began in late 1983 and was completed in June 1989. The progression of the mining is illustrated by the mined bench elevations shown on the sections in Appendix A. Slopes were completed to the 5690 level by mid-1987. During the winter of 1987/1988, the slope was mined from the 5690 level to the 5630 level. Two failures developed on the pit slopes during the spring thaw of May/June 1988. The failure of the south wall involved approximately 250,000m^3 of fractured and sheared serpentinite between the 45° Shear and the footwall contact of the serpentinite sill (Section 2.6.5). This failure was stabilized by flattening the slope to 40° to 42° by the removal of 150,000m^3 (460,000 tonnes) of waste.

In June 1988, a second area of instability was noted on the northeast wall of the open pit. This area was first identified by the development of a crack along the Serpentinite Dyke as shown in Fig. 2. Additional prisms and a surface extensometer were installed on the slope in this area in July 1988 to assess slope deformation rates.

By mid-August 1988 it was apparent that an extremely large portion of the pit wall in excess of three million tonnes had become unstable as a result of mining and the onset of spring thaw. The large volume of the failure did not enable the slope to be economically flattened or regraded. Hence, a decision was made to accelerate the mine production and complete the mining prior to spring breakup in May 1989. In addition, a program of slope depressurization using drainholes was recommended to reduce water pressures during the completion of mining.

Accelerated mining began in late September 1988 and continued until June 2, 1989. During this period, a total of 3.0 million tonnes of ore and waste was

mined from the pit at an average mining rate of 22,000 tonnes/day. A total of 2.5 million tonnes of ore was mined, of which 1.68 million tonnes of ore were stockpiled outside the pit. Drainholes were installed in late October and early November on the 5600 and 5570 levels. Monitoring was continued throughout the mining. Additional prisms and extensometers were installed and monitored as mining progressed.

Slope movements slowed considerably after installation of drainholes and the onset of winter conditions. With the onset of spring thaw in mid-April 1989, movement rates began accelerating. Additional prisms were installed and monitoring frequency was increased. Movement rates reached 90mm/day (3.5 in/day) for prisms and 125mm/day (5 in/day) for surface extensometers by early June 1989.

Mining operations were suspended on June 2, 1989 due to the high movement rates and occurrence of rockfalls from the failure area. Monitoring was continued through the summer of 1989 during which time movement rates greater than 125mm/day were recorded, and some very large rockfalls of the order of several hundred tonnes occurred from the failure area. Movement rates again slowed to less than 35mm/day in January 1990 and the pit was re-opened to recover the remaining mineable ore in the bottom of the pit and on the haulroad. A total of 144,000 tonnes of ore was mined in a scavenging operation between late February 1990 and early May 1990. By early May, movement rates were again beginning to increase as spring thaw advanced.

4.1 MOVEMENT MONITORING SYSTEMS

Monitoring systems installed on the slope consisted of movement monitoring prisms and surface extensometers. Prisms consisted of ground glass reflective prisms which provided effective coverage over the entire slope area (see Fig. 2). Prisms were replaced when lost and additional prisms placed in areas of high movements, as required.

Prism monitoring was conducted using a Wild DI 1600 EDM with a T2 theodolite. Frequency of prism monitoring was determined from the movement rates and mining activity at the base of the slope. Monitoring was conducted weekly when mining was not active in the pit. During periods of mining activity, monitoring frequency varied from once a week to twice per day depending on the monitored movement rates. In general, when movement rates were less than about 12mm/day (0.5 in/day), monitoring was conducted between two and five times per week. For movement rates between 12 and 50mm/day (0.5 to 2.0 in/day), prism monitoring was conducted daily. Movements in excess of 50mm/day generally required monitoring to be conducted twice daily.

In addition to prisms, surface wire extensometers were placed on the slope to monitor movements across the major cracks which developed. These extensometers provided a simple, rapid method to assess slope movements in critical areas near the slope crest. Surface extensometers were monitored daily during the bulk of the mining activity. One extensometer was fitted with an automatic trip wire and radio transmitter in the event that movement exceeded 100mm between readings. When movement rates exceeded 50mm/day, monitoring frequency was increased to every four to eight hours. Extensometer movements in excess of 100mm/day required monitoring every one to three hours.

In addition to the above, visual inspections were conducted on a regular, daily basis during mining activity. When movement rates exceeded 50mm/day, sentries were posted to observe the unstable area and provide visual warning to equipment in the pit bottom.

4.2 ASSESSMENT OF PRISM MONITORING DATA

Slope movements were assessed primarily by examination of prism monitoring records. Monitoring records consisting of surveyed co-ordinates and elevations were compiled using a spreadsheet on a personal computer. Data was

presented using wander plots and movement vs time graphs, as shown for typical prisms in Appendix B. The wander plots, movement vs time graphs and raw data printouts were used to determine trends and changes in the movement direction and/or movement rates for individual prisms. These results were related to mining activity and climatic changes by inspection of the mining plans and temperature and precipitation records.

The various pulses of total movement, movement direction, plunge, and movement rate are summarized in Table VII. The main pulses of movement are plotted as vectors showing magnitude of total movement and direction of total movement on plans of the open pit on Figs. 10 and 11. These pulses are also plotted as vectors showing the magnitude of total movement and apparent plunge in the plane of the section on the representative sections in Appendix A.

Examination of Table VII and the vector plots indicate that the movement directions of individual prisms have been relatively consistent for the duration of the records. However, the vector direction of movement, plunge and movement rates vary considerably for different prisms, depending on location on the slope as discussed in the following.

4.2.1 Prisms on East and South Walls

Prisms on the east and south walls are not involved in active instability. These prisms have indicated movement which appears to be related to natural long term slope relaxation in response to mining. Movement directions are generally normal to the slope. Movement rates for prisms 16, 18, 30, 31, 36 and 45 located in argillite in the east wall range from 0.03 to 0.3mm/day (0.001 to 0.01 in/day). These prisms were installed some time after the slope was exposed and hence any short term deformation experienced immediately after mining is not represented from these prisms. Prisms 3, 21, 27 and 28 were established in serpentinite, lower on the east wall. These prisms were installed

shortly after the slope had been exposed by mining but were subsequently lost due to rockfalls and snow. Initial movement rates for these prisms ranged from 0.6 to 9.7mm/day (0.02 to 0.38 in/day). However, the bulk of the long term movement of these prisms range from 0.5 to 2.5mm/day (0.02 to 0.10 in/day). Near horizontal movements were initially recorded in most cases indicating a squeezing, rebound and/or relaxation mechanism to the movement of these prisms. Long term movement rates of these prisms are expected to be comparable with other prisms outside the area of active instability provided that the slope remains stable.

4.2.2 Prisms in Main Area of Instability

Movement directions, plunges and movement rates of prisms in the area of active instability are strongly related to climate, assumed groundwater conditions, prism location and elevation on the slope.

Prism movements indicate four distinct areas of movement in the northeast wall. The main area of active instability is bounded by the North Fault, the Serpentinite Dyke and Fault A1 which defines the main area of instability (Figs. 10 and 11). This area appears to have been the initial area of active failure which developed after spring thaw in June 1988.

The area between Fault A1 and Fault A2 appears to have become involved in active failure after mid-April 1989, i.e. after spring thaw of 1989.

The area between Fault A2 and Fault A3 also appears to have become involved in active failure after mid-April 1989; however, movement rates in this area are considerably less than those experienced in the main area of active instability.

The fourth area of instability involves the area west of the North Fault, much of which is covered by waste rock.

Individual prisms in the area of active instability have markedly different direction and plunge of movement depending on location on the slope. All prisms west of the Serpentinite Dyke and above about the 6050 level have a vector direction of movement to the northwest at an oblique angle to the pit wall as shown in Figs. 10 and 11. Average plunge of these prisms varies from 40° to 50° (see Appendix A). These movement directions have remained consistent over the duration of the movement records.

Prisms below the 6060 level have vector directions of movement to the southwest out of the slope. Average plunge of the movement vector of these prisms varies from 14° to 35°. Prism 20, which is located lower on the slope, had a subhorizontal movement in the first few weeks after being installed. The plunge of movements of this prism have steepened as mining progressed and spring thaw began in 1989.

Movement rates of all prisms in the area of instability increased significantly after the onset of spring thaw between mid-April and early May 1989. Movement rates increased to rates in excess of 100mm/day in mid-summer before decreasing late in 1989. Movement rates again increased in late April and early May 1990 in response to spring thaw.

It is noteworthy that movement records for the initial phases of movement indicate that total movement and movement rates in the upper section of the slope (Prisms 11, 13 and 14) are 1.7 to 4.1 times as great as movement rates in the lower section of the slope (Prism 20). Prisms located in the waste dump west of the North Fault have indicated generally less consistent movement rates, most likely due to their location on broken waste.

4.3 ASSESSMENT OF FAILURE GEOMETRY

Results of geological mapping in the open pit and prism movement data were used to determine the failure geometry and failure mechanism. Figure 12 shows the specific geometry of the failure. Photos 8 to 13 illustrate salient features within the failure zone.

The initial failure zone is bounded on the east by the Serpentinite Dyke, on the west by the North Fault and on the south by Fault A1, as shown on Fig. 12. The failure has progressively expanded to the south to include an area of secondary failure bounded by Fault A2 and an area of tertiary failure bounded by Fault A3, as shown in Fig. 12. In addition, the waste dump and fractured serpentinite north of the North Fault has undergone considerable movement.

The locations and orientations of the Serpentinite Dyke, North Fault, Fault A1, Fault A2 and Fault A3 were determined from geological mapping, as shown in Fig. 2 and Photos 8 to 12. Field examination has also revealed the presence of several steeply dipping cracks, designated Cracks B, C, D and E as shown in Photo 13, an oblique photo taken from the south side of the failure. These cracks appear to have formed by failure of the rock mass along an irregular surface formed by the intersection of short discontinuous joints of the various joint sets mapped in the rock mass. These cracks appear to dip to the northeast at an estimated angle of 80° as shown in Fig. 12 and Photo 13.

The extent of these cracks is more clearly defined in the main failure zone between the North Fault and Fault A1. Hence, subsequent analyses of the failure geometry and failure mechanisms have been concentrated on the main (initial) failure zone to assess the specific conditions which led to failure.

4.3.1 Volume of Failure

Structural contours of the Serpentinite Dyke, North Fault, Fault A1, Fault A2 and Fault A3 were plotted on a plan to determine the geometry and volume of the failure, as shown in Fig. 12. The plan area of the failure bounded by these structures and the pit wall was determined for each level using a digital planimeter. The average area on each level and distance between each level were used to calculate the volume between each level. Total volumes and weights calculated in this manner are as follows:

Main (initial) failure zone	1.1×10^6 m^3	(3.2×10^6 tonnes)
Zone of secondary failure	1.6×10^6 m^3	(4.9×10^6 tonnes)
Zone of tertiary failure	3.1×10^6 m^3	(9.3×10^6 tonnes)
Zone west of North Fault	0.1×10^6 m^3	(0.4×10^6 tonnes)
Total volume of failure	5.9×10^6 m^3	(17.8×10^6 tonnes)

4.3.2 Failure Mechanism

The actual failure mechanism has been determined by a detailed assessment of field mapping data, photographs and prism monitoring records. Examination of the structural contour plans of the Serpentinite Dyke and Fault A1 indicate that the line of intersection of these structures has an orientation of 308/52 (Fig. 12). This orientation is consistent with the movement vectors of prisms in the upper part of the slope which have an average azimuth of 271° to 315° and an average plunge of 40° to 54°. The upper section of the slope is not buttressed by the pit wall, and hence it is free to move at an oblique angle to the slope.

Below about the 6060 level, there is substantial rock in the pit wall to the west of the North Fault. As a result, movement is out of the slope

within the large wedge shaped block bounded by the North Fault and Fault A1. As shown in Fig. 12, the line of intersection of the North Fault and Fault A1 plunge to the northeast (i.e. away from the slope) at about 25°. Although a kinematically possible sliding wedge does not occur, it appears that the stress on the rock mass as a result of the upper sliding block has led to the formation of a deep seated toppling mechanism involving shearing along cracks B, C, D and E which form the boundaries of large blocks as shown on Section A-A in Fig. 12. Formation of cracks B, C, D and E may also have been facilitated by the squeezing of serpentinite in the toe which created room for initial tensile failure and shearing along these cracks.

The progressively shallower plunge angles of the prism movements in the lower section of the active failure area indicate that a combination of sliding and toppling may be occurring in the lower blocks. Some plunges may be steeper than anticipated because the blocks are not deforming as rigid blocks and it is likely that internal crushing, shearing and squeezing is occurring at the corners of the blocks.

The consistent movement directions of individual prisms indicates that the postulated failure mechanism is continuing without significant changes. The increase in movement rate in response to temperature and precipitation indicates that the slope movements are extremely sensitive to the water pressures acting on the backs of the blocks. Lower movement rates were recorded after installation of the drainholes (November 1988) and during winter months (December to mid-April) due to the lack of groundwater recharge at that time.

Movement rates also slowed in late fall of 1989, probably due to the lower water table as well as the buttressing effect of debris in the lower part of the slope. The effects of slope deformation and ravelling of debris has been to reduce the slope angle to about 38° by mid-October

1989. Even at this relatively shallow slope angle, significant movement has been recorded on the remaining prisms and movement rates have increased during the spring thaw of 1990.

During spring thaw, recorded movement of surface extensometers indicates that the slope movements vary on an approximate time cycle. Slope movements appear to increase under the influence of high water pressure. Movement of the blocks results in drainage and associated depressurization of the slope, which reduces the movement rate until water pressures can again build up due to groundwater recharge. This results in a "rachet mechanism" of movement rates which vary from minimal movement to movement rates in excess of 100mm/day in a cycle of three to five days.

5. LIMIT EQUILIBRIUM BACK ANALYSIS

A three-dimensional limit equilibrium back analysis was conducted to assess the likely rock mass strength and groundwater conditions at failure for the graben toppling mechanism identified in Section 4.3. The back analysis was conducted for the main (initial) failure zone bounded by the Serpentinite Dyke, North Fault and Fault A1. The slope was divided into five blocks based on the locations of these structures and the locations of the cracks, as shown in Fig. 12. The upper block is considered as a truncated tetrahedral wedge, whereas the other blocks may be visualized as inverted triangular prisms as shown on Fig. 12. The volume and surface area of each block were calculated by extrapolating the lengths and areas between the various levels on the structural contour plans, as discussed above. The weights and surface areas of the individual blocks as calculated using this method are given in Fig. 12. It should be noted that different surface areas were used for the same plane, depending on whether it is considered as the front or back of the block. The difference in surface area is based on the fact that some shearing and crushing may be expected in the toe area of each block to accommodate the room required for toppling to occur.

A failure of this nature is very difficult to model because of the three-dimensional effects of the blocks which are essentially inverted triangular prisms. Calculation of the weights, water pressures and shearing resistance on the surfaces of each block is also difficult because of the irregular geometry.

A conventional factor of safety approach is not valid because the slope is failing by overturning and the slope condition is expected to change dramatically once the conditions of moment equilibrium are exceeded. Hence, the analyses have been conducted to assess the variation in strength and

groundwater conditions likely to be acting on the blocks at limiting equilibrium.

The analysis method presented by Goodman and Bray (1976) was used as a basis to conduct the three dimensional limit equilibrium analysis. Using this method, a free body diagram is prepared for each block and forces acting on the block are resolved normal and perpendicular to the planes. Resultant forces are transferred to succeedingly lower blocks and the resultant force on the toe block is calculated. The upper graben (Block 1) is considered to be a sliding block. Blocks 2, 3 and 4 are considered to be toppling blocks. Block 5 is checked for stability against both sliding and toppling.

In order to simplify the analysis, the forces on the sides of the blocks have not been considered in Blocks 1 to 4. Side forces on Block 5 have been approximated for the triangular area of Section A-A shown on Fig. 12. In addition, the base of Block 2 is assumed to form a point, thereby reducing the requirements for calculation of overturning forces due to the shear strength along Plane A*.

Analyses were conducted for a dry slope and three water levels in the slope, as shown in Fig. 12. The low water condition is expected to approximate fully drained conditions in the slope. The medium and high water conditions shown in Fig. 12 represent assumed water levels during winter and spring conditions, respectively.

Freebody diagrams and the equations of limiting equilibrium for each block are given in Appendix C. Analyses were conducted using a spreadsheet to calculate the resultant forces on each block using the equations of limiting equilibrium derived for each block in Appendix C. Resultant forces calculated for Block 1 were transferred to Block 2 and the calculations continued for each of Blocks 2 to 5. Limiting equilibrium conditions for Block 5 were assessed in terms of a zero unbalanced force for sliding or toppling.

The analyses were conducted assuming constant shear strength parameters on the Serpentinite Dyke (Plane A) and the base (i.e. line of intersection of the North Fault and Fault A1). The cohesion and friction angle of these discontinuities were assumed to be 70 kPa (10 psi) and 26.5°, respectively. The variation in shear strength along Planes B, C, D and E was evaluated by varying friction angle for seven cohesion values, namely 0, 69, 345, 690, 965, 1724, 2069 kPa (0, 10, 50, 100, 140, 250 and 300 psi). The friction angle which resulted in zero net unbalanced force on Block 5 (the toe block) for both sliding and toppling was determined for the various cohesions for each water condition.

Analysis results are plotted in terms of the friction angle required for each cohesion on cracks B, C, D and E for various water conditions for both sliding and toppling of the toe block. Results are shown in Figs. 13a and 13b. Based on rock mass strengths determined from the previous investigation at the site discussed in Section 2.6, a nominal rock mass cohesion of 700 kPa (14,400 psf or 100 psi) and a rock mass friction angle of 32° were determined to be appropriate for design. Results in Fig. 13 indicate that for a nominal cohesion of 700 kPa (14,400 psf or 100 psi), a friction angle of about 18° would be sufficient to control toppling for the high water condition, whereas a friction angle of about 44° would be required for limiting equilibrium against sliding of Block 5 for the high water condition. A friction angle of about 31° is required for limiting equilibrium against sliding for the intermediate water condition. The low water condition only requires a friction angle of 17° for limiting equilibrium against sliding for a rock mass cohesion of 690 kPa (100 psi).

These results indicate that the design rock mass cohesion of 690 kPa (100 psi) is valid and that slope stability is extremely sensitive to groundwater level and friction angle. The results indicate that the toe block is more likely to slide than topple, which is confirmed by subsequent numerical modelling

studies discussed in Section 6. The sensitivity to groundwater level is confirmed by the observed increase in movement rates during spring thaw and summer, and the rachet mechanism observed for the failure.

6. NUMERICAL MODELLING OF SLOPE FAILURE

A numerical modelling study has been conducted to assess the deformation behaviour of the deep seated graben toppling mechanism observed at Cassiar. Numerical modelling was conducted using the UDEC program marketed by the Itasca Consulting Group (1989). The background and results of the modelling study are described in the following.

6.1 DESCRIPTION OF THE PROGRAM

The Cassiar failure was modelled using the two-dimensional program known as the universal distinct element code (UDEC). This complex program applies an explicit, time domain finite difference method of solution to model large displacements and rotations of block systems. The rock mass is represented by an assemblage (blocks) that are separated by discontinuities with prescribed behaviour, allowing the blocks to disconnect and interact with each other (Pritchard, 1989). The distinct element method is similar to the finite-element method in that the problem domain (in this case, a rock mass) is discretized into a system of solid elements. The principal difference of the two methods is that the distinct element method permits the geometry of the elements to be defined by the spacing and orientation of the rock mass discontinuities (ITASCA, 1989. This allows a jointed rock mass to be represented by an assemblage of distinct blocks that interact along their boundaries. In addition to the discontinuum modelling of the block interactions, each block can be allowed to deform as a continuum modelled by finite differences. It is designed to model large deformations and displacements, and non-linear changes in rock and joint strengths with more realistic results than the finite element and the limit equilibrium methods.

Deformation is determined by using an explicit solution procedure time stepping algorithm. In UDEC, the quantities calculated in each step are

incremental displacements or strains. The time increment is based on the mass and material stiffness of blocks or zones. The increment is small enough that displacements cannot travel from one block to an adjacent block in one time step, but will travel between the continuum finite difference zones within the block.

Using the force-displacement laws, the program calculates the net force on each block resulting from the interaction with itself and the surrounding blocks. Accelerations and displacements are calculated from a motion law using the above unbalanced forces and the time cycle increment. By examining the time histories of displacements, velocities or any other chosen parameter, the user can determine when the problem stabilizes or fails.

6.2 DESCRIPTION OF THE MODEL

The UDEC program only permits a two-dimensional analysis to be conducted. In terms of the slope failure at Cassiar, the representative section through the failure, as shown in Fig. 12, was used to set up the model and run the analysis. Figure 14 (Fig. D1) shows the model used for analysis.

The Cassiar model was initially prepared as a solid material with two lithologies. A fully deformable mesh was constructed for the model, as shown in Fig. D2. The model was allowed to consolidate under internal and boundary in-situ stress conditions for 1000 computer time cycles. The pit was then excavated in a series of eight lifts to the June 1988 slope profile, as shown on Section D-D in Appendix A. Each excavation was followed by a 1000 cycle time interval to allow rock mass deformation due to unbalanced stresses. This model state was saved as the "root-model" for all subsequent simulations.

The material properties used to develop the root model are summarized on Table VIII. The properties of the fault trace intersection and the contact between the argillite and serpentinite were unchanged for all simulations.

Discontinuities mapped as cracks in the active failure zone (i.e. cracks B, C, D, E and F) were assigned very high strengths during excavation to inhibit movement prior to exposure of the assumed slide toe between August 1988 and April 1989. These pre-failure strengths are given in brackets on Table VIII. The lower strength values were reassigned to these discontinuities after the toe was excavated. The time cycle after the excavation is 9000 counts.

After the initial excavation model was set up, a number of cases were run with different water table elevations and values for discontinuity cohesion and friction angle. Individual models were assessed by evaluating the plots showing the vector direction of movement and velocity at nodes on the mesh for each model run. In addition, time history plots were prepared for seven representative monitoring points on the model, as shown in Fig. 14. These points were selected to correspond with selected prisms located on the slope (Fig. 10, Fig. 11 and Appendix A). By comparing the deformation of the model with the observed slope deformation, an assessment of slope behaviour and material properties could be prepared. Yield plots showing the plastic state at each node in the fully deformable mesh were also examined for two specific cases.

Analysis results are summarized in Table IX and Appendix D, and discussed below.

6.3 ANALYSIS RESULTS FOR MODEL WITHOUT CRACKS

One model was run with two materials without the six cracks observed during the field mapping. Maximum displacements indicated for this model are of the order of 0.39m, as shown in Fig. D3a. Figure D3a indicates considerable shearing on the discontinuities and internal deformation of the rock mass, with the result that only small movements are indicated in the lower portion of the slope. The yield plot in Fig. D3b indicates that most areas of the slope have yielded with a concentration of yielding along the major

discontinuities. It is interesting to note that tensile failure is indicated to occur at one point on the slope surface near the argillite/serpentinite contact (Fig. D3b). This yield plot indicates that generation of tensile stress may have occurred on the slope surface as a result of the deformation of the weaker serpentinite rock mass. This fact could explain the development of cracks observed in the open pit. Further assessment of slope deformation properties would be required to verify this hypothesis.

6.4 ASSESSMENT OF MODEL WITH ONE ROCK TYPE WITH CRACKS

Four models were conducted assuming only one rock type, i.e. argillite, with the presence of the cracks observed on the slope. In this case, the model was prepared and consolidated assuming a high strength on the discontinuities. Discontinuity strength was reduced and the model allowed to come to equilibrium for two different values of friction on the discontinuities, and for an intermediate and a high water table. Analysis results included in Figs. D4 to D7 indicate that velocity vectors are relatively small and movements are inconsistent for the case of the high water table and high friction angle, as shown in Fig. D4. A reduction in the friction angle along a discontinuity of 2° indicates significantly greater velocity vectors and magnitudes and direction of movement consistent with the documented deformation of the slope (Fig. D5). An intermediate water table indicates inconsistent movement for both higher and lower friction angles indicating the slope to be stable (Figs. D6 and D7). The model shown in Fig. D5 supports the graben toppling mechanism presented in Section 4.3. The relative movements in the crest and toe of the slope are consistent with those observed in the field. However, the ratio of movements at the crest to the movement in the toe is higher than that documented from the prism records and the predicted plunge of monitoring points is generally less than that documented.

These discrepancies could be explained due to the absence of deformable serpentinite in the lower portion of the active failure area in the model. In

addition, the absence of the hanging wall contact between argillite and serpentinite precludes shearing along that discontinuity.

6.5 ASSESSMENT OF MODEL WITH TWO ROCK TYPES WITH CRACKS

The analyses described above clearly indicate the strong influence of rock type, discontinuities, water pressure and strength on the model behaviour. In order to assess the combined effect of these parameters, a series of models was conducted using two rock types with cracks, as shown in Fig. 14. The material properties and groundwater conditions were varied to compare the model behaviour for the various cases to the documented slope behaviour.

The model was first conducted with a high water table and friction angles of 30° and 24° for the cracks in argillite and serpentinite, respectively. Cohesions of 700 kPa and 200 kPa were used for cracks in argillite and serpentinite, respectively. These high cohesions were used to provide initial cohesions similar to the estimated rock mass strengths derived from laboratory testing and core logging, as summarized in Section 2.6.4. Figure D8a indicates the response of the model to excavating the remainder of the slope and allowing deformation to occur in both the rock mass as well as along all major discontinuities and cracks. The model summarized in Fig. D8a provides a very realistic assessment of slope deformation behaviour in terms of the magnitude, plunge and ratio of movement between the crest and toe of the slope. This case also supports shear on the various planes and development of the graben toppling mechanism with sliding in the toe area.

In order to better appreciate slope behaviour and sensitivity to strength, the rock mass cohesion and joint shear stiffness on the cracks for the case shown in Fig. D8a was successively reduced by 20%, 10%, 5%, 5% and 5% to simulate strain softening of the discontinuity strength. Approximately 1500 time steps were run after each reduction in cohesion to assess the slope behaviour. Results are shown in Figs. D8b to D8f and summarized in Table IX.

It is interesting to note that even with strain softening, the deformation behaviour of the slope remains consistent for all strain softening cycles. The bulk of the model displacement occurs in the first two cycles of softening with progressively smaller amounts of displacement occurring at succeeding intervals.

The model shown in Figs. D8a to D8f were also conducted for a cohesion of 70 kPa (instead of 200 kPa) for the cracks in serpentinite. Results of these analyses appear to be identical to those for a cohesion of 200 kPa. These results may be explained by the deep seated nature of the failure in which cohesion has less influence than friction on the planes due to the extremely high normal loads and shear stresses on the individual planes.

6.6 VARIATION OF GROUNDWATER CONDITIONS FOR THE SLOPE MODEL

The model assessed in Section 6.5 (Figs. D8a to D8f) was reassessed for intermediate and low groundwater conditions, as shown in Figs. D9 and D10. These analyses include the total behaviour after full strain softening of 20%, 10%, 5%, 5% and 5% as discussed above. Results shown in Figs. D9 and D10 and summarized in Table IX clearly indicate that magnitudes and velocity of movement decrease dramatically as the water table is lowered. Results shown in Figs. D9 and D10 are generally less consistent indicating that the slope may be stable for these two water conditions.

6.7 VARIATION OF DISCONTINUITY STRENGTH FOR HIGH GROUNDWATER CONDITIONS

The model was further assessed for high groundwater conditions for an increased joint friction of 6° (Fig. D11) and a decreased joint friction angle of 2° (Fig. D12). Results indicate that while the deformation behaviour of the model for these cases is similar to the previous model, the magnitude of movements and velocities vary significantly with the friction angle.

6.8 COMPARISON OF PREDICTED DISPLACEMENT FOR THE VARIOUS MODELS AND DOCUMENTED DISPLACEMENT OF THE SLOPE

One limitation of the UDEC model is that it predicts the displacement and velocities in terms of computer time and not real time. Furthermore, because of the nature of the failure, the slope conditions are expected to change dramatically after the onset of failure. Hence, the main value of the model is to obtain an appreciation of the failure mechanism, sense of movement and relative sensitivity to the various material properties and groundwater pressures. At Cassiar, the detailed monitoring data from the prisms in the failure area have been used to compare the actual slope deformation and those predicted by the various models. Actual documented displacements are given on the plans in Figs. 10 and 11 and on the sections in Appendix A.

In order to compare the observed movements to the predicted movements, the initial failure movements are most important. The information in Table VII was used to assess the movement rates of prisms which correspond to the monitoring points in the model in the initial phases of movement. The movement rates in the first few weeks of failure were compared with the predicted deformation of the model. Results are summarized on the bottom of Table IX.

These results clearly show that the sense and mechanism of deformation predicted by the model is similar to that documented from the prisms. The documented deformation most closely resembles the deformation shown in Fig. D8a which represents a high water condition with discontinuity friction angles of 30° in argillite and 24° in serpentinite. The results of the numerical model, limit equilibrium model and observed failure mechanisms are consistent. It is clear that the observed variation in movement rates on the actual slope confirms the sensitivity to groundwater level indicated by the model. The model is generally sensitive to friction angle of the discontinuities and relatively insensitive to changes in the discontinuity cohesion.

6.9 SUMMARY OF NUMERICAL MODELLING

The results of the UDEC modelling have confirmed the failure mechanisms and sense of failure predicted from the documented displacements and limit equilibrium analysis methods. Although the model only provides a two-dimensional assessment, the rock mass strength and deformation properties and the discontinuity strength properties are consistent with material properties determined previously from rock mechanics testing and back analysis at the mine.

The slope is highly sensitive to groundwater levels and friction angle of discontinuities. It appears to be less sensitive to the cohesion of the discontinuities. If this is the case, the model would predict that deep seated graben toppling failures of this nature could develop in any rock mass, where there is sufficient deformation to develop tensile stresses on the slope surface. Development of tensile stresses would then lead to the propagation of cracks such as those observed which have subsequently become involved in deep seated toppling failure.

Additional numerical modelling assessments to more rationally assess elastic properties and sensitivity to other material properties are recommended. This is beyond the scope and budget of the current project but would provide a useful contribution to the field. Three-dimensional modelling would also be extremely useful for this slope.

7. CONCLUSIONS

The results of this study have demonstrated that failure of high rock slopes is possible even when structural discontinuities are at a favourable orientation for stability, and the slopes are designed so that kinematically possible failures are controlled. In the case of Cassiar Mine, three major discontinuties namely the Serpentinite Dyke, the North Fault and Fault A1 have played a contributory role in the failure although the location and geometry of the excavated slope are such that kinematically possible failures involving sliding on these discontinuties did not occur. Even though a relatively shallow slope of 40 to 42° was excavated in the serpentinite rocks, there has been sufficient squeezing deformation of the serpentinite to enable development of the large graben toppling failure documented. The squeezing phenomena has created sufficient room to generate tensile stresses on the slope face which have led to formation of large blocks by a combination of shear and tensile failure of the fractured rock mass. These large blocks have failed by a combination of sliding in the toe, toppling in the middle section of the slope and sliding of an upper graben block. The failure is extremely sensitive to changes in the friction angle and is exacerbated by high groundwater pressures. The fact that movement rates fluctuate in response to climate conditions indicate that the slope is very close to limiting equilibrium and that small changes in the groundwater level are sufficient to cause changes in the movement rate.

This project has illustrated the importance of assessing the rock mass deformability as well as structural geology and strength when designing high rock slopes. It is clear that the failure documented at Cassiar could not have developed without the presence of weak deformable rock in the toe. The numerical modelling study provides an insight into the deformation mechanisms of the slope and the importance of understanding the deformation properties of the rock mass. Results from numerical modelling indicate the sensitivity of

the deformation to the rock mass parameters selected. It is important to note that these studies can only give an indication of the type and sense of movements. The structural analyses and limit equilibrium analyses provide a good appreciation of the slope behaviour and, when combined with the numerical modelling, provide an accurate picture of the slope deformation processes at Cassiar.

The facility with which a failure such as that documented at Cassiar could be predicted is very difficult to determine. The presence of soft deformable rock in any slope should be a warning that such a failure could develop. However, accurate prediction of such failures requires a complete understanding of all the material properties, structural geology and groundwater conditions. Design constraints and requirements are even more difficult to predict. Numerical modelling may be used as a tool to provide an indication of slope behaviour; however, actual slope performance can only be determined by field documentation. In this regard, the combination of structural analyses, conventional stability analyses and numerical modelling are all components of a rational design for an open pit slope. The design of any slope must be evaluated in light of the state of the art in understanding of material properties and deformation behaviour.

Even though displacement in excess of 30 metres and movement rates in excess of 125mm/day (5 in/day) have been documented at Cassiar, by understanding the failure mechanisms and installing the appropriate monitoring system, it has been possible to complete the slope and recover all the mineable ore in the open pit under controlled conditions.

8. REFERENCES

Call Nicolas Inc., 1981. "Slope Design Study for the Cassiar Open Pit". Report to Cassiar Mine, April. Three Volume Set.

Coates, D.F. and Sage, R., 1974. "Supplement for Rotational Shear Analysis". Design Chapter. Pit Slope Manual, CANMET Pit Slope Project 1872/77 Ottawa.

Goodman, R.E. and Bray J.W., 1976. "Toppling of Rock Slopes in Rock Engineering for Foundations and Slopes". Proceeding ASCE Specialty Conference. Boulder, Colorado, August 1975. Vol. II, pp. 201-234.

Gabrielse, H., 1963. "McDame Map Area British Columbia". Geological Survey of Canada Memoir 319. Department of Energy, Mines and Resources, Ottawa.

Herget, G., 1977. "Pit Slope Manual Chapter 2 - Structural Geology". Energy, Mines and Resources Canada, CANMET Report 76-44. October 123p.

Hoek, E. and Brown, E.T., 1980. "Underground Excavations in Rock". IMM London 527p.

Houlding, S.W., Slezak, G. and Spiers, C, 1982. "GEOSLP: Computer Program for Analysis of Circular and Irregular Failure Surfaces". Copyright Geomin Computer Services Corp., West Vancouver, B.C.

Itasca Consulting Group, 1989. Universal Distinct Element Code: UDEC Program and Manual Version ICG 1.5 - UDEC Minneapolis, Minnesota.

Martin, D.C., 1986. Geotechnical Data Collection, Geological Association of Canada Short Course No. 10, October. 543p.

Martin, D.C. and Carew, T.J., 1986. "Application of a Rock Buttress for design of Slopes at Cassiar Mine". Vol. 79, No. 896, pp. 60-66, December.

Martin, D.C., Hawley, P.M. and Holmes, A.T., 1984. "Slope Stability Analysis and Design of the Open Pit Slopes". Unpublished Geotechnical Report to Cassiar Mining Division, February. 87p.

Nelson, J., Bradford, J., MacLean M., and Maddison, L., 1989. "Geology and Metallogeny of the Cassiar and McDame Map Areas NTS 104P/5, 104 P/3". B.C. Ministry of Energy Mines and Petroleum Resources, Geological Survey Branch Open File 1989-9, 8 Sheets.

O'Hanley, D.S., 1990. "Structural Geology of the Mount McDame Area, North Central British Columbia (104/P)". British Columbia Ministry of Energy Mines and Petroleum Resources, Geological Survey Branch, Geological Field Work 1989. Paper 1990-1, pp. 223-228.

Piteau, D.R., Stewart, A.F., Martin, D.C. and Trenholme, B.S., 1985. "A Combined Limit Equilibrium and Statistical Approach for Designing Rock Slopes". ASCE Spring Meeting, July 1985.

Piteau, D.R. and Stewart, C.D., 1977. "Slope Stability Analysis and Design Based on Probability Techniques at Cassiar Mine". CIM Bulletin, March. 12p.

Piteau Gadsby Macleod, 1975 "Slope Stability Analysis and Design of the Hanging Wall Slope". Geotechnical report to Cassiar Mine, November 29, 1975. 96p.

Plumb, W.N., 1968. "Geology of the Cassiar Asbestos Deposit". Unpublished Report, June. 8p.

Pritchard, M.A., 1989. "Numerical Modelling of Large Scale Toppling". M.A.Sc Thesis, University of British Columbia, September. 171p.

JOB NUMBER

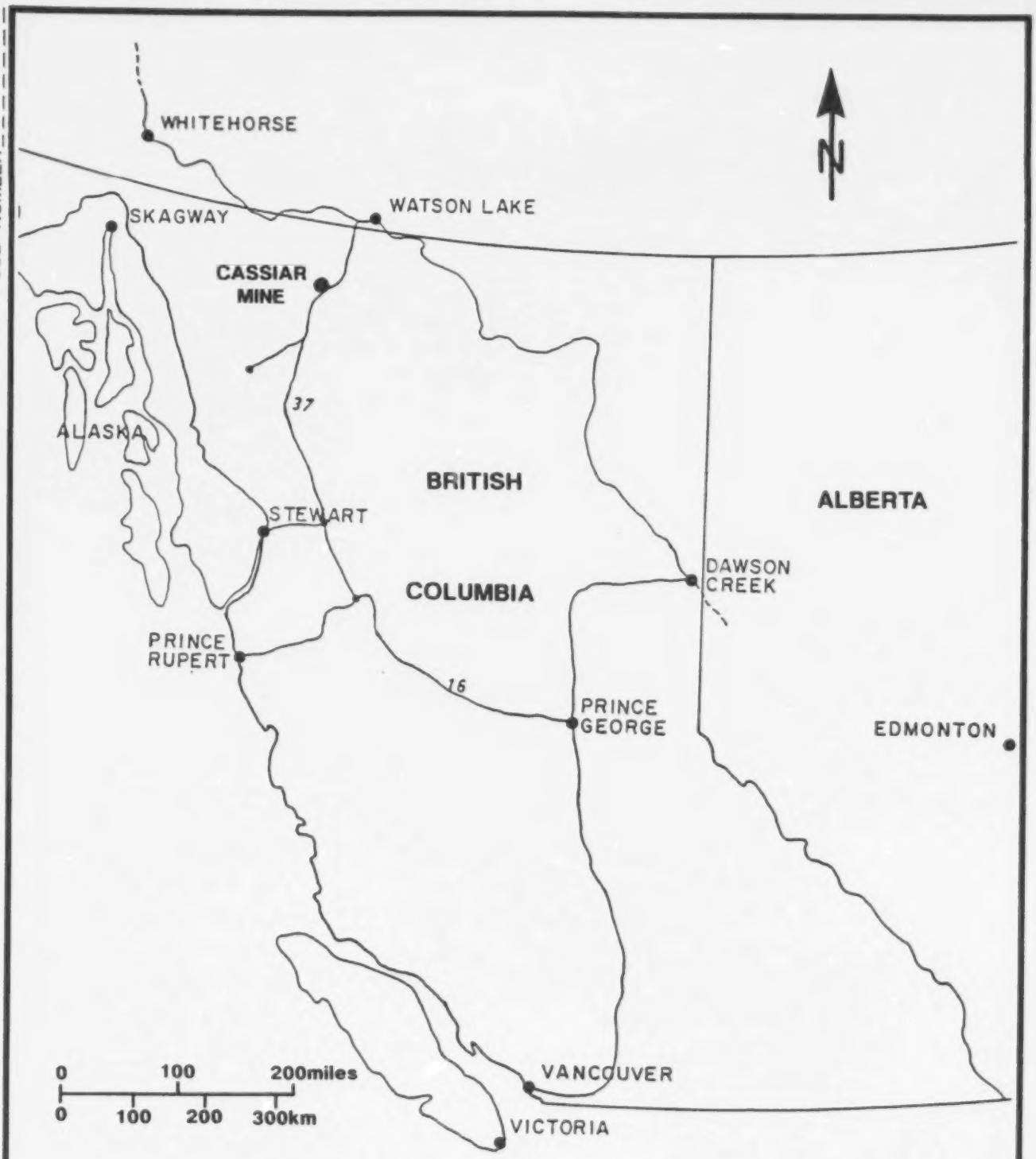

FIG. 1

CANMET/SUPPLY AND SERVICES CANADA
CASSIAR OPEN PIT
SLOPE DEFORMATION STUDY

PITEAU ASSOCIATES
GEOTECHNICAL CONSULTANTS
VANCOUVER CALGARY

LOCATION MAP

BY	DATE
DCM	7/4/90
APPROVED	DWG:
DCM	718G-1

SYLVESTER GROUP ROCKS

McDAME INTRUSION NORTH OF NORTH FAULT

JOINTS

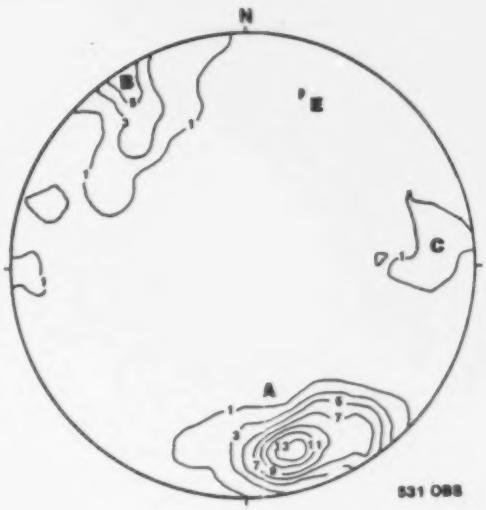

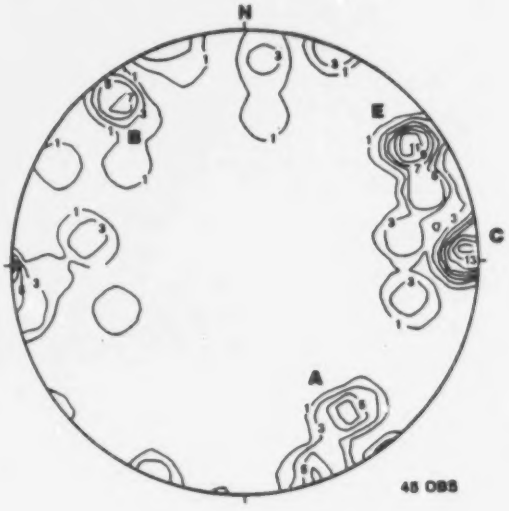

SHEARS and FAULTS

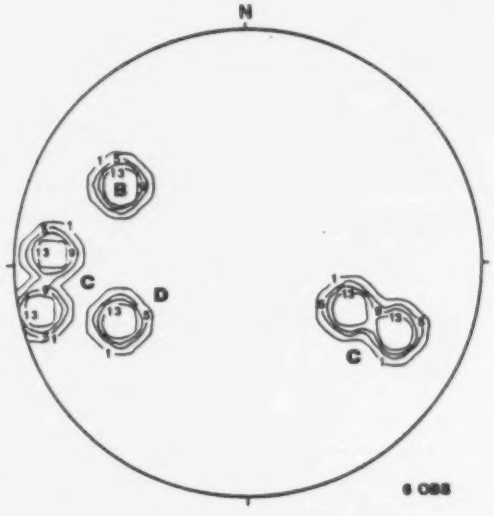

BEDDING

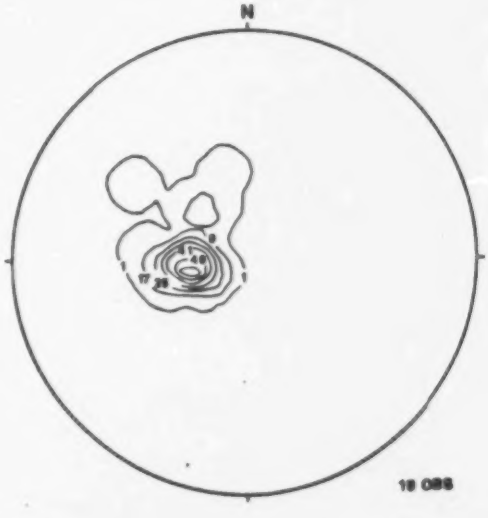

1. Contours are the percen
from a grid count on the

2. Average orientations of
from the peak of the co

CANMET
CASSIAR
SLOPE D

LOWER
DISCONT
OPEN PI

ER GROUP ROCKS

McDAME INTRUSION
NORTH OF NORTH FAULT

McDAME INTRUSION
SOUTH OF NORTH FAULT

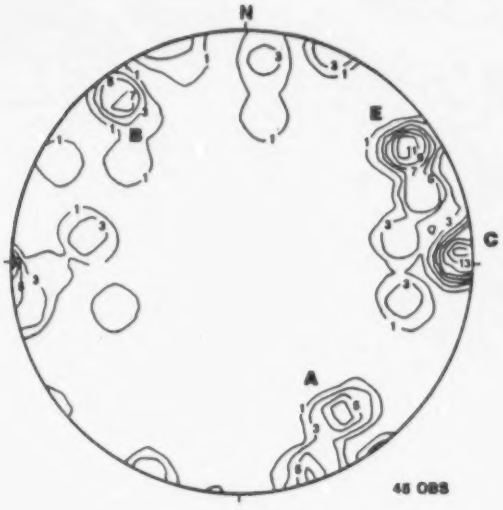

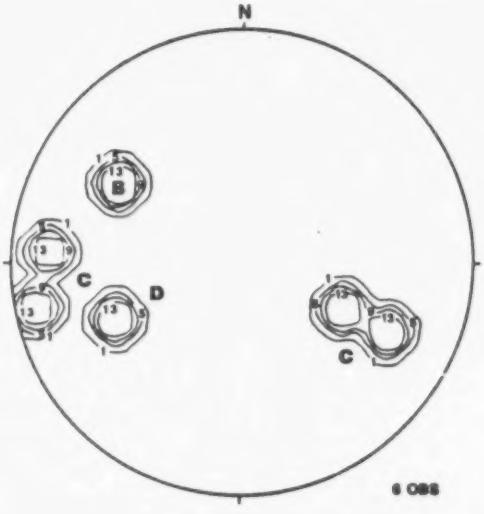

NOTES

1. Contours are the percent of the population in a one percent area as determined from a grid count on the equal area net.

2. Average orientations of discontinuity populations as determined from the peak of the contour populations are summarized in Table I

FIG. 3

CANMET/SUPPLY AND SERVICES CANADA CASSIAR OPEN PIT SLOPE DEFORMATION STUDY	PITEAU ASSOCIATES GEOTECHNICAL CONSULTANTS VANCOUVER CALGARY	
LOWER HEMISPHERE EQUAL AREA PROJECTIONS OF DISCONTINUITY POPULATIONS ON EAST WALL OF THE OPEN PIT	BY: JDT	DATE: MAY 90
	CHKD:	APPD:

JOB NUMBER 83-582

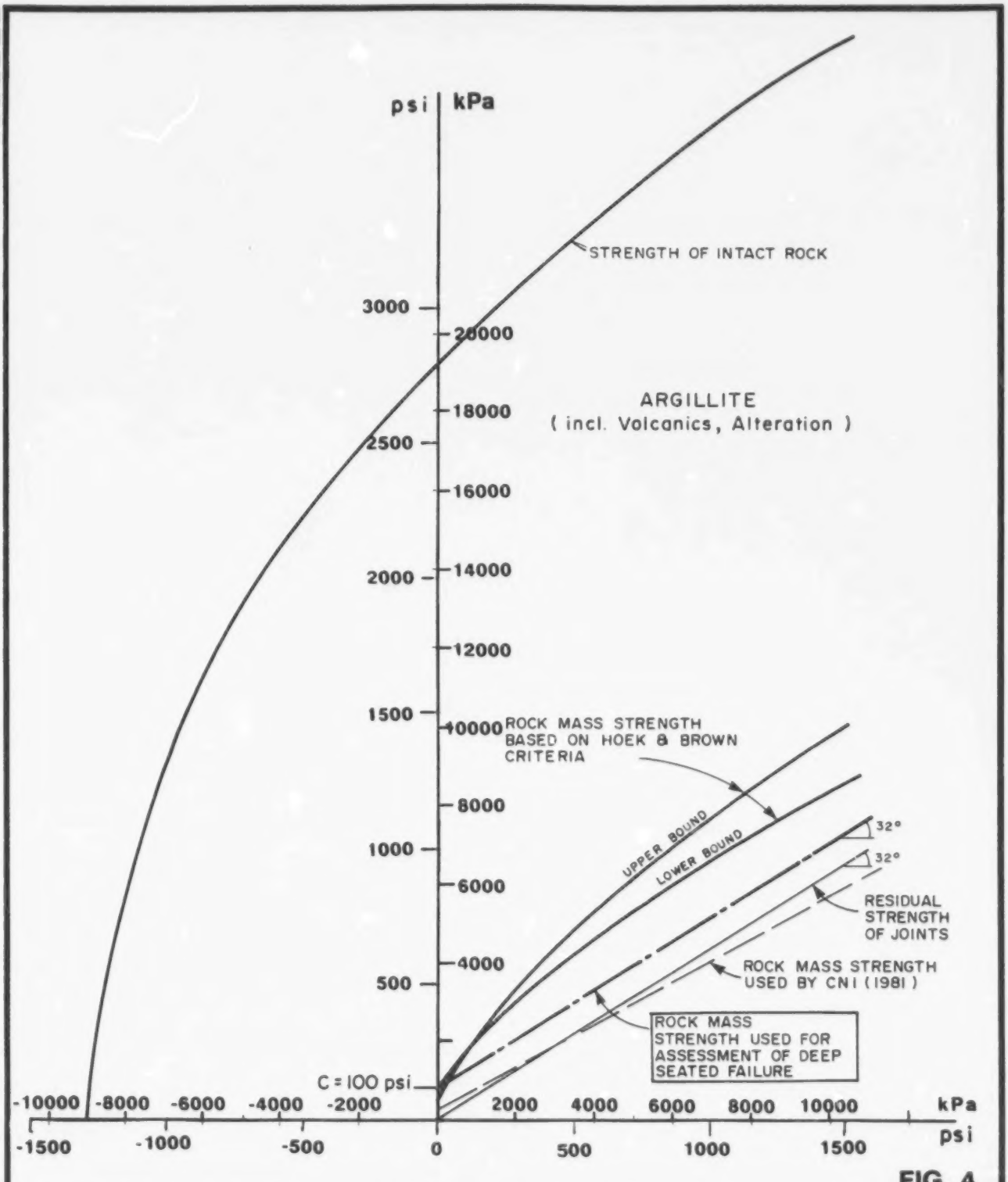

FIG. 4

CANMET/SUPPLY AND SERVICES CANADA CASSIAR OPEN PIT SLOPE DEFORMATION STUDY	PITEAU & ASSOCIATES GEOTECHNICAL CONSULTANTS VANCOUVER CALGARY
ESTIMATED STRENGTH OF INTACT ROCK DISCONTINUITIES AND ROCK MASS STRENGTH FOR ARGILLITE, VOLCANICS AND ALTERATION ON THE HANGING WALL	BY MH DATE MAY 90 APPROVED: DCM

JOB NUMBER 83-542

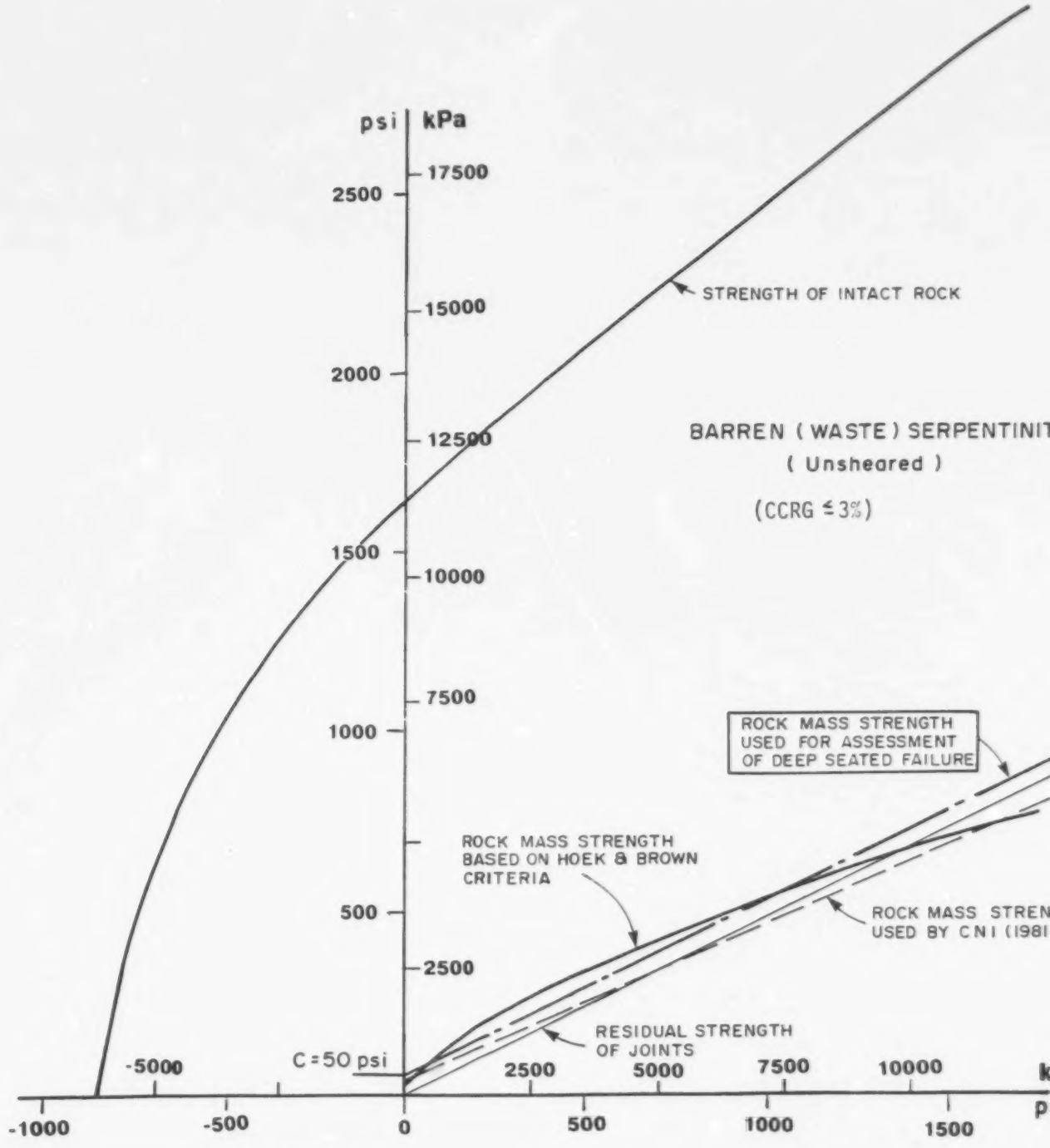

(a) BARREN (WASTE) SERPENTINITE

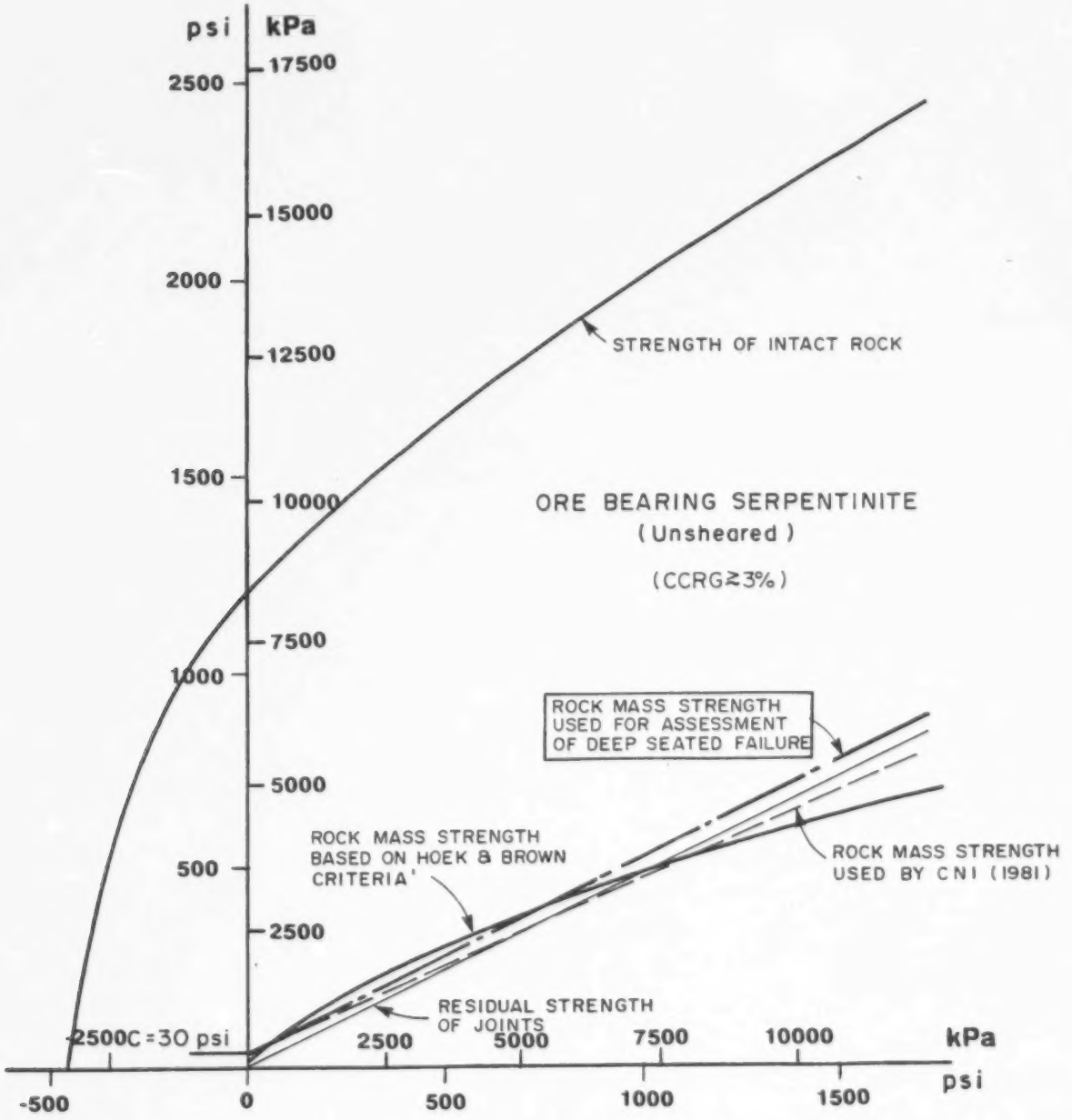

(b) ORE BEARING SERPENTINITE

FIG. 5

CANMET/SUPPLY AND SERVICES CANADA **CASSIAR OPEN PIT** **SLOPE DEFORMATION STUDY**	**PITEAU & ASSOCIATES** GEOTECHNICAL CONSULTANTS VANCOUVER CALGARY	
ESTIMATED STRENGTH OF INTACT ROCK, DISCONTINUITIES AND ROCK MASS STRENGTH FOR SERPENTINITE WASTE AND ORE	BY: **MH**	DATE: **MAY 90**
	APPROVED: DCA	

JOB NUMBER

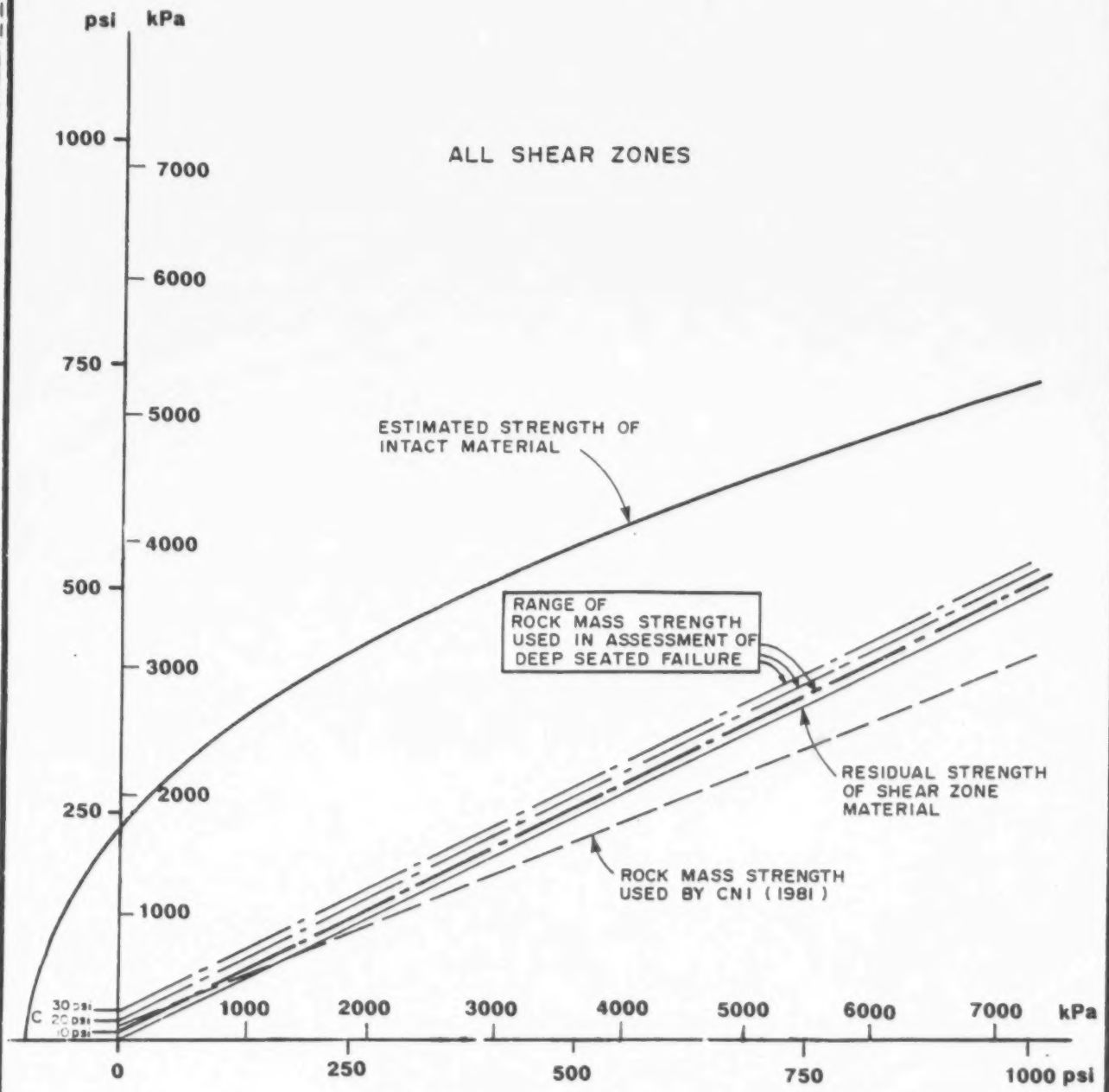

NOTE: STRENGTHS ARE BASED ON TESTING OF MATERIALS FROM SHEAR ZONES IN SERPENTINITE ONLY

FIG. 6

CANMET/SUPPLY AND SERVICES CANADA **CASSIAR OPEN PIT** **SLOPE DEFORMATION STUDY**	**PITEAU & ASSOCIATES** GEOTECHNICAL CONSULTANTS VANCOUVER CALGARY	
ESTIMATED STRENGTH OF INTACT MATERIAL, DISCONTINUITIES AND ROCK MASS STRENGTH FOR SHEAR ZONES	BY: MH	DATE: MAY 90
	APPROVED: DCM	

JOB NUMBER

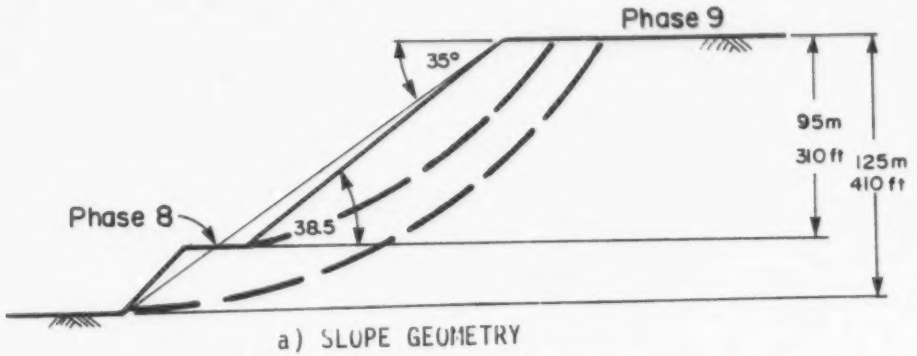

a) SLOPE GEOMETRY

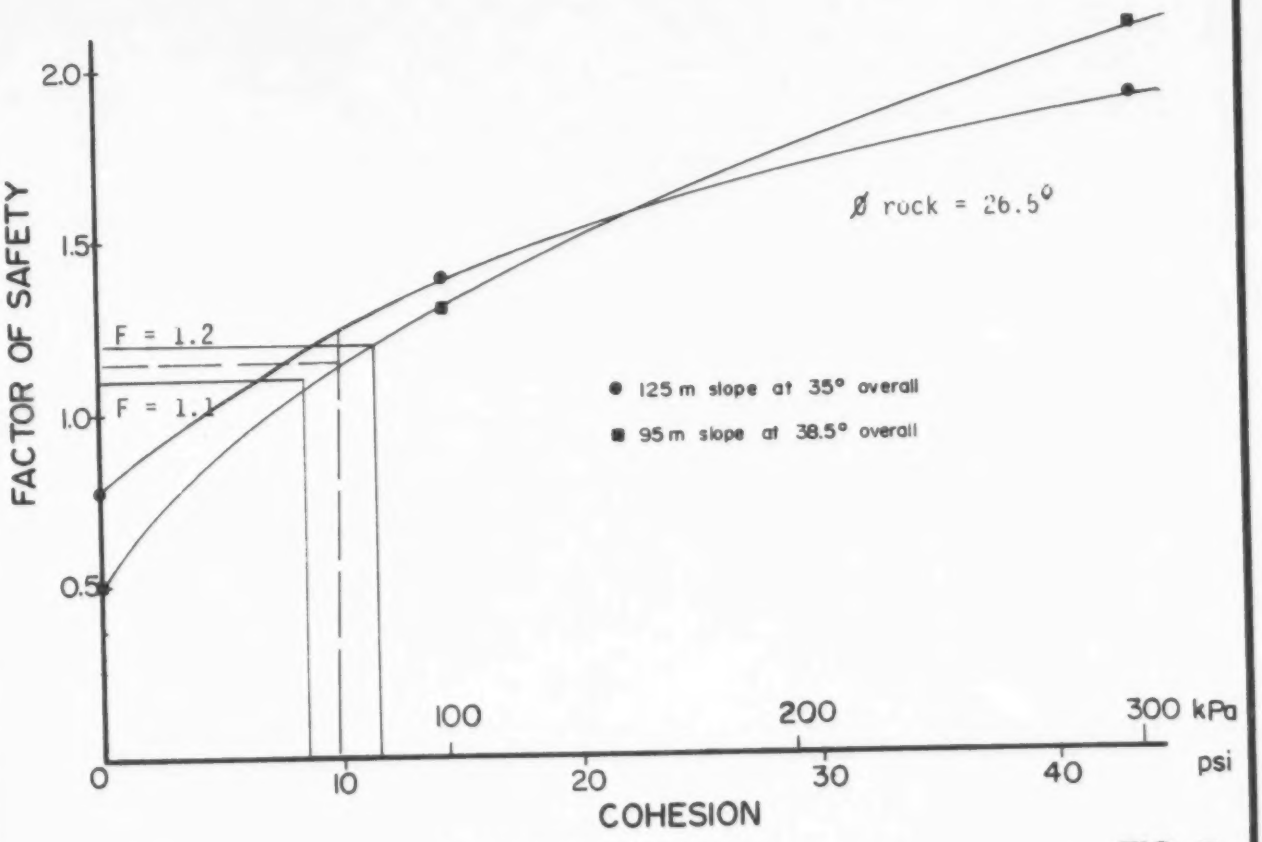

b) ANALYSIS RESULTS

FIG. 7

CANMET/SUPPLY AND SERVICES CANADA
CASSIAR OPEN PIT
SLOPE DEFORMATION STUDY

PITEAU & ASSOCIATES
GEOTECHNICAL CONSULTANTS
VANCOUVER CALGARY

BACK ANALYSIS RESULTS FOR SLOPES IN SHEARED SERPENTINITE

BY:	DATE:
DCM	JUN 90
APPROVED: DCM	DWG:

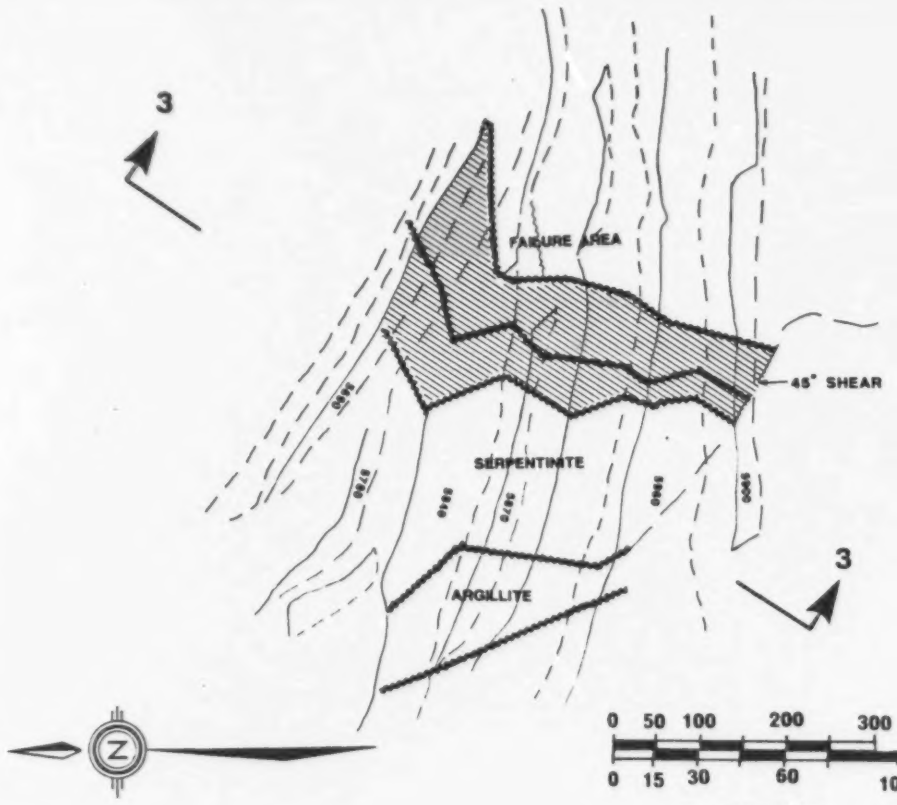

SCALE

PLAN

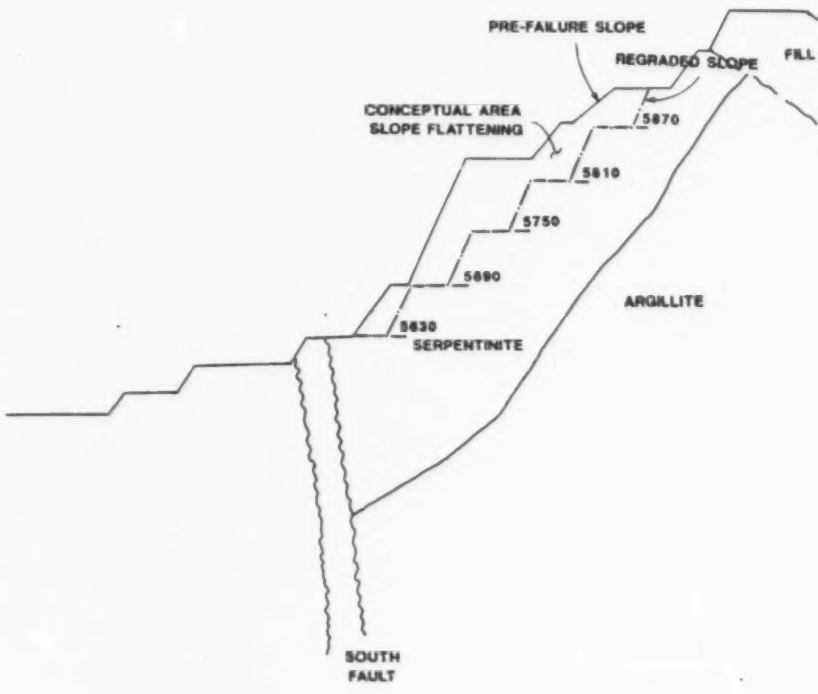

SECTION 3-3

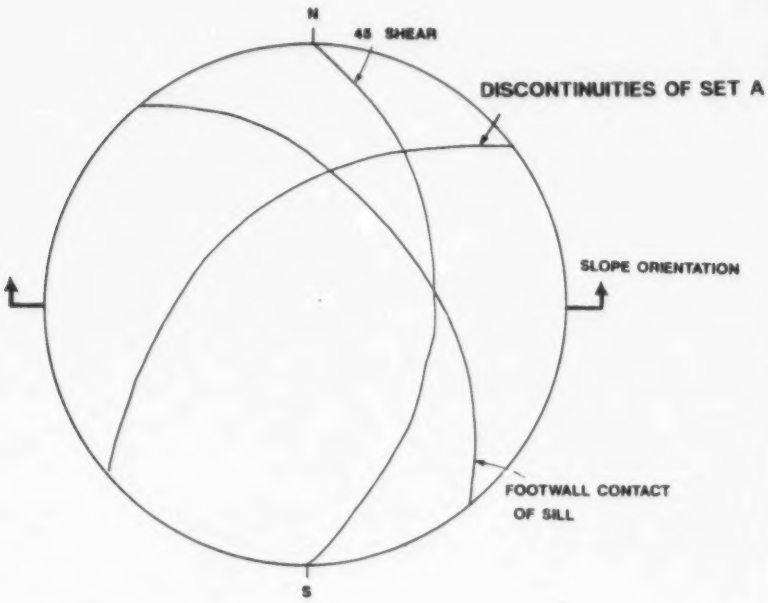

LOWER HEMISPHERE PROJECTION
OF DISCONTINUITIES IN FAILURE ZONE

eet

metres

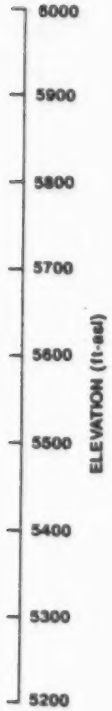

FIG. 8

CANMET/SUPPLY AND SERVICES CANADA CASSIAR OPEN PIT SLOPE DEFORMATION STUDY	PITEAU & ASSOCIATES GEOTECHNICAL CONSULTANTS VANCOUVER CALGARY

SOUTH WALL FAILURE MAY, 1988

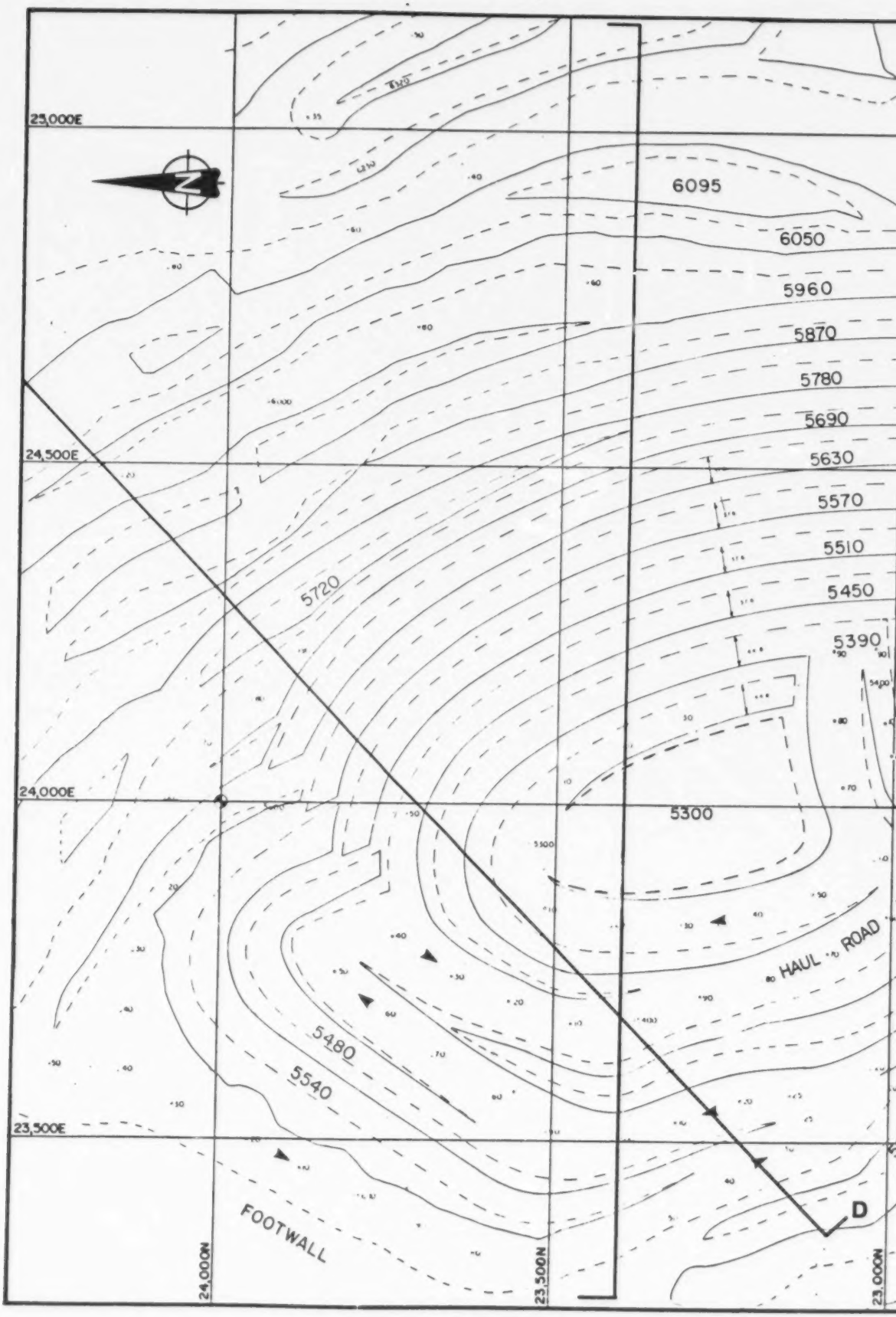
23,000E
24,500E
24,000E
23,500E
N
6095
6050
5960
5870
5780
5690
5630
5570
5510
5450
5390
5720
5300
5480
5540
HAUL ROAD
FOOTWALL
D
24,000N
23,500N
23,000N

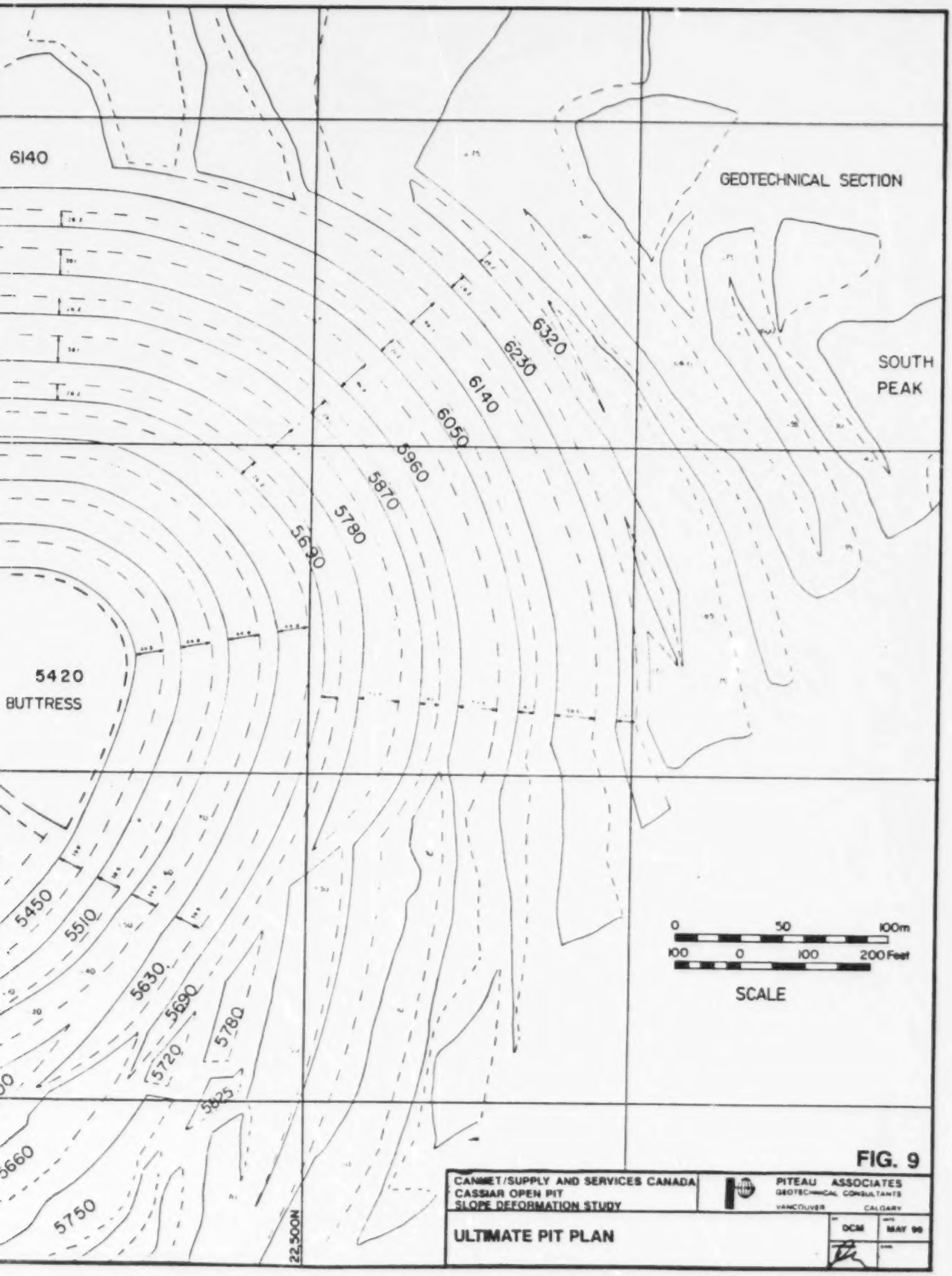

FIG. 9

CANMET/SUPPLY AND SERVICES CANADA
CASSIAR OPEN PIT
SLOPE DEFORMATION STUDY

PITEAU ASSOCIATES
GEOTECHNICAL CONSULTANTS
VANCOUVER CALGARY

ULTIMATE PIT PLAN

DCM MAY 90

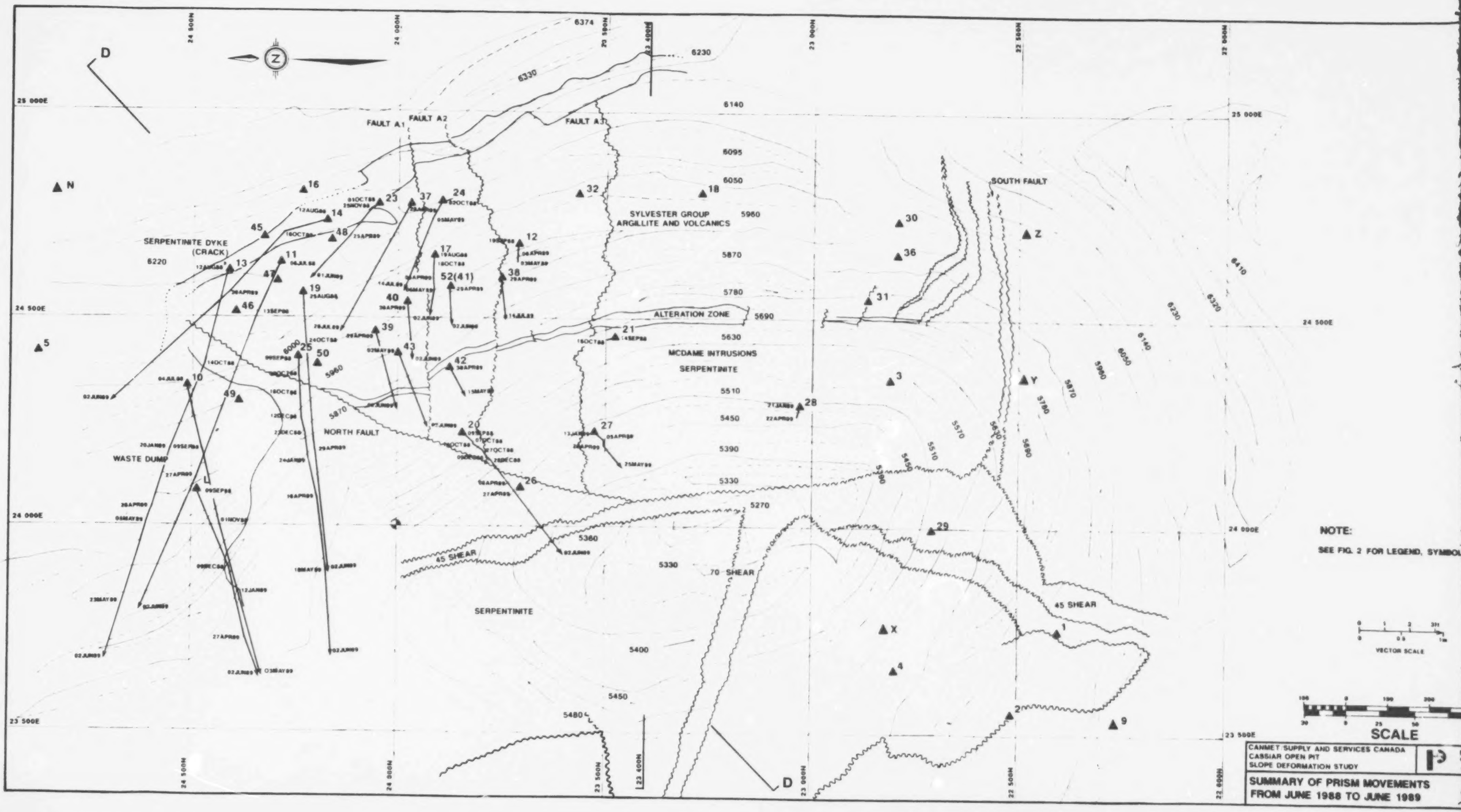

NOTE:

SEE FIG. 2 FOR LEGEND, SYMBOL

VECTOR SCALE

SCALE

CANMET SUPPLY AND SERVICES CANADA
CASSIAR OPEN PIT
SLOPE DEFORMATION STUDY

SUMMARY OF PRISM MOVEMENTS FROM JUNE 1988 TO JUNE 1989

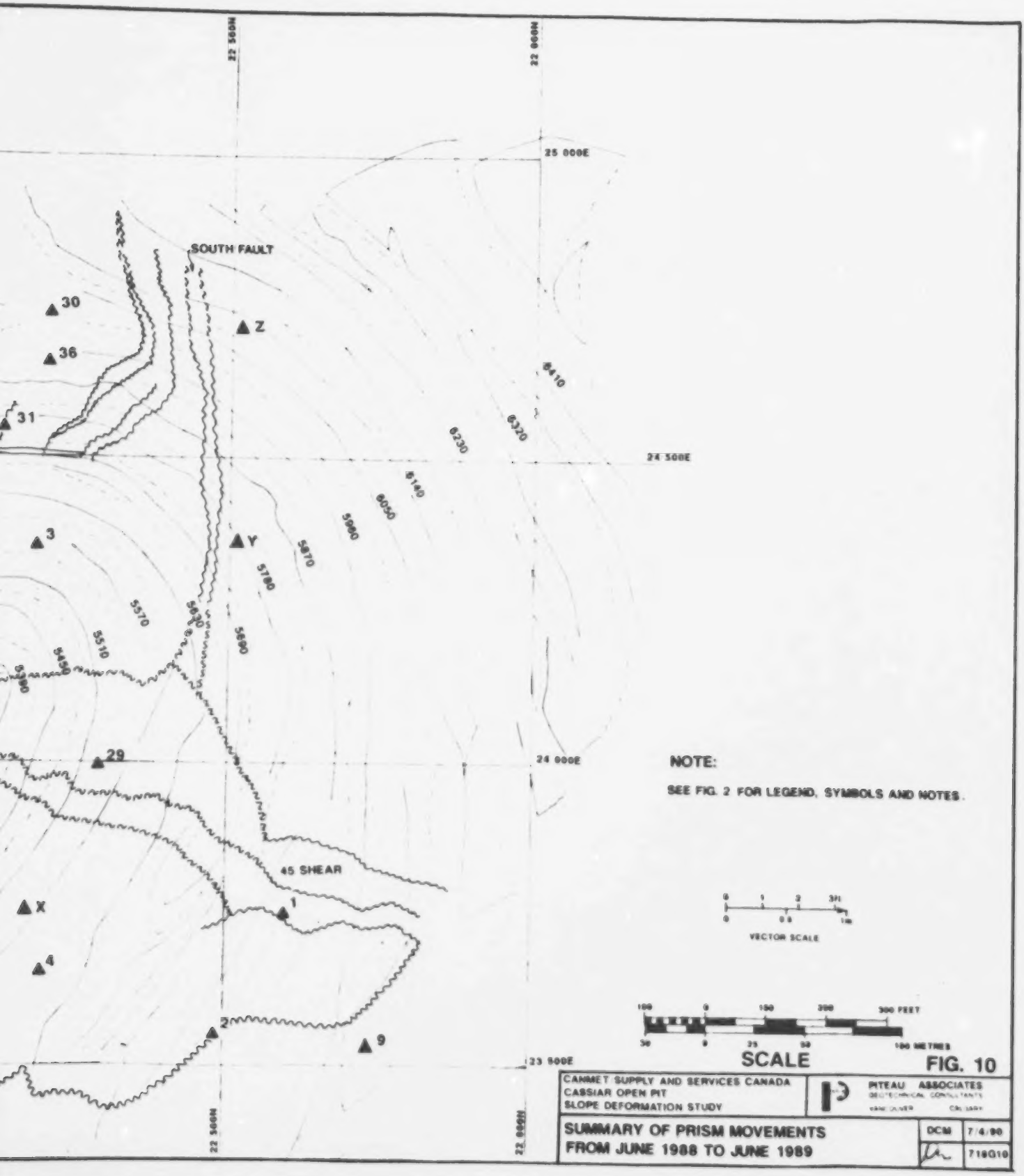

NOTE:

SEE FIG. 2 FOR LEGEND, SYMBOLS AND NOTES.

VECTOR SCALE

SCALE

FIG. 10

CANMET SUPPLY AND SERVICES CANADA CASSIAR OPEN PIT SLOPE DEFORMATION STUDY	PITEAU ASSOCIATES GEOTECHNICAL CONSULTANTS VANCOUVER CALGARY	
SUMMARY OF PRISM MOVEMENTS FROM JUNE 1988 TO JUNE 1989	DCM	7/4/90
		719Q10

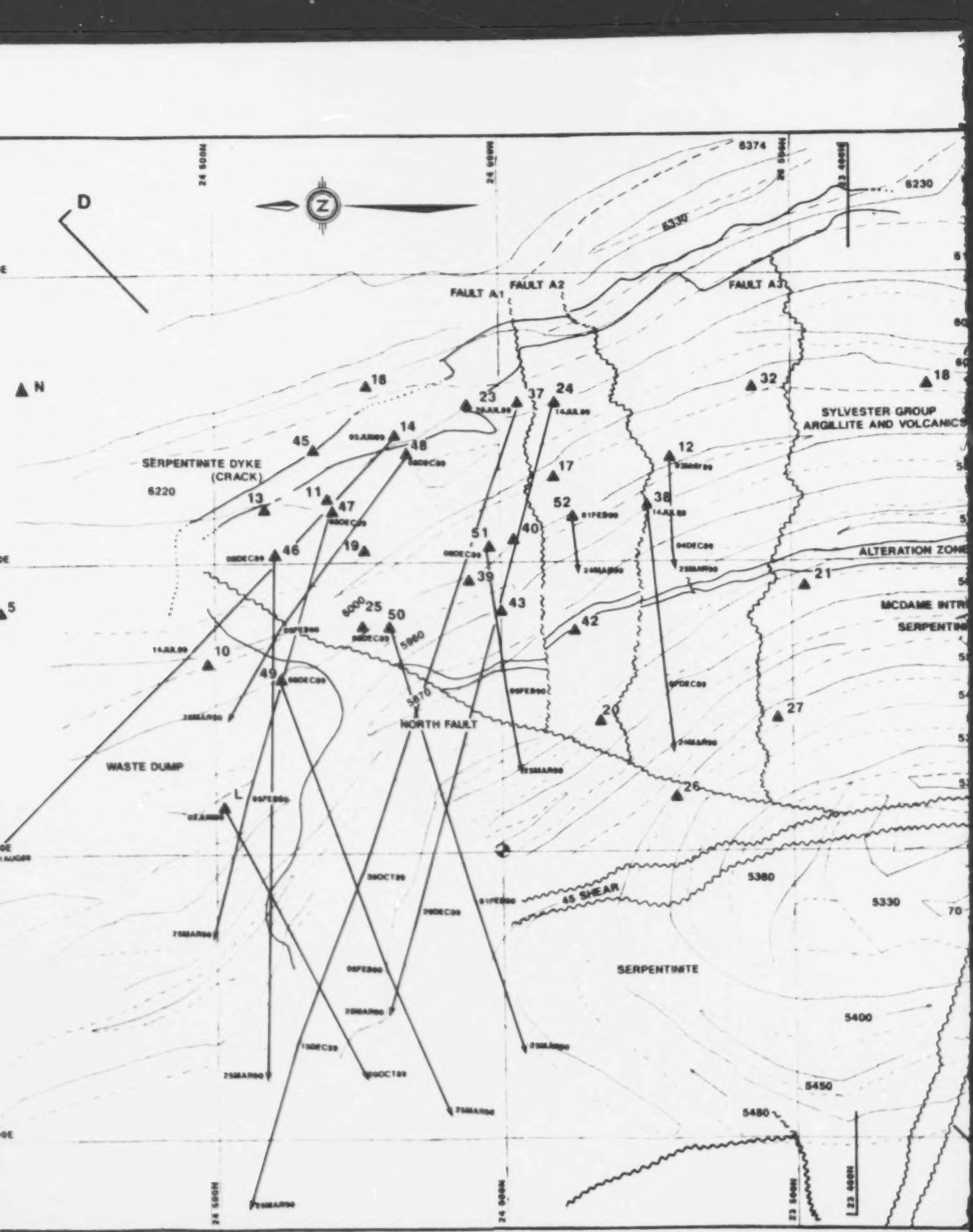
D
N
FAULT A1
FAULT A2
FAULT A3
SERPENTINITE DYKE
(CRACK)
6220
SYLVESTER GROUP
ARGILLITE AND VOLCANICS
ALTERATION ZONE
NORTH FAULT
WASTE DUMP
45 SHEAR
SERPENTINITE
8374
8230
6330
5380
5330
5400
5450
5480
5870
5960
6000

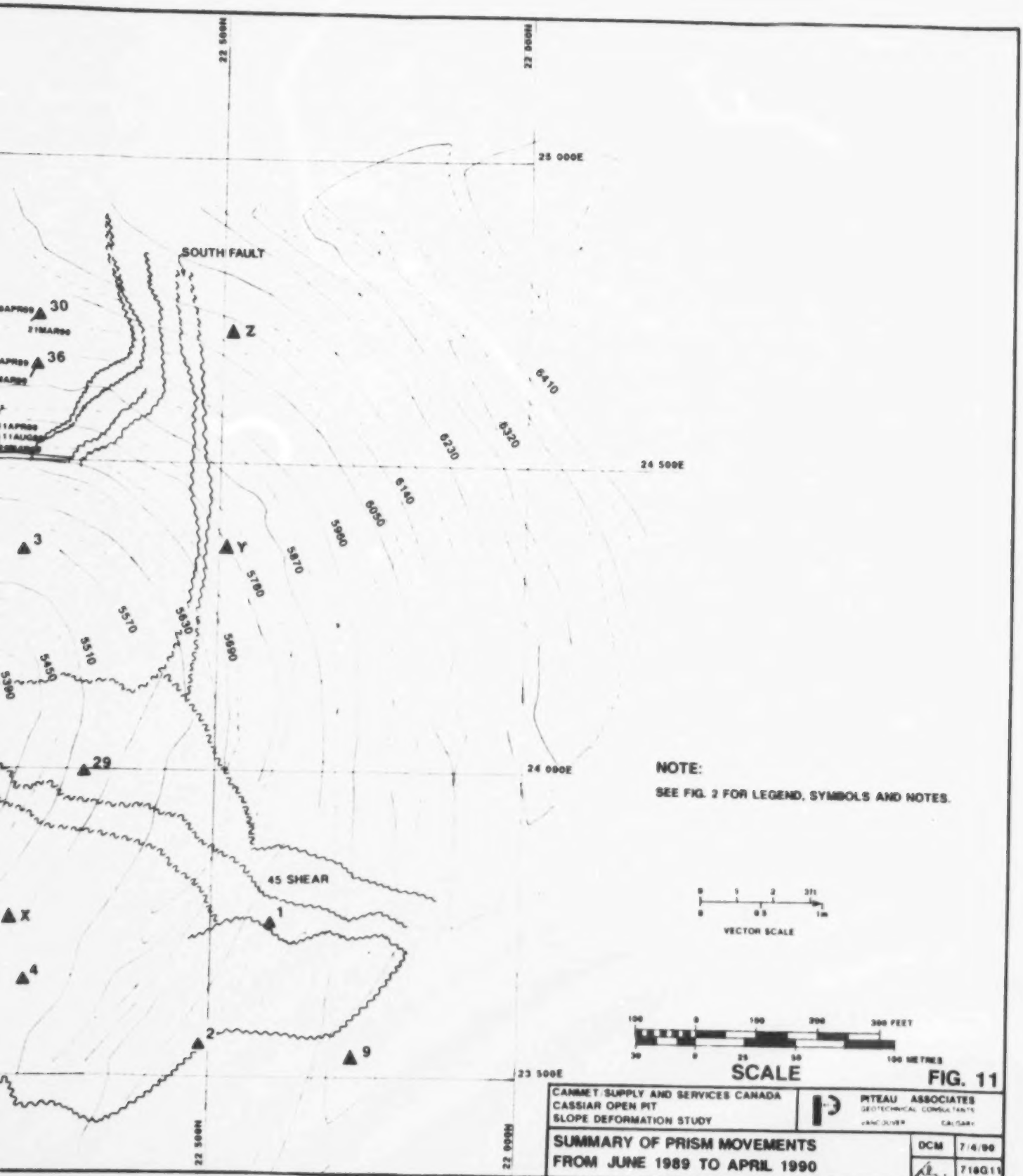
22 500N
22 000N
23 500E
24 000E
24 500E
25 000E
SOUTH FAULT
45 SHEAR
30
36
Z
Y
X
1
2
3
4
9
29
6410
6320
6230
6140
6050
5960
5870
5780
5690
5630
5570
5510
5450
5390
NOTE:
SEE FIG. 2 FOR LEGEND, SYMBOLS AND NOTES.
VECTOR SCALE
SCALE
FIG. 11
CANMET SUPPLY AND SERVICES CANADA
CASSIAR OPEN PIT
SLOPE DEFORMATION STUDY
PITEAU ASSOCIATES
GEOTECHNICAL CONSULTANTS
VANCOUVER CALGARY
SUMMARY OF PRISM MOVEMENTS
FROM JUNE 1989 TO APRIL 1990
DCM
7/4/90
718G11

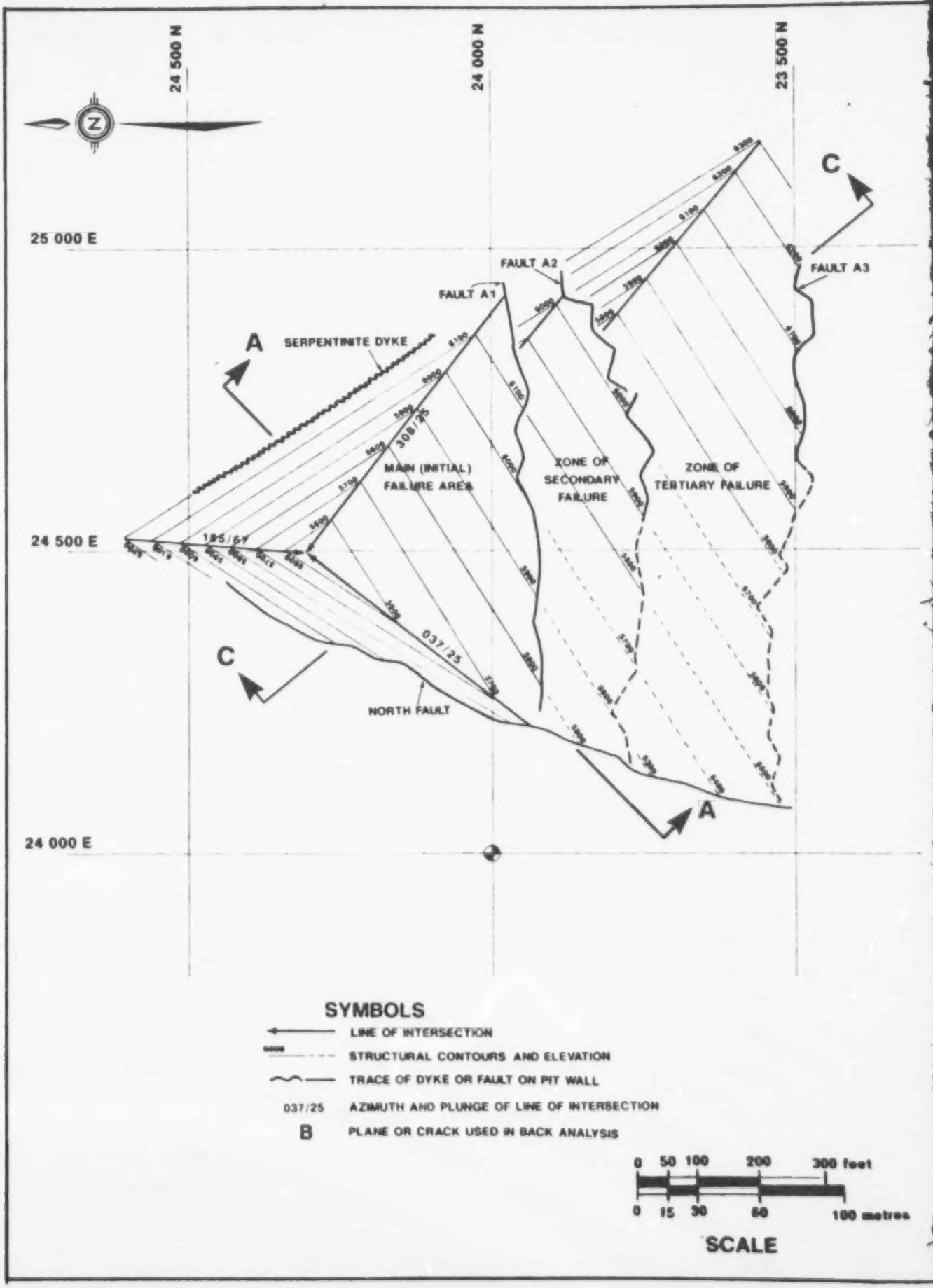

SYMBOLS

- LINE OF INTERSECTION
- STRUCTURAL CONTOURS AND ELEVATION
- TRACE OF DYKE OR FAULT ON PIT WALL
- 037/25 — AZIMUTH AND PLUNGE OF LINE OF INTERSECTION
- B — PLANE OR CRACK USED IN BACK ANALYSIS

0 50 100 200 300 feet

0 15 30 60 100 metres

SCALE

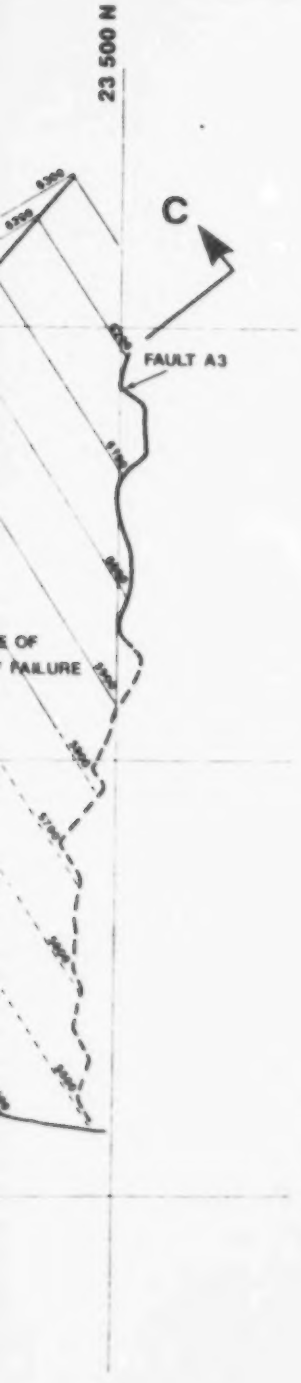

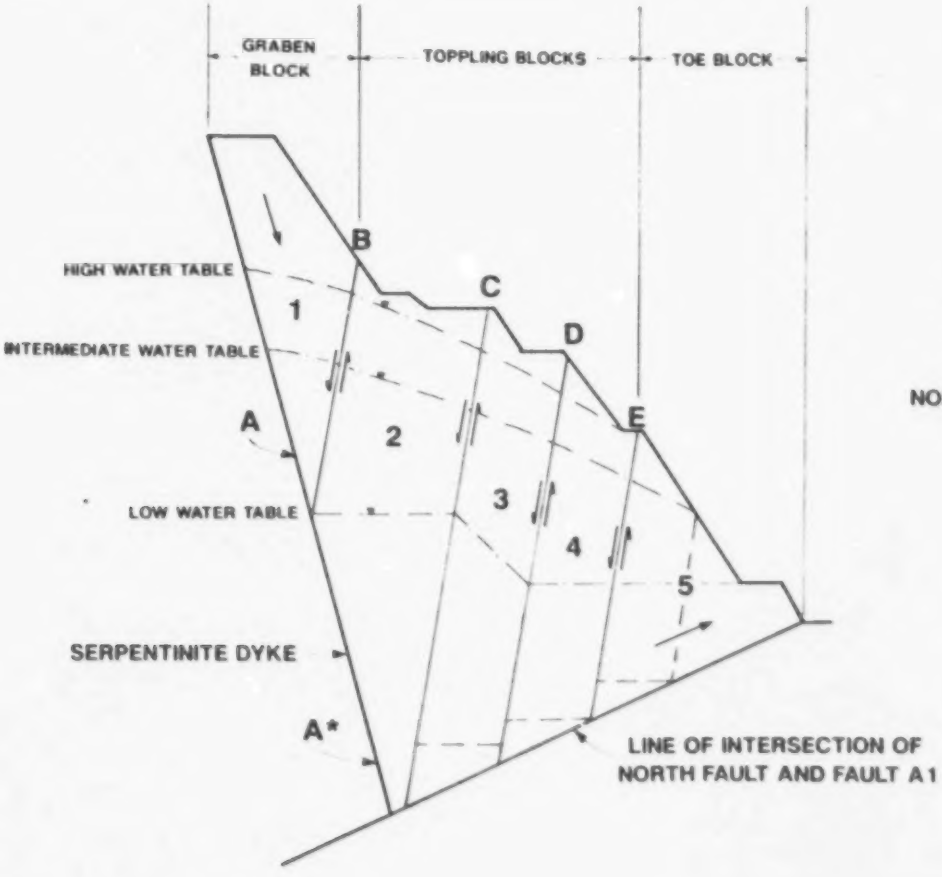

NOR

SECTION A-A

GEOMETRY OF MAIN (INITIAL) FAILURE

BLOCK	VOLUME (ft^3)	WEIGHT (lb)	SURFACE AREA (ft^2)	
			back of block	front of block
1	8.71×10^6	1.14×10^9	2.05×10^5	9.20×10^4
2	1.70×10^7	2.89×10^9	upper: 9.20×10^4 lower: 4.20×10^4	1.02×10^5
3	8.41×10^6	1.09×10^9	9.82×10^4	6.28×10^4
4	4.24×10^6	7.21×10^8	6.20×10^4	2.20×10^4
5	7.53×10^5	1.28×10^8	2.13×10^4	—
TOTAL	3.51×10^7	5.97×10^9	—	—

200 300 feet
60 100 metres
CALE

AL SECTIONS

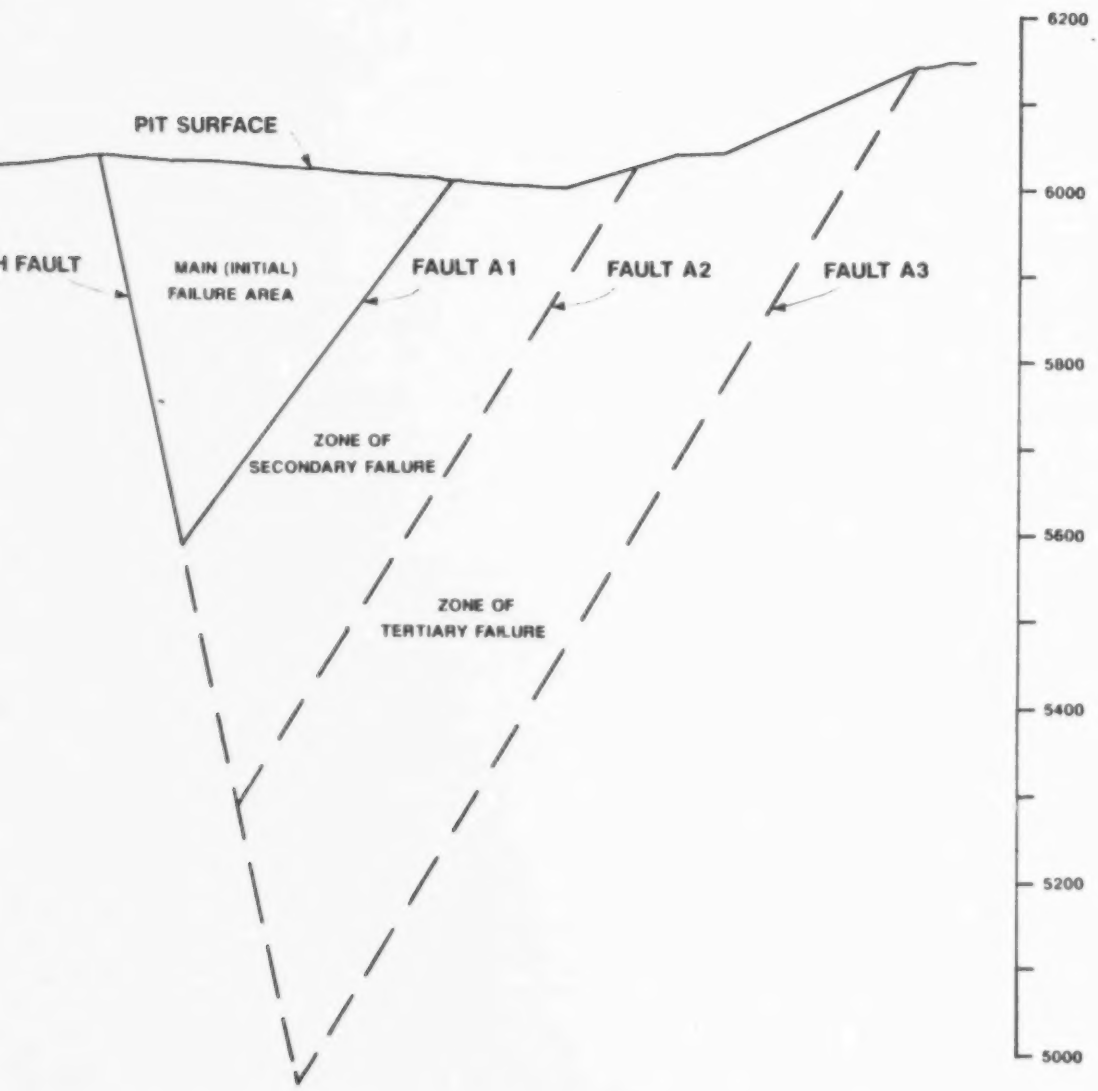

FIG. 12

SECTION C-C

CANMET/SUPPLY AND SERVICES CANADA
CASSIAR OPEN PIT
SLOPE DEFORMATION STUDY

PITEAU ASSOCIATES
GEOTECHNICAL CONSULTANTS
VANCOUVER CALGARY

FAILURE GEOMETRY AND FAILURE MECHANISM

HNICAL SECTIONS

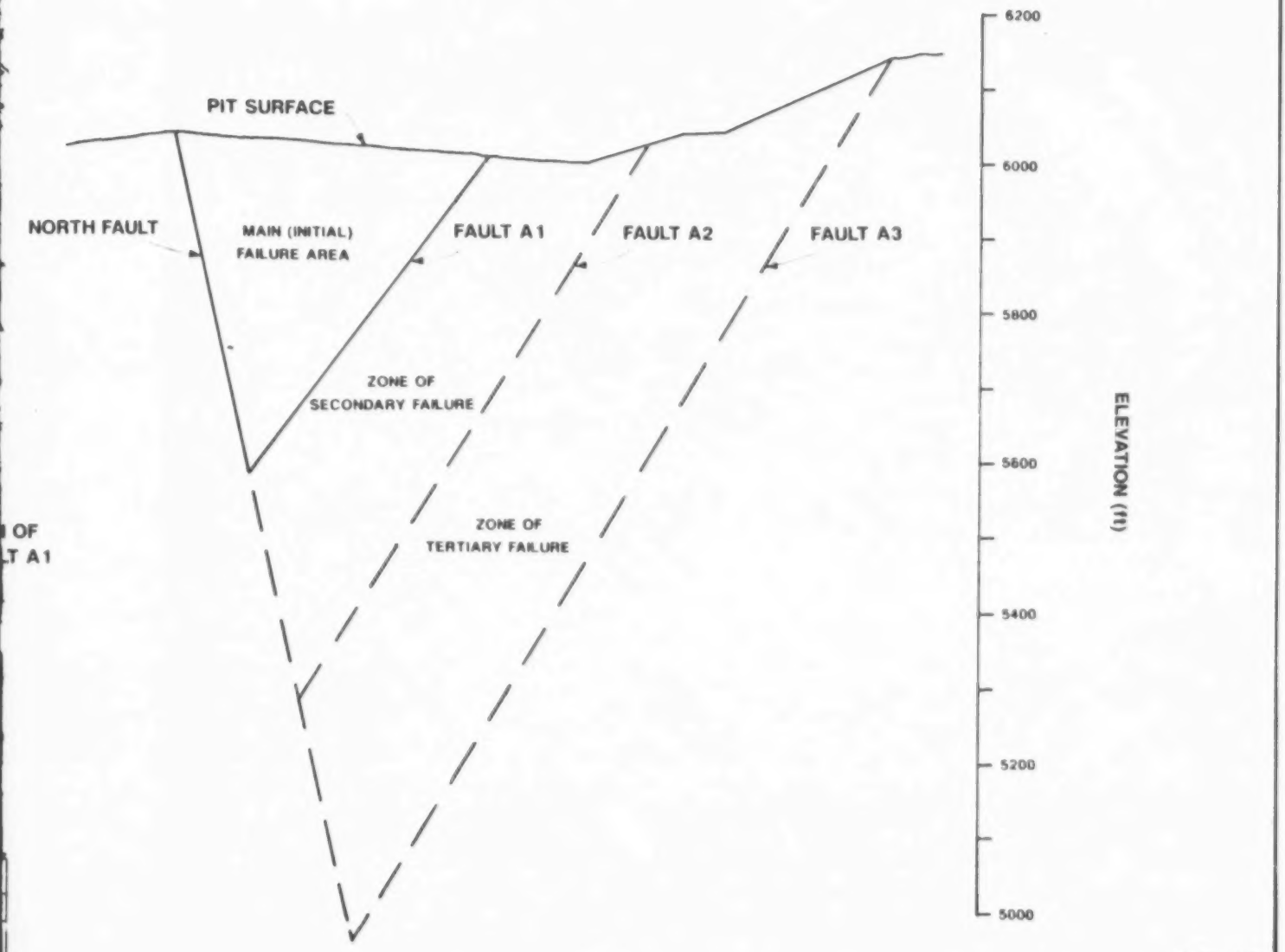

OF
T A1

FIG. 12

SECTION C-C

CANMET SUPPLY AND SERVICES CANADA
CASSIAR OPEN PIT
SLOPE DEFORMATION STUDY

PITEAU ASSOCIATES
GEOTECHNICAL CONSULTANTS
VANCOUVER CALGARY

FAILURE GEOMETRY AND FAILURE MECHANISM

JOB NUMBER

SLIDING

BASAL COHESION = 10 psi

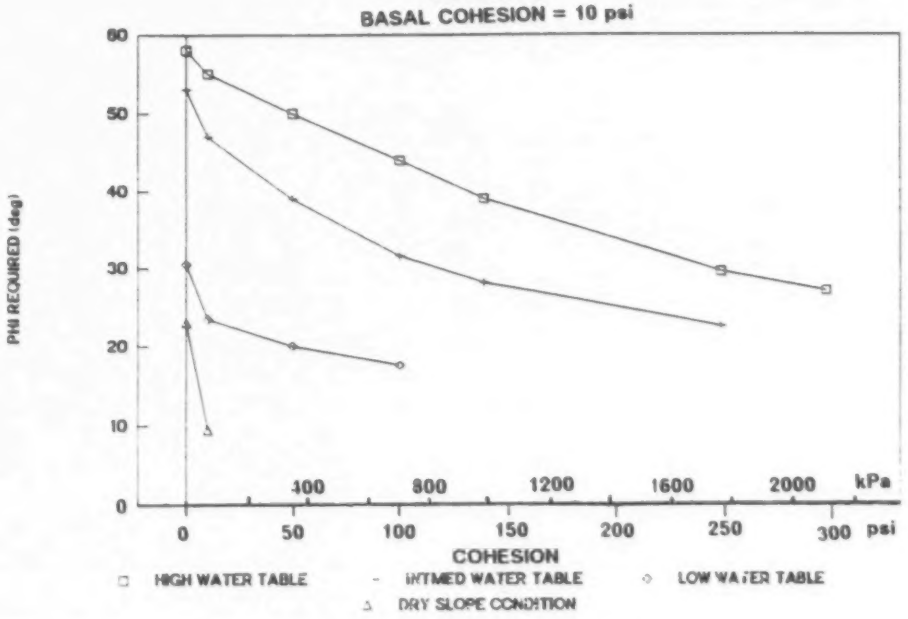

a. SLIDING OF THE TOE BLOCK (BLOCK 5)

TOPPLING

BASAL COHESION = 10 psi

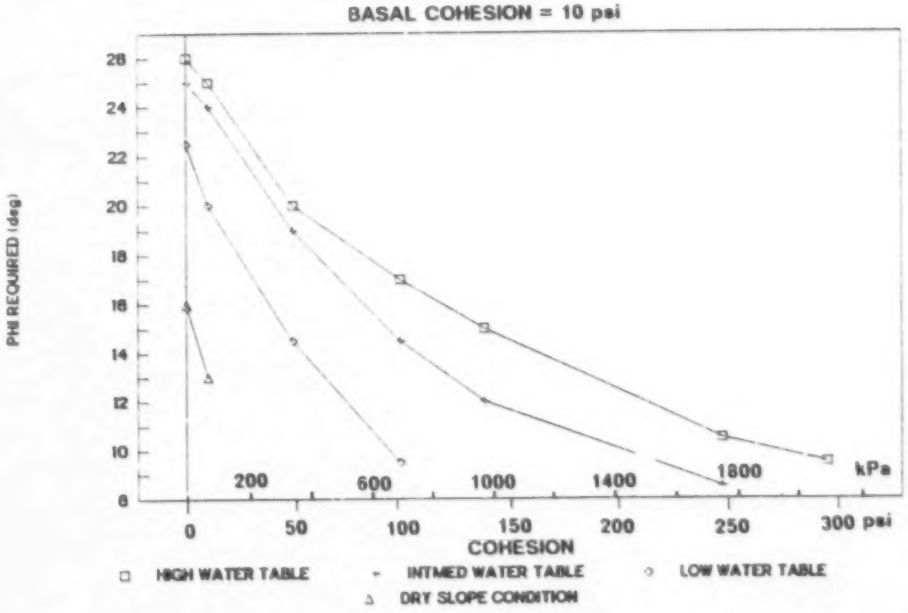

b. TOPPLING OF THE TOE BLOCK (BLOCK 5)

FIG. 13

CANMET/SUPPLY AND SERVICES CANADA
CASSIAR OPEN PIT
SLOPE DEFORMATION STUDY

PITEAU ASSOCIATES
GEOTECHNICAL CONSULTANTS
VANCOUVER CALGARY

SUMMARY OF THREE DIMENSIONAL LIMIT EQUILIBRIUM ANALYSIS OF MAIN FAILURE AREA FOR VARIOUS STRENGTH AND GROUNDWATER CONDITIONS

BY	DATE
LAS	JUN 90
APPROVED	DWG

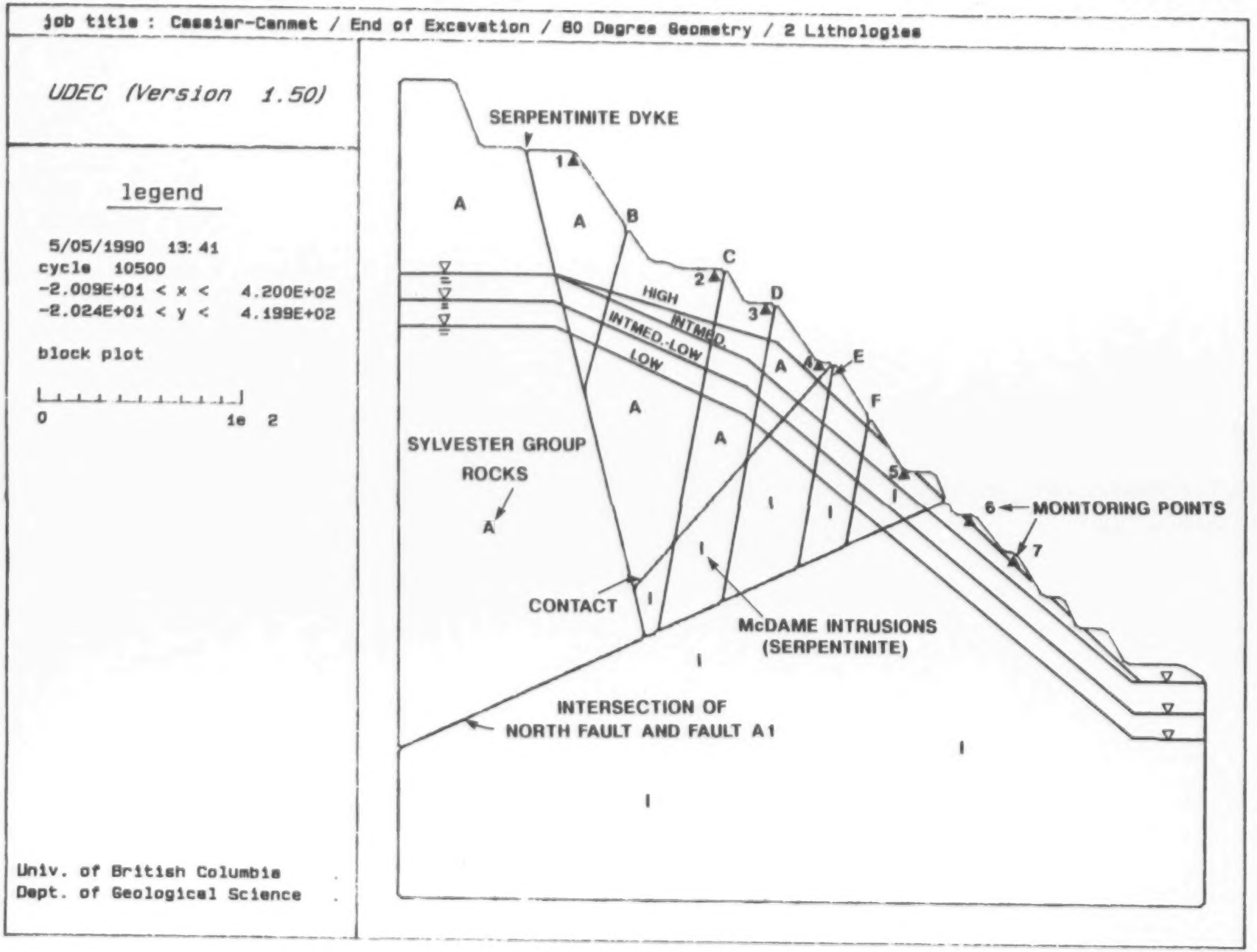

Fig. 14 Slope model used for numerical modelling

TA

SUMMARY OF DISCONTINUITY

ROCK TYPE/AREA (STRUCTURAL DOMAIN)	BEDDING (POPULATION = 19)					SET A			SET B		
	DIP DIRECTION (°)	DIP (°)	%/No.		POPULATION	DIP DIRECTION (°)	DIP (°)	%/No.	DIP DIRECTION (°)	DIP (°)	%
SYLVESTER GROUP ROCKS (A3)	080 137	21 23	55/10 9/2	JOINTS	531	346 326	71 78	14/74 9/48	147 108	82 79	6 2
				FAULTS AND/OR SHEARS	38	353 023 316 334	66 64 80 80	19/7 6/2 5/2 5/2	163	82	
McDAME INTRUSION NORTH OF THE NORTH FAULT (S1)	-	-	-	JOINTS	45	327 342	68 86	9/4 7/3	144	75	9
				FAULTS AND/OR SHEARS	6	-	-	-	122	50	6
McDAME INTRUSION SOUTH OF THE NORTH FAULT (S2)	-	-	-	JOINTS	212	013	80	3/6	113 126 164	63 66 47	7/ 5/ 4/
				FAULTS AND/OR SHEARS	48	020 010	43 70	6/3 3/1	138 172	37 60	7/ 7/

NOTES: 1. Orientations are given as the dip direction and dip of the peak or average orientation of each discontinu

2. %/No refers to the percent population and number of poles in a one percent area at the peak orientation

TABLE I

DISCONTINUITY POPULATIONS ON THE EAST WALL

DISCONTINUTY SETS														
SET B			SET C			SET D			SET E			MISCELLANEOUS SETS		
DIP DIRECTION (°)	DIP (°)	%/No.	DIP DIRECTION (°)	DIP (°)	%/No.	DIP DIRECTION (°)	DIP (°)	%/No.	DIP DIRECTION (°)	DIP (°)	%/No.	DIP DIRECTION (°)	DIP (°)	%/No.
147 108	82 79	6/32 2/11	266 88	75 84	2/11 2/11	–	–	–	197	70	2/11	–	–	–
163	82	9/3	–	–	–	–	–	–	186 218	77 74	9/3 3/1	335 086	26 60	3/1 3/1
144	75	9/4	268	83	16/7	–	–	–	235	76	12/5	–	–	–
122	50	16/1	295 073 093	60 80 73	16/1 16/1 16/1	065	45	16/1	–	–	–	–	–	–
13 26 64	63 66 47	7/15 5/11 4/8	252 255	49 70	4/8 3/6	–	–	–	206 221	56 76	5/11 5/11	–	–	–
38 72	37 60	7/3 7/3	064 309	35 10	9/4 6/3	038	86	6/3	203 220	74 77	8/4 6/3	–	–	–

f each discontinuity set

eak orientation

TABLE II

SUMMARY OF STRENGTH TESTING OF INTACT ROCK SAMPLES[1]

ROCK TYPE	POINT LOAD INDEX TESTS on ROCK CORES (1975)		RESULTS OF PREVIOUS ROCK MECHANICS TESTING (1981)												
				Unconfined Compressive Strength (psi)		Youngs Modulus, E (x 10^6 psi) (number of samples in brackets)		Poissons Ratio, (number of samples in brackets)		Tensile Strength (psi)			Unit Weight LB/ft^3	
	No. of[2] Test Suites	Average Estimated Unconfined Compressive Strength (psi)	No. of Samples	Mean	Standard Deviation	Mean	Standard Deviation	Mean	Standard Deviation	No. of Tests	Mean	Standard Deviation	No. of Samples	Mean
Argillites	-	-	4	11,036	2049	25.3 (4)	3.3 (4)	0.23 (4)	0.09 (4)	6	1361	244	3	170
Volcanics	-	-	4	20,923	8797	37.7 (3)	3.7 (3)	0.24 (3)	0.04 (3)	6	2030	293	3	190
Alteration	-	-	-	-	-	-	-	-	-	5	1976	895	3	177
All Sylvester Group Rocks	-	-	8	15,721	7032	30.6 (7)	7.35 (7)	0.24 (7)	0.06 (7)	17	1778	589	9	179
Jointed Serpentinite	23	7170	7	4,981	4087	14.0 (7)	10.4 (7)	0.30 (7)	0.09 (7)	3 3	877 452	59 36	3	161
Serpentinite Rock Shear	-	-	3	1,181	931	2.6 (3)	2.0 (3)	0.33 (1)	-	-	–	-	-	–

NOTES: 1. Point load index tests were carried out by Piteau, Gadsby Macleod Ltd. (1975). All other rock mechanics testing was carried out by Call, Nicolas, Inc. (1981).
2. Each test suite consists of a minimum of twelve point load tests on rock core.

TABLE III

DIRECT SHEAR STRENGTH OF DISCONTINUITIES[1,2]

DISCONTINUITY TYPE	SPECIMEN/ TEST TYPE	SOURCE OF INFORMATION								RECOMMENDED SHEAR[5,6] STRENGTH OF DISCONTINUITIES FOR SLOPE DESIGN		NO. OF SAMPLES/ NO. OF TEST RUNS	DISCONTINUITY[7] STIFFNESS	
		RESULTS FOR DATA COLLECTED IN 1975			RESULTS OF LINEAR REGRESSION ANALYSIS OF 1981 DATA			ESTIMATION OF RESIDUAL FRICTION ANGLE FOR 1981 DATA[4]						
		No. of Samples	Friction Angle ϕ_r (°)	Cohesion C (psi)	No. of Samples	Friction Angle ϕ_r (°)	Cohesion C (psi)	No. of Samples	ϕ_r (°)	Friction Angle ϕ_r (°)	Cohesion (psi)		Shear Stiffness K_S Pa/m	Shear Stiffness K_N Pa/m
SERPENTINE SHEAR ZONES	Cores and large scale specimens	7	26.5	21	4	22.9	12.4	4	27.0	26.5	0 - 10	7/12	2.70×10^8	2.03×10^9
SERPENTINE JOINTS	Cores: Normal stress <250 psi	3	30.0	0	-	-	- -	-	-	26.0	0	2/3	8.60×10^8	9.52×10^9
	Normal stress >250 psi		26.0	0	-	-	- -	-	-					
	Large scale specimen	-	-	-	1	19.8	20.7	1 Forward 1 Reverse	21.0 28.0					
ASBESTOS FIBRE VEIN	<0.5" veins	3	26.0	NC[3]	-	-	-	-	-	26.0	NC[3]		NC[3]	NC[3]
	>0.5" veins	3	21.0	NC[3]	-	-	-	-	-	21.0	NC[3]		NC[3]	NC[3]
ARGILLITE SHEAR ZONES	-	-	-	-	-	-	-	-	-	26.5	0 - 10		NC[3]	NC[3]
ARGILLITE JOINTS	Cores	-	-	-	3	29.7	-14.7	3	27.3	32	0	2/7	6.77×10^8	4.32×10^{10}
	Large scale specimens	2	33.0	0	8	28.7	29.0	8	32.2					
JOINTS IN ALTERATION ZONE	Cores	-	-	-	-	31.2	-12.5	2	28.3			-	NC[3]	NC[3]
JOINTS IN VOLCANICS	Cores	-	-	-	4	27.4	- 3.9	4	26.8					

NOTES:

1. Shear Strength is defined in terms of cohesion, C and Angle of Friction, ϕ_r.
2. Data sources include direct shear testing carried out by Piteau, Gadsby Maclead Ltd. (1975) and Call, Nicolos, Inc. (1981).
3. NC = not calculated.
4. Friction angles are estimated from an assessment of test results reported by Call Nicolos Inc. in 1981.
5. A range of cohesion is indicated for fault gouge. A cohesion of 0 psi should be used for analysis of bench failures, whereas cohesion of 10 psi may be used for analysis of major failures along faults or shears.
6. Shear strength of joints in argillites, volcanics, and alteration are asssumed to be similar based on results of large scale direct shear tests.
7. Discontinuity stiffness was determined as the ratio of peak strength to maximum strain and/or maximum dilation for the direct shear tests.

TABLE IV

SUMMARY OF GEOTECHNICAL PARAMETERS LOGGED IN DIAMOND DRILL CORE

DESCRIPTION OF ROCK MASS	PARAMETER[1]													
	CORE RECOVERY		NATURAL RQD[2]		RQD (+ 4")[3]		NATURAL JOINT SPACING		HARDNESS		DEGREE OF BREAKAGE		CCRG	
	LENGTH[4] (FT)	WEIGHTED[5] MEAN AND RANGE [6] (%)	LENGTH[4] (FT)	WEIGHTED[5] MEAN AND RANGE [6] (%)	LENGTH[4] (FT)	WEIGHTED[5] MEAN AND RANGE [6] (%)	LENGTH[4] (FT)	WEIGHTED[5] MEAN AND (RANGE)[6] (%)	LENGTH[4] (FT)	WEIGHTED[5] MEAN AND RANGE [6]	LENGTH[4] (FT)	WEIGHTED[5] MEAN AND RANGE [6]	LENGTH (FT)	WEIGHTED[5] MEAN AND (RANGE)[6] (%)
Alteration	125	91 (84-96)	125	88 (84-96)	-	-	125	3.1 (1.5-massive)	60	R4.5 (R3-R5)	125	D+	-	-
Argillite	817	88 (72-97)	817	85 (73-96)	-	-	818	7.8 (2.5 massive)	460	R5 (R4-R5)	809	D (C+ to D+)	-	-
Volcanics	144	95	142	91	-	-	141	7.4 (2.5-massive)	-	-	143	D	-	-
All Argillites and Volcanics	1002	89 (86-95)	1002	86 (83-90)	-	-	1002	8.1 (6.2-11.9)	460	R5 (R4-R5)	998	D	-	-
Ore bearing Serpentine (Unsheared)	2301	89 (84-93)	2553	81 (71-89)	3400	19 (13-35)	2557	2.3 (1.2-5.0)	2590	R3 (R2-R3)	2543	D- (C+-D)	3440	6.6 (1.8-8.5)
Barren Serpentine (Unsheared)	2575	88 (63-91)	2898	(53-81)	1714	22 (9-30)	2870	2.1 (1.3-4.5)	2650	R3	2901	D- (C+ to D)	3010	1.2 (.7-1.6)
Shear Zones in Ore Bearing Serpentine	316	84 (82-89)	389	75 (62-83)	425	7 (2-14)	381	2.6 (1.8-3.8)	408	R0.5 (S3-R3)	387	C+ (C to D)	427	4.9 (1.6-9.1)
Shear Zones in Barren Serpentine	896	85 (81-87)	1036	43 (22-83)	1015	7 (0-14)	970	1.7 (1.4-3.1)	968	R1 (S6-R2)	972	C+ (C to D-)	1008	1.4 (1.3-1.7)
All Shear Zones in Serpentine	1212	85 (81-89)	1425	52 (22-83)	1440	7 (0-14)	1351	1.9 (1.4-3.8)	1376	R1 (S6-R2)	1359	C+ (C to D)	1435	2.4 (1.3-7.9)
Shear Zones in Argillite	168	67 (58-81)	168	38 (20-75)	-	-	168	7.0 (1.7-massive)	168	R4 (R1-R5)	168	C+ (C to D)	-	-

NOTES: 1. A complete description of the geotechnical parameters logged and cusums analysis technique is given in Appendix B.

2. Natural RQD refers to percentage of length drilled where the spacing between naturally occurring fractures is greater than 4".

3. RQD + 4" refers to percentage of length drilled where the spacing between both natural and drill induced fractures is greater than 4".

4. Length refers to the length of core over which a given parameter was logged within a particular rock type/zone.

5. Weighted means of geotechnical parameters are based on current mean values determined from the cumulative sums analysis.

6. Range refers to the interval within which approximately 80% of all current mean values fall and is given in brackets.

TABLE V

ROCK MASS STRENGTHS ESTIMATED FROM

LABORATORY TESTING AND CORE LOGGING

ROCK MASS GROUP	ROCK MASS STRENGTH[1]		
	FRICTION ANGLE ϕ (°)	COHESION, C	
		psi	kPa
ARGILLITE (VOLCANICS AND ALTERATION)	32	100	690
BARREN (WASTE) SERPENTINITE (CCRG < 3%)	26	50	345
ORE BEARING SERPENTINITE (CCRG > 3%)	26	30	207
SHEAR ZONES	26.5	10	69

NOTE: 1. Rock mass strengths have been used for assessing maximum overall slopes in various areas of the open pit. Analyses were also carried out to assess the sensitivity of overall slope stability to changes in the assumed cohesion of shear zones.

TABLE VI

DEEP SEATED ROTATIONAL FAILURE ANALYSES RESULTS

SECTION	SLOPE ANALYZED	CONDITIONS	CALCULATED[1] FACTOR OF SAFETY
SECTION 23,400N	Overall hanging wall	Anticipated strength and groundwater conditions.	1.25
	Hanging wall slope below elevation 5690	Anticipated strengths; high groundwater	1.06
		Anticipated strength; depressurized slope.	1.35
SOUTH WALL	Overall slope	Anticipated strength and groundwater conditions.	1.25
	Slope in Serpentinite and 45° Shear below elevation 5690	Anticipated strength and groundwater conditions; cohesion = 10 psi (69 kPa) in 45° Shear.	0.64
		Cohesion = 20 psi (138 kPa) in 45° Shear; anticipated groundwater conditions.	0.76
		Cohesions 30 psi (207 kPa) in 45° Shear; anticipated groundwater conditions.	0.87
		Cohesion = 10 psi (69 kPa) in 45° Shear; depressurized slope.	0.99
	Slope in serpentinite and 45° Shear with buttress of intact rock at elevation 5420	Anticipated strength and groundwater conditions.	0.78
		Anticipated strength and groundwater conditions; flattened between El.5240 and El.5690.	0.92
		Anticipated strengths; depressurized slope.	1.10
		Anticipated strengths; depressurized slope; flattened between El.5420 and El.5690.	1.20

NOTES: 1. Factors of safety given are calculated values based on the assumed rock mass strengths. Results should be viewed in terms of relative slope stability and sensitivity to variation in slope conditions. More accurate assessment of rock mass strength based on performance of mined slopes is necessary to clearly assess the absolute slope stability.

AREA DESCRIPTION	PRISM NO.	START ELEVATION (ft)
BEDROCK AND WASTE DUMPS EAST OFTHE NORTH FAULT	10	6047
	49	5998
	L	5889
MAIN AREA OF THE GRABEN TOPPLING	13	6206
	46	6128
	11	6195
	47	6140
	14	6192
	48	6150
	23	6183
	37	6177
	19	6053
	25	6032
	50	5998
	39	6012
	51	6008
	40	6007
	43	5958
AREA OF SECONDARY GRABEN TOPPLING EAST OF MAIN AREA	24	6170
	17	6009
	41	5998
	52	5994
	42	5798
	20	5641
AREA OF TERTIARY GRABEN TOPPLING ON EAST WALL	32	5990
	12	5988
	38	5965
NORTH OF UNSTABLE AREA	16	6212
	45	6204
EAST WALL	18	5968
	30	6011
	36	5924
	31	5760
	21	5642
	3	5555
	27	5493
	28	5488
SOUTH WALL	Z	
	9	6008
	Y	5760
	2	5821

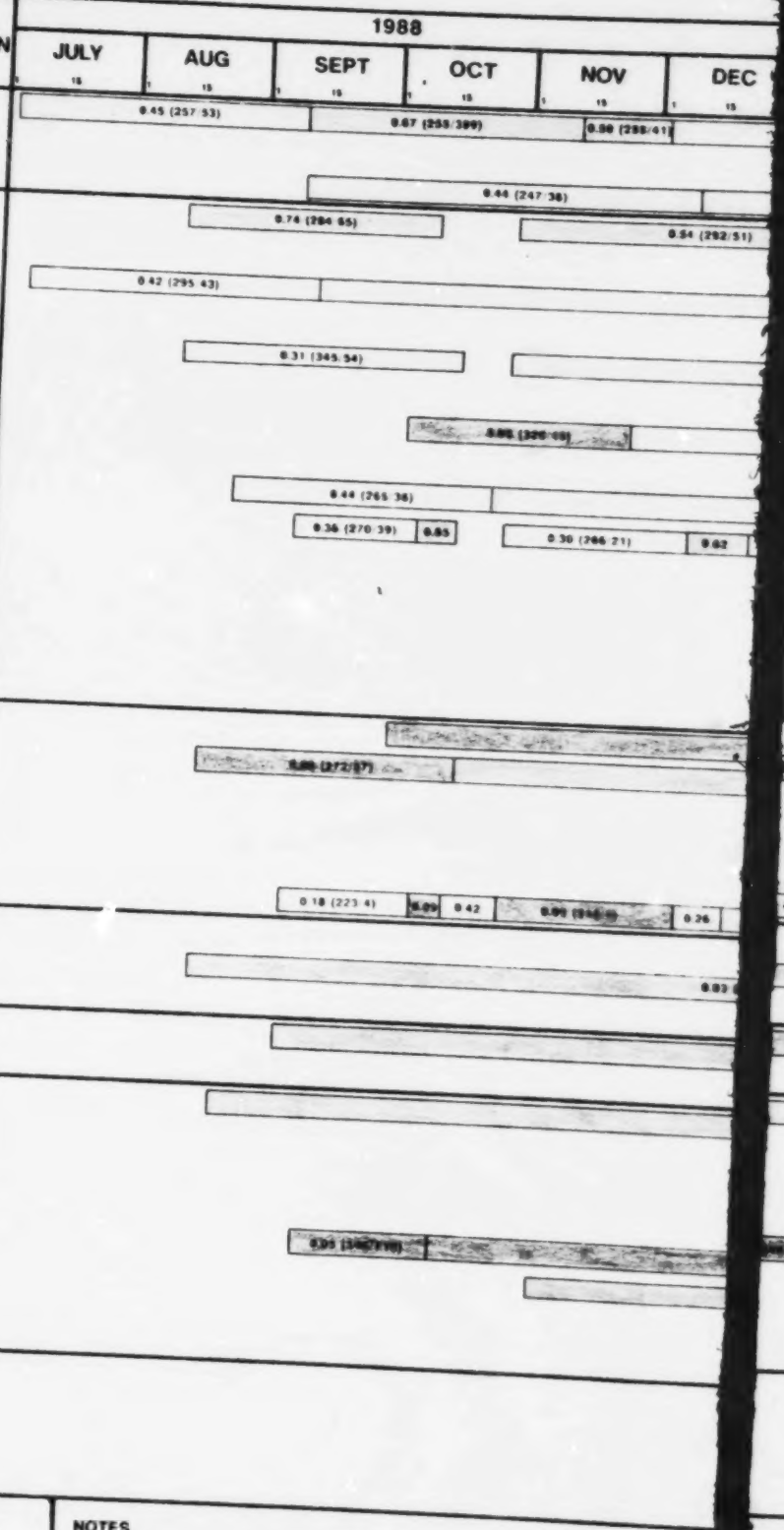

NOTES

1. Prism locations given in Fig. 2
2. Total movement and movement rate were calculated from the prism monitoring data collected by mine personel between July 1988 and May

MOVEMENT RATE IN INCHES/DAY (AZIMUTH AND PLUNGE OF MOVEMENT VECTOR IN BRACKETS)

(PLUNGE OF VECTORS IS NEGATIVE UNLESS OTHERWISE NOTED)

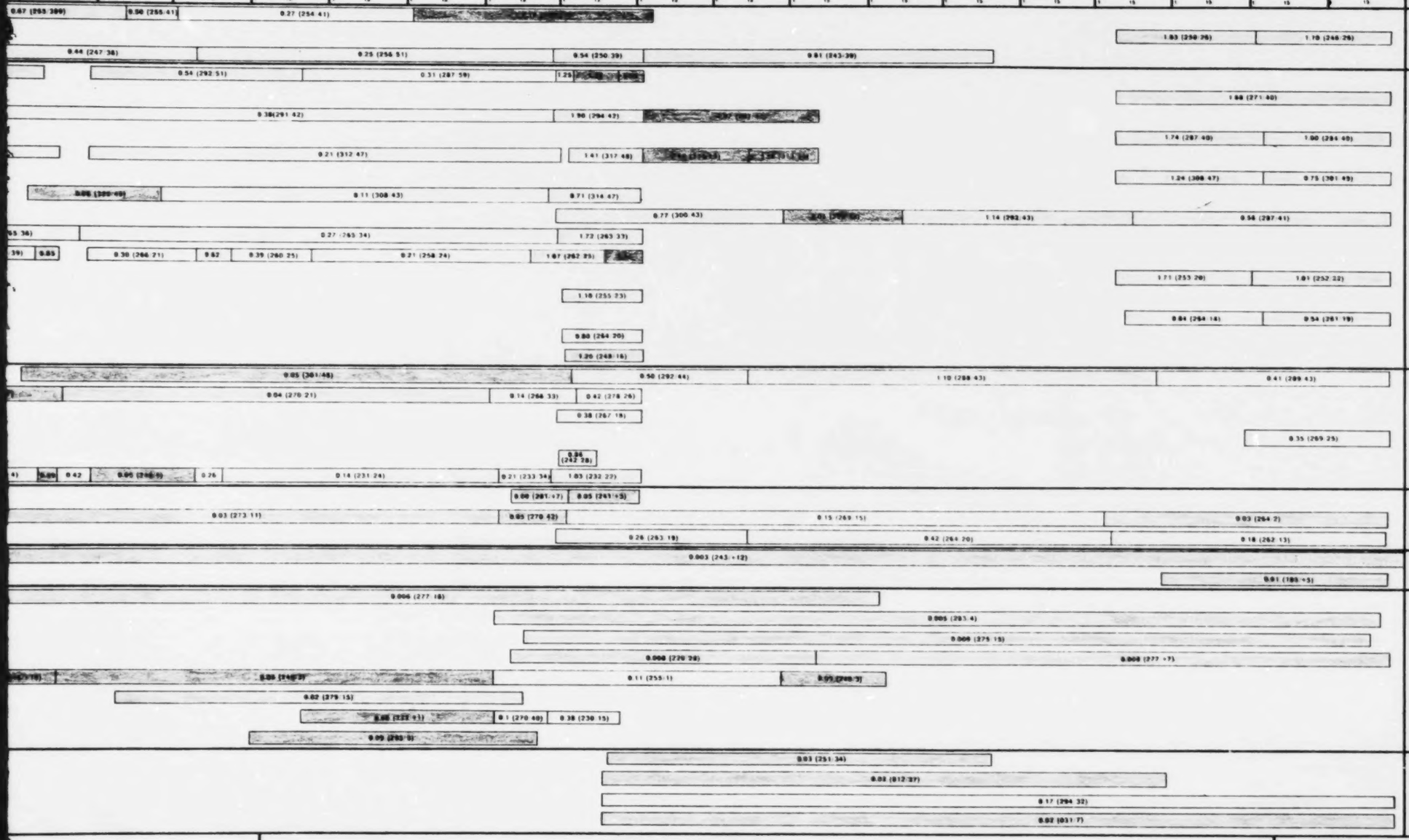

SUMMARY OF TOTAL MOVEMENT [2]

PRISM NO. [1]	TOTAL MOVEMENT (feet)	AZIMUTH	PLUNGE	AVERAGE MOVEMENT RATE (inches/day)
10	41.7	254	43	1.55
49	13.3	249	26	1.50
L	15.8	246	37	0.47
13	14.7	289	54	0.81
46	15.0	271	40	1.68
11	44.0	289	40	1.31
47	12.6	286	40	1.42
14	25.7	315	49	0.84
48	9.1	306	48	1.02
23	4.0	312	45	0.20
37	30.4	292	44	1.11
19	11.1	264	34	0.47
25	13.2	264	25	0.64
50	12.2	252	21	1.37
39	3.1	255	23	1.10
51	6.3	263	16	0.71
40	2.21	264	20	0.80
43	3.1	248	16	1.20
24	22.0	289	43	0.49
17	2.2	273	26	0.09
41	1.1	267	18	0.38
52	1.6	269	25	0.35
42	1.2	242	28	0.86
20	5.9	231	22	0.26
32	0.27	255	+6	0.06
12	3.3	269	14	0.07
38	8.4	264	18	0.31
16	0.14	243	+12	0.003
45	0.11	185	5	0.01
18	0.20	277	16	0.006
30	0.13	283	4	0.005
36	0.24	275	15	0.009
31	0.22	259	5	0.008
21	1.61	245	3	0.05
3	0.27	279	15	0.02
27	1.49	232	12	0.14
28	0.75	285	5	0.09
Z	0.37	251	34	0.03
9	0.42	012	27	0.022
Y	0.17	294	32	0.007
2	0.39	031	7	0.02

Fig. 2
ement rate were calculated from the prism
d by mine personel between July 1988 and May 1990

LEGEND FOR MOVEMENT RATE

- > 2 in/day
- 1.0 to 2.0 in/day
- 0.5 to 0.99 in/day
- 0.1 to 0.49 in/day
- 0.05 to 0.099 in/day
- < 0.05 in/day

CANMET SUPPLY AND SERVICES CANADA
CASSIAR OPEN PIT
SLOPE DEFORMATION STUDY

PITEAU & ASSOCIATES
GEOTECHNICAL CONSULTANTS
VANCOUVER CALGARY

SUMMARY OF PRISM MONITORING

TABLE VII

TABLE VIII

MATERIAL PROPERTIES USED FOR NUMERICAL MODELLING WITH THE UDEC PROGRAM[1]

	DENSITY Kg/m^3	BULK MODULUS (K) Pa	SHEAR MODULUS (G) Pa	COHESION Pa	FRICTION[2] ANGLE (°)	TENSILE STRENGTH Pa	DILATION ANGLE (°)	NORMAL STIFFNESS Pa/m	SHEAR[2] STIFFNESS Pa/m
ARGILLITES/VOLCANICS ROCK MASS	2870	1.35×10^{10}	8.51×10^{9}	7.00×10^{5}	32	3.44×10^{5}	0.0		
ARGILLITE/VOLCANIC DISCONTINUITIES				7.00×10^{5} (1.00×10^{8})	32 (45)	0.0		4.40×10^{7}	6.80×10^{6} (1.00×10^{8})
SERPENTINITE ROCK MASS	2580	8.04×10^{9}	3.71×10^{9}	2.00×10^{5}	26	1.03×10^{5}	0.0		
SERPENTINITE DISCONTINUITIES				7.00×10^{4} (1.0×10^{8})	26 (45)	0.0		4.30×10^{7}	2.70×10^{6} (1.00×10^{8})
FAULT TRACE INTERSECTION				7.00×10^{4}	26	0.0		4.30×10^{7}	2.00×10^{6}
ALTERATION ZONE CONTACT				7.00×10^{5}	32	0.0		4.40×10^{7}	6.80×10^{6}

NOTES: 1. Material properties are based on laboratory testing of rock samples as modified, based on the behaviour of the model.

2. Value in brackets is a higher strength value used during the excavation phase of the model to prevent displacement before the toe is exposed.

SUMMARY OF

DESCRIPTION	WATER TABLE	DISCONTINUITY STRENGTH				MOVEMENT (metres) (PLUNG		
		ARGILLITE		SERPENTINITE		MONITORING POINT 1	MONITORING POINT 2	MONITORING POINT 3 M
		C (kPa)	Ø (°)	C (kPa)	Ø (°)			
TWO MATERIALS WITHOUT CRACKS	HIGH	–	–	–	–	0.39 (86)	0.39 (88)	0.40 (88)
ONE MATERIAL (ARGILLITE) IN ACTIVE FAILURE AREA WITH CRACKS PRESENT	HIGH	700	34	70	28	0.50 (76)	–	0.27 (05)
		700	30	70	24	0.83 (75)	–	0.47 (05)
	INTMED	700	34	70	28	0.16 (76)	–	0.13 (+52)
		700	30	70	24	0.50 (76)	–	0.25 (+02)
TWO MATERIALS (ARGILLITE AND SERPENTINITE) AND CRACKS IN THE ACTIVE ZONE WITH STRAIN SOFTENING	HIGH	700	30	70	24	1.52 (79)	1.06 (59)	0.79 (41)
		595	30	60	24	1.03 (76)	1.08 (+44)	0.70 (07)
		536	30	54	24	0.47 (82)	0.15 (20)	0.14 (23)
		509	30	51	24	0.05 (77)	0.04 (52)	0.04 (50)
		483	30	48	24	0.02 (74)	0.02 (00)	0.01 (09)
		459	30	46	24	0.08 (75)	0.06 (10)	0.05 (19)
	INTMED–LOW	700–459	30	70–46	24	0.30 (76)	0.22 (11)	0.20 (07)
	LOW	700–459	30	70–46	24	0.21 (76)	0.15 (19)	0.13 (14)
	HIGH	700–459	36	70–46	30	1.98 (78)	1.31 (46)	1.06 (29)
		700–459	30	70–46	24	3.17 (78)	1.57 (09)	1.66 (25)
		700–459	28	70–46	22	3.57 (77)	2.15 (28)	1.99 (22)
OBSERVED DEFORMATION RATE AND APPARENT PLUNGE IN EARLY PHASE OF INSTABILITY [3]						PRISM 13 0.74 (65)	PRISM 25 0.38 (39)	–

NOTES: 1. Total movment and plunge are based on time history plots for monitoring points shown in Fig. D1. Predicted plunges are negative unless otherwise noted.

2. Models shown in Fig. D8a to f to D12 represent a strain softening sequence with successive reductions in di scon Figs D8a and D8f give the individual movements after each strain softening event. Fig.D9 to D12 represent the t

3. Based on observed movement rates (in./day) of prisms on Section D–D during the initial stages of failure. These However the plunges and ratios of movement between prisms is used as a basis to assessing the validity of t he m

TABLE IX

MARY OF NUMERICAL MODELLING RESULTS

) (PLUNGE (degrees)) PREDICTED BY UDEC MODEL[1,2]

TORING INT 3	MONITORING POINT 4	MONITORING POINT 5	MONITORING POINT 6	MONITORING POINT 7	COMMENTS	APPENDIX FIGURE
0 (88)	0.34 (83)	0.15 (36)	0.08 (14)	0.09 (13)		D3a,D3b
7 (05)	–	0.17 (06)	0.10 (09)	–	Velocity plots indicate inconsistent movement and probably stable.	D4
7 (05)	–	0.28 (03)	0.18 (09)	–	Magnitudes and velocities indicate failure as observed.	D5
(+52)	–	0.05 (+11)	0.01 (13)	–	Velocity plots indicate inconsistent movement and probably stable.	D6
(+02)	–	0.16 (00)	0.08 (09)	–	Velocity plots indicate inconsistent movement and probably stable.	D7
(41)	0.73 (44)	0.49 (16)	0.06 (43)	0.05 (23)	Note 2. The bulk of the movement occurs after the first two strain softening events.	D8a
(07)	0.57 (12)	0.31 (09)	0.20 (07)	0.16 (03)		D8b
(23)	0.12 (11)	0.09 (13)	0.09 (07)	0.06 (03)		D8c
(50)	0.03 (07)	0.02 (15)	0.02 (09)	0.02 (09)		D8d
(09)	0.01 (10)	0.01 (16)	0.01 (11)	0.01 (01)		D8e
(19)	0.04 (12)	0.03 (15)	0.02 (07)	0.02 (01)		D8f
(07)	0.16 (23)	0.08 (10)	0.04 (09)	0.03 (03)	Note 2.	D9
(14)	0.11 (27)	0.05 (14)	0.03 (09)	0.03 (04)	Note 2.	D10
(29)	0.96 (36)	0.63 (15)	0.06 (43)	0.05 (23)	Note 2.	D11
(25)	1.45 (27)	0.44 (13)	0.39 (13)	0.32 (07)		D8f
(22)	1.73 (24)	1.13 (12)	0.06 (43)	0.05 (23)		D12
	–	PRISM 20 0.18 (04)	PRISM 21 0.05 (+18)	–	The ratios of movement between various prisms and plunge of prisms most closely resembles the model shown in Fig. D8a	A2,A3

s in di scontinuity cohesion of 20%, 10%, 5%, 5% and 5%.
sent the total movement after all strain softening.

re. These rates cannot be compared directly with the models.
y of the model.

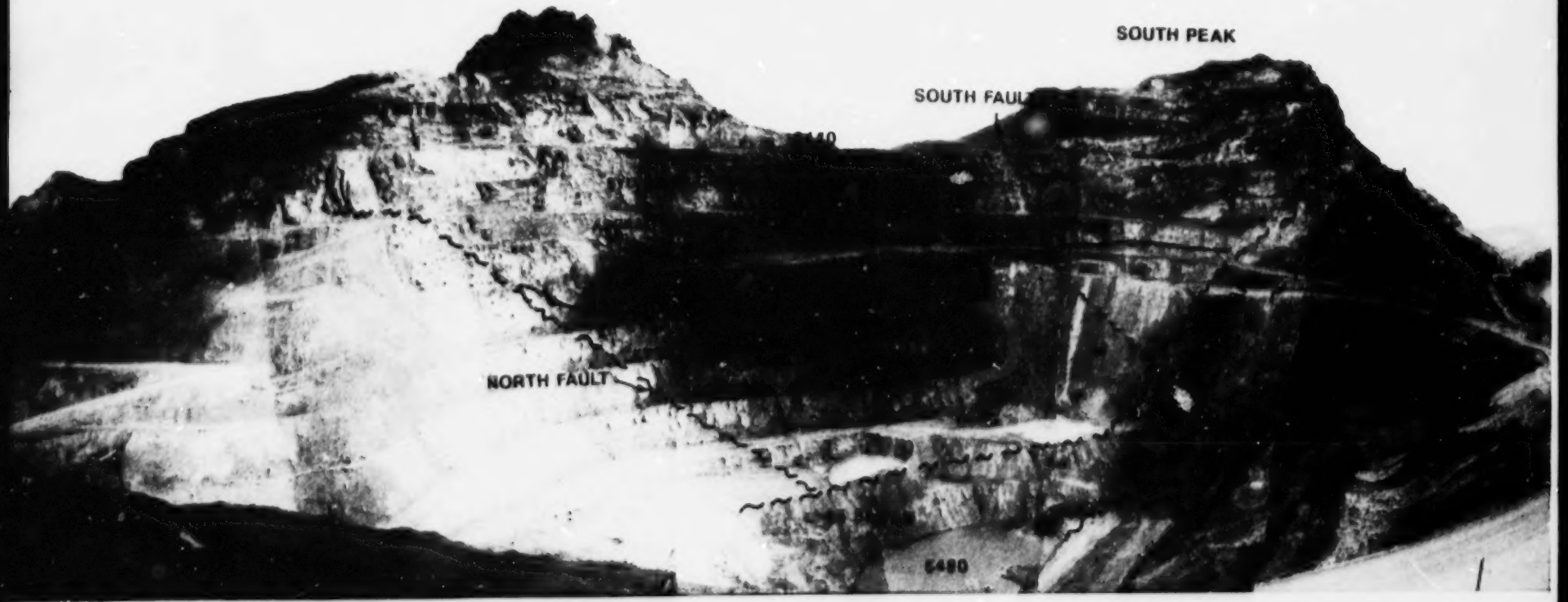

PHOTO 1: PANORAMIC VIEW OF THE OPEN PIT IN AUGUST 1983 DURING THE EARLY STAGE OF THE FINAL MINING PHASE.

Photo 2. Hard, indurated argillite and volcanic rocks of the Sylvester Group on the hanging wall. Note well developed discontinuities of Set A.

Photo 3. Fractured and blocky serpentinite of the McDame Intrusion in the open pit.

Photo 4. Sheared and fractured serpentinite in the ore zone.

Photo 5. Footwall contact, 70° Shear and Footwall Fault on the footwall (west) side of the open pit.

Photo 6. 45° Shear and North Fault on the 5360 bench.

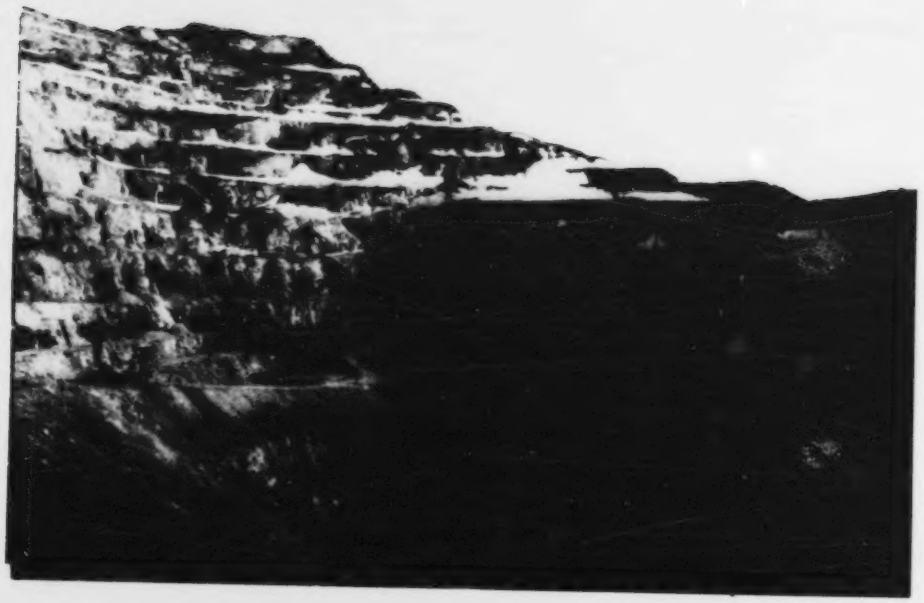

Photo 7. South wall failure which occurred in May 1988 involving the 45° Shear and footwall contact of the serpentinite

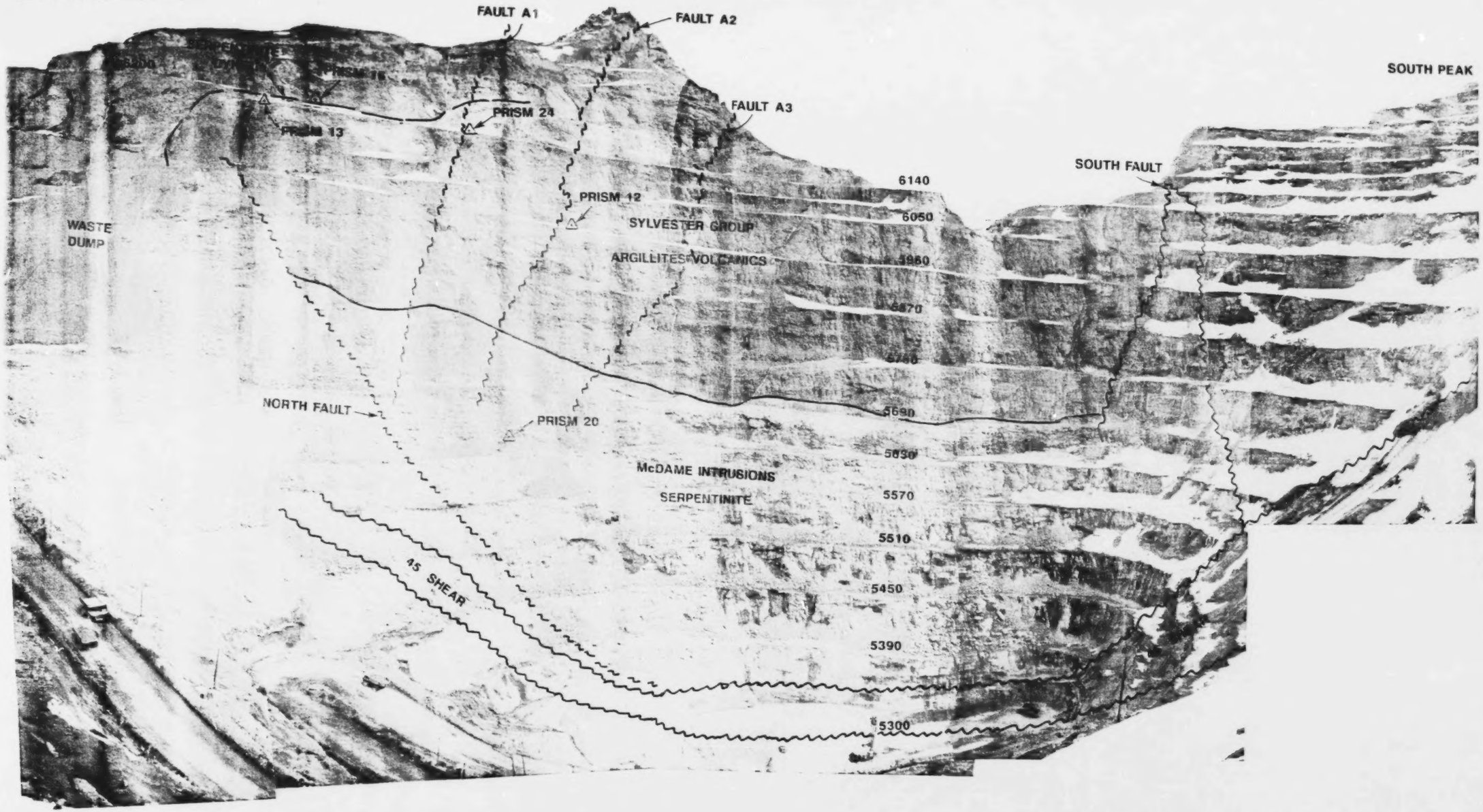

PHOTO 8: PANORAMIC VIEW OF THE EAST WALL ON MAY 18, 1989.

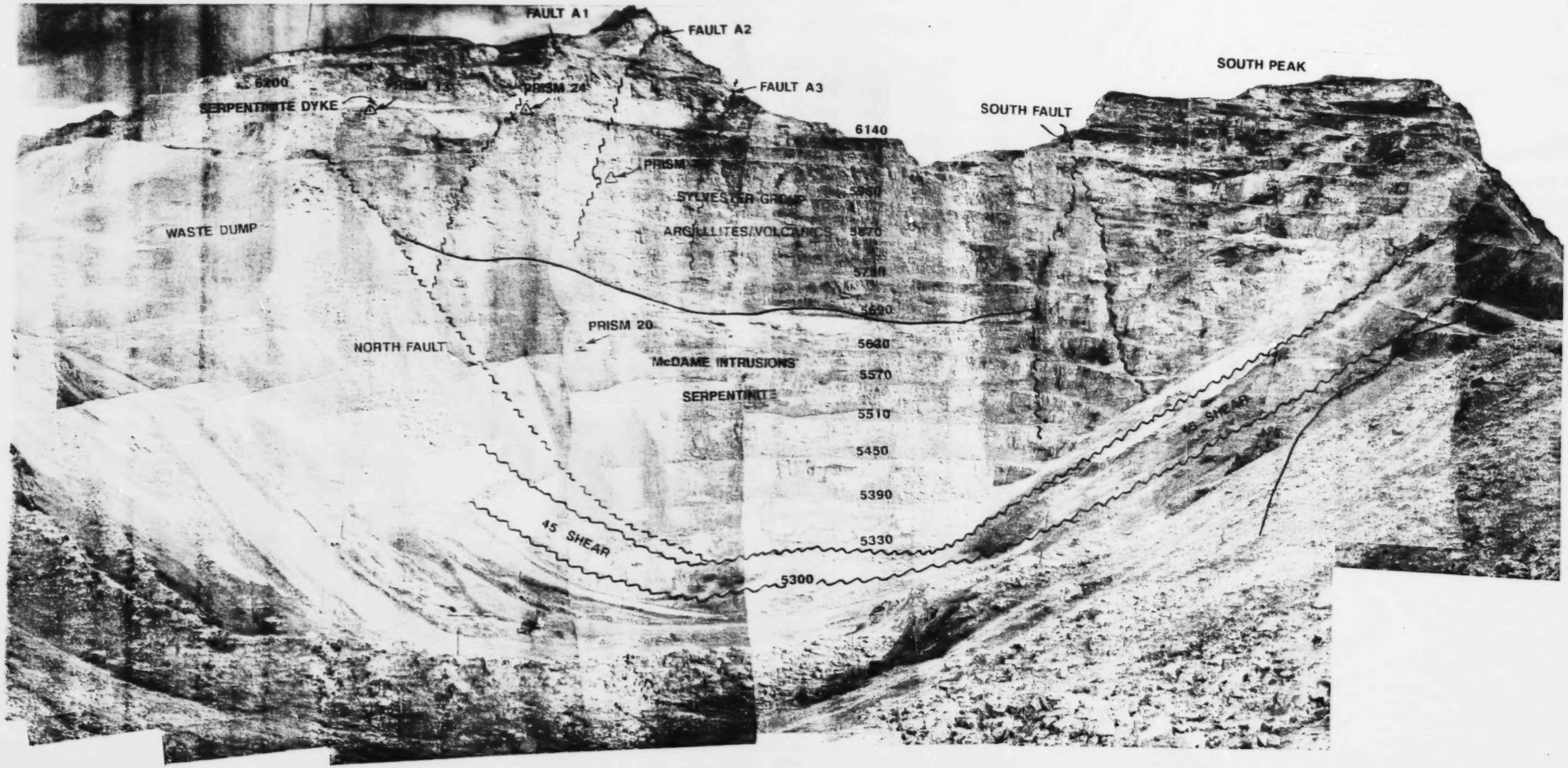

PHOTO 9: PANORAMIC VIEW OF THE EAST WALL ON AUGUST 1, 1989 SHOWING ADVANCED DEVELOPMENT OF THE GRABEN TOPPLING FAILURE.

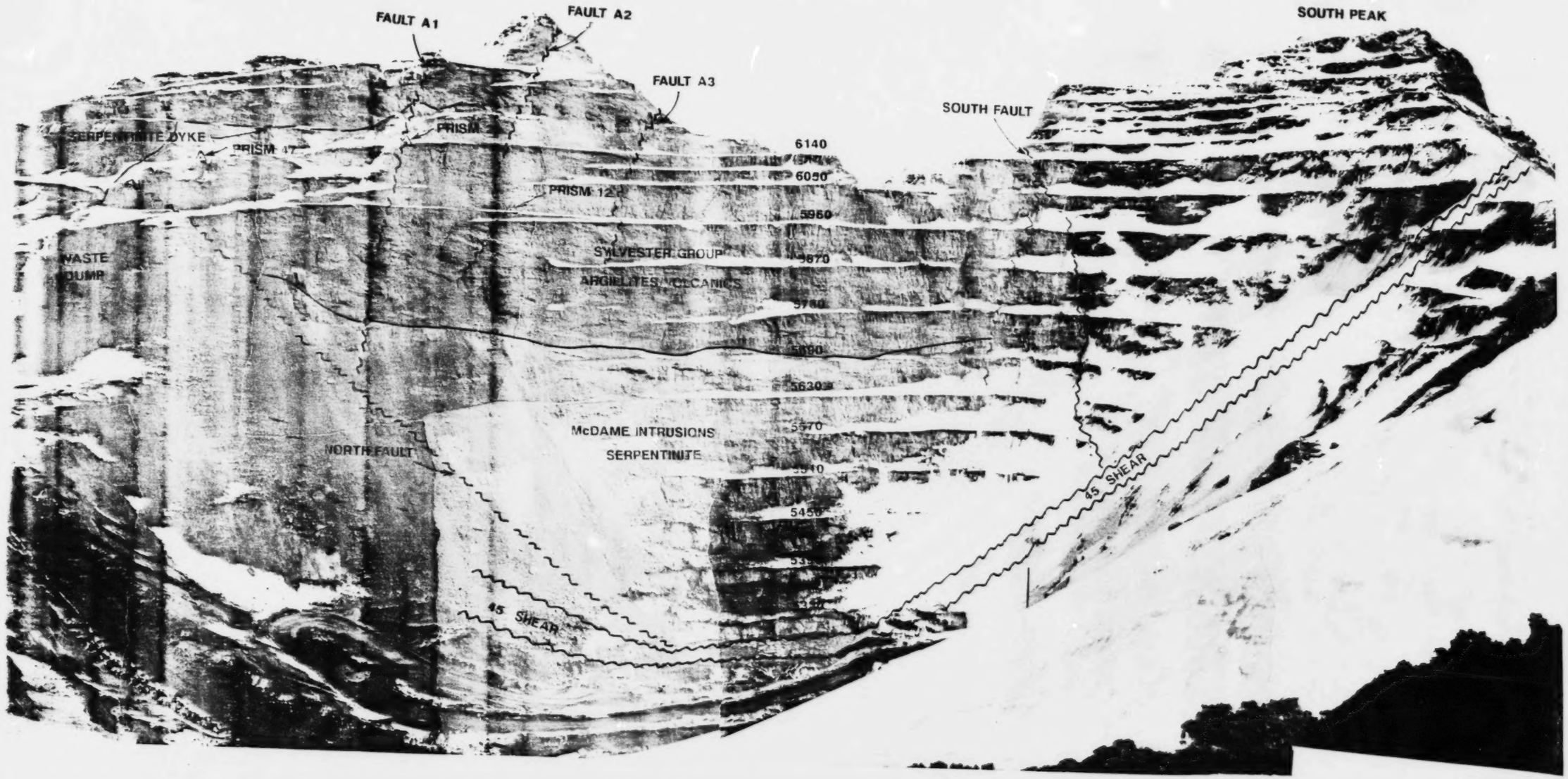

PHOTO 10: PANORAMIC VIEW OF THE EAST WALL ON MAY 14, 1990 SHOWING ADVANCED DEVELOPMENT OF THE GRABEN TOPPLING FAILURE.

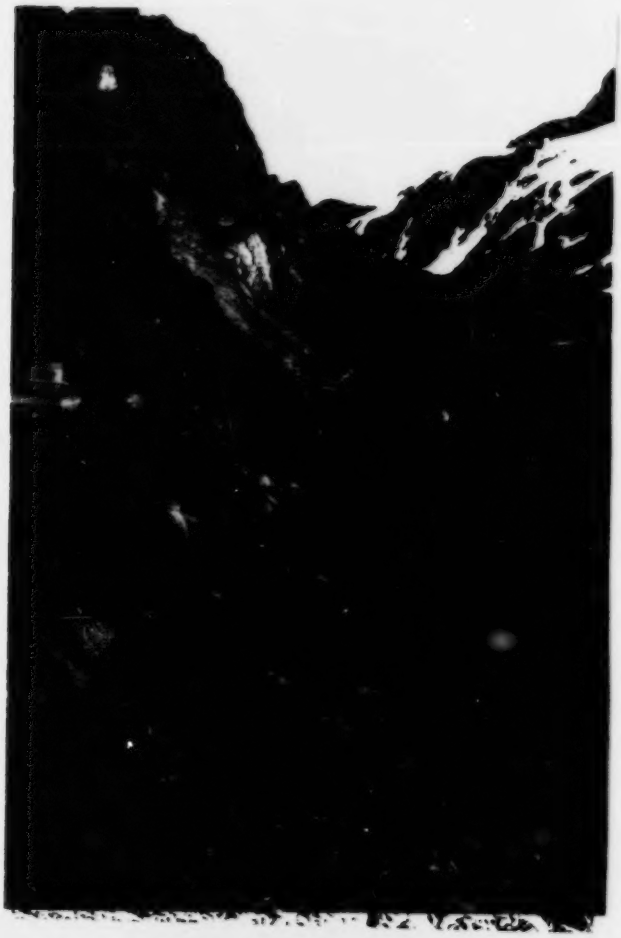

Photo 11. View looking south along the Serpentinite Dyke showing displacement of graben block. Surface extensometer is shown to the right of the pick-up truck.

Photo 12. View looking north showing approximately 12 metres of displacement along the Serpentinite Dyke by mid-September 1989.

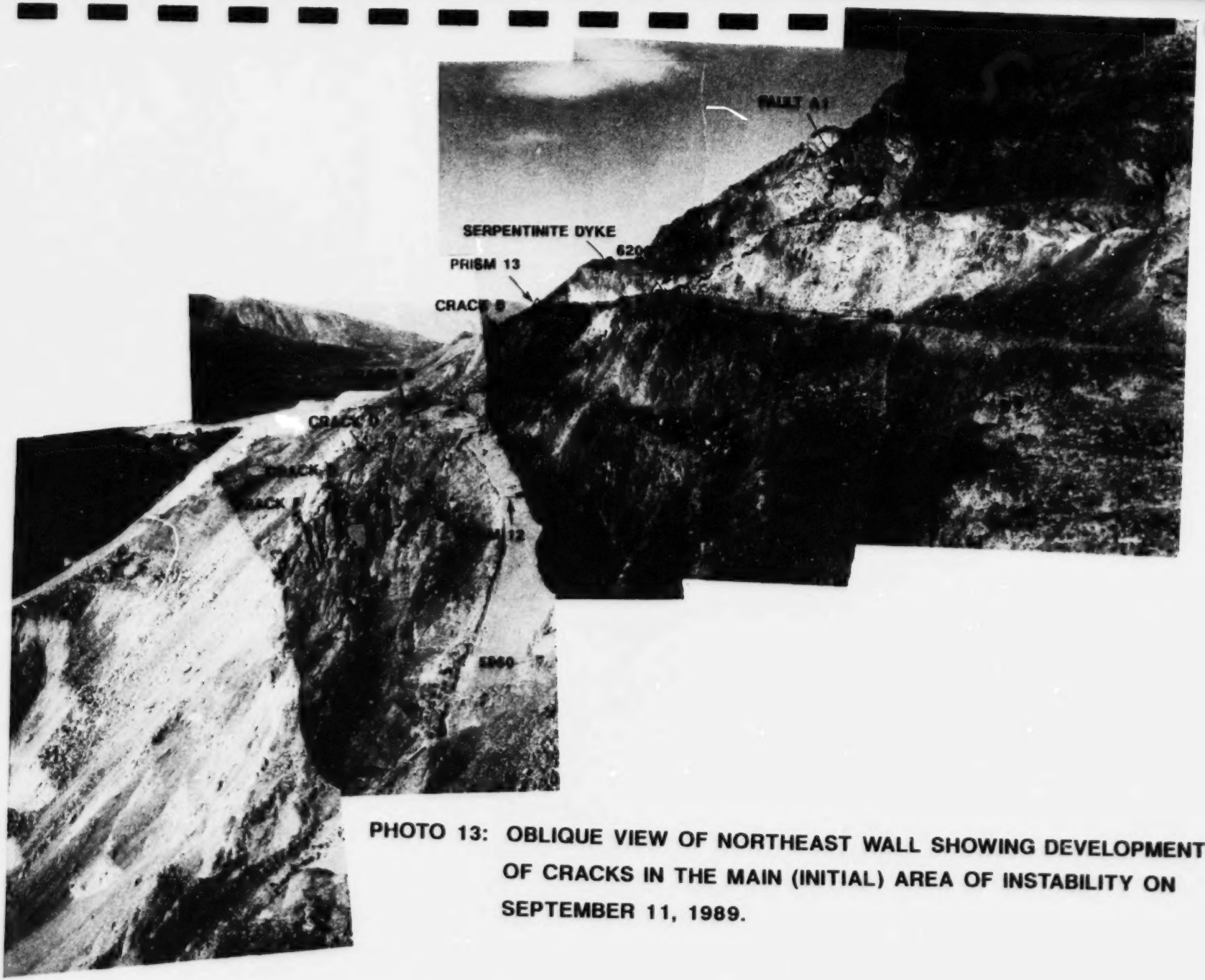

PHOTO 13: OBLIQUE VIEW OF NORTHEAST WALL SHOWING DEVELOPMENT OF CRACKS IN THE MAIN (INITIAL) AREA OF INSTABILITY ON SEPTEMBER 11, 1989.

APPENDIX A

REPRESENTATIVE GEOTECHNICAL SECTIONS SHOWING ENGINEERING GEOLOGY AND MOVEMENT SUMMARIES

LOOKING NORTH

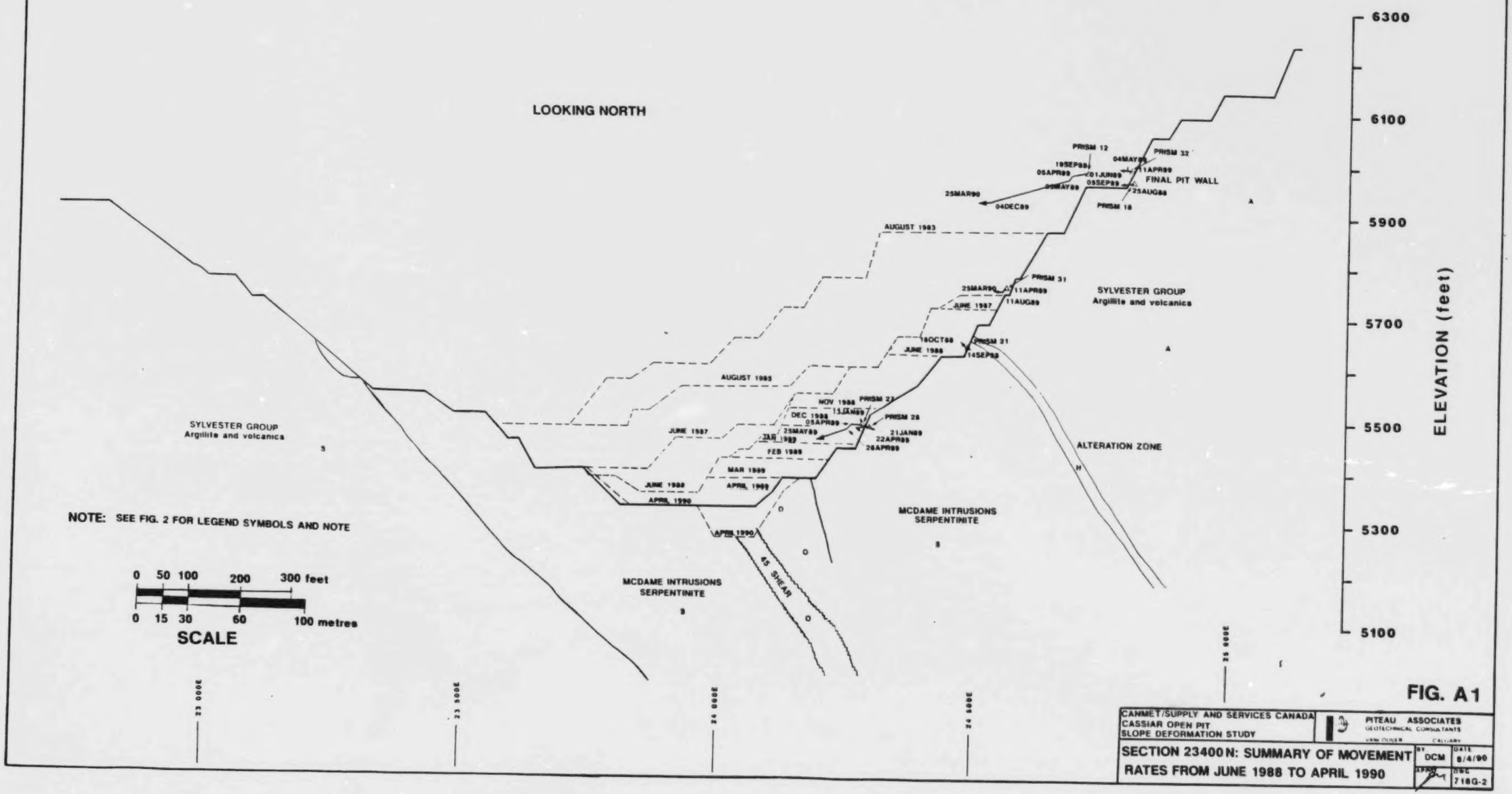

NOTE: SEE FIG. 2 FOR LEGEND SYMBOLS AND NOTE

0 50 100 200 300 feet

0 15 30 60 100 metres

SCALE

FIG. A1

CANMET/SUPPLY AND SERVICES CANADA CASSIAR OPEN PIT SLOPE DEFORMATION STUDY	PITEAU ASSOCIATES GEOTECHNICAL CONSULTANTS VANCOUVER CALGARY		
SECTION 23400N: SUMMARY OF MOVEMENT RATES FROM JUNE 1988 TO APRIL 1990	BY DCM	DATE 8/4/90	
	APP'D	DWG 718G-2	

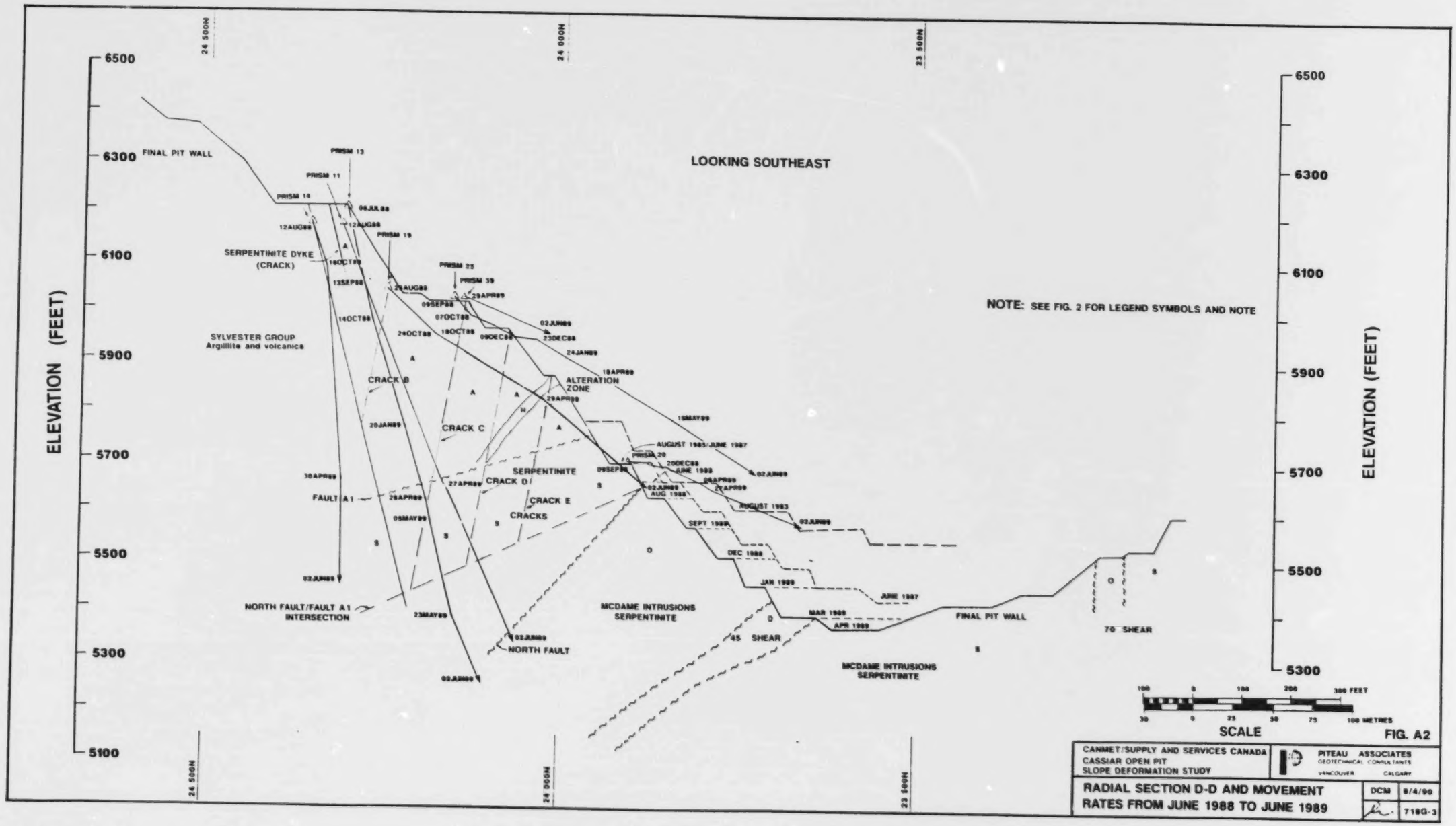

FIG. A2

CANMET/SUPPLY AND SERVICES CANADA
CASSIAR OPEN PIT
SLOPE DEFORMATION STUDY

PITEAU ASSOCIATES
GEOTECHNICAL CONSULTANTS
VANCOUVER CALGARY

RADIAL SECTION D-D AND MOVEMENT RATES FROM JUNE 1988 TO JUNE 1989

DCM 8/4/90

719G-3

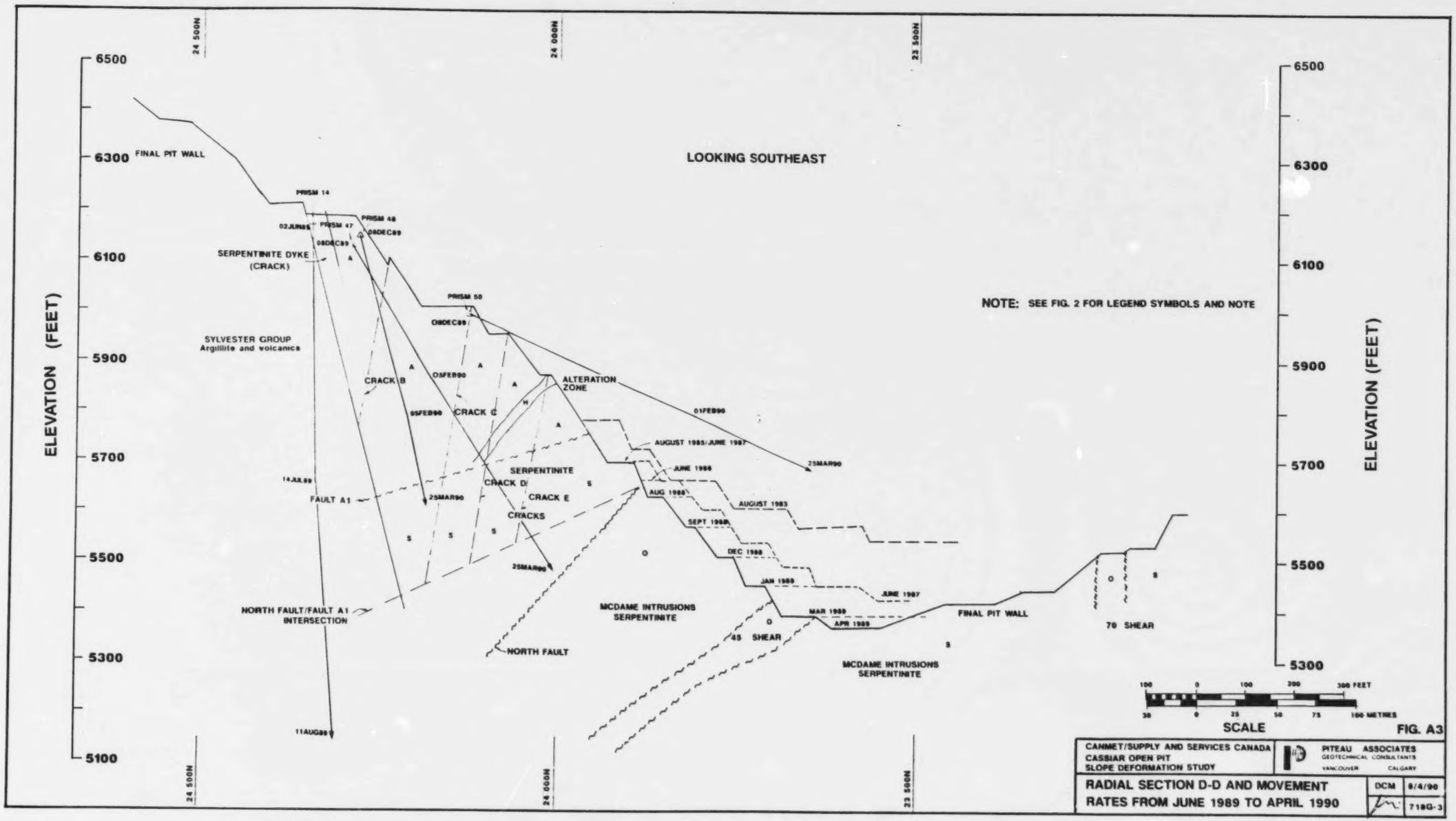
24 500N
24 000N
23 500N
6500
6300
6100
5900
5700
5500
5300
5100
ELEVATION (FEET)
LOOKING SOUTHEAST
NOTE: SEE FIG. 2 FOR LEGEND SYMBOLS AND NOTE
FINAL PIT WALL
PRISM 14
PRISM 48
02JUN89
PRISM 47
08DEC89
SERPENTINITE DYKE
(CRACK)
SYLVESTER GROUP
Argillite and volcanics
PRISM 50
CRACK B
05FEB90
ALTERATION
ZONE
05FEB90
CRACK C
01FEB90
AUGUST 1985/JUNE 1987
25MAR90
SERPENTINITE
JUNE 1988
14JUL89
CRACK D
CRACK E
AUG 1988
AUGUST 1988
FAULT A1
25MAR90
CRACKS
SEPT 1988
DEC 1988
JAN 1989
JUNE 1987
MAR 1989
APR 1989
NORTH FAULT/FAULT A1
INTERSECTION
MCDAME INTRUSIONS
SERPENTINITE
45 SHEAR
FINAL PIT WALL
70 SHEAR
NORTH FAULT
MCDAME INTRUSIONS
SERPENTINITE
11AUG89
100 0 100 200 300 FEET
30 0 25 50 75 100 METRES
SCALE
FIG. A3
CANMET/SUPPLY AND SERVICES CANADA
CASSIAR OPEN PIT
SLOPE DEFORMATION STUDY
PITEAU ASSOCIATES
GEOTECHNICAL CONSULTANTS
VANCOUVER CALGARY
RADIAL SECTION D-D AND MOVEMENT
RATES FROM JUNE 1989 TO APRIL 1990
DCM 9/4/90
718G-3

APPENDIX B

SUMMARY OF PRISM MOVEMENTS FOR SELECTED REPRESENTATIVE PRISMS

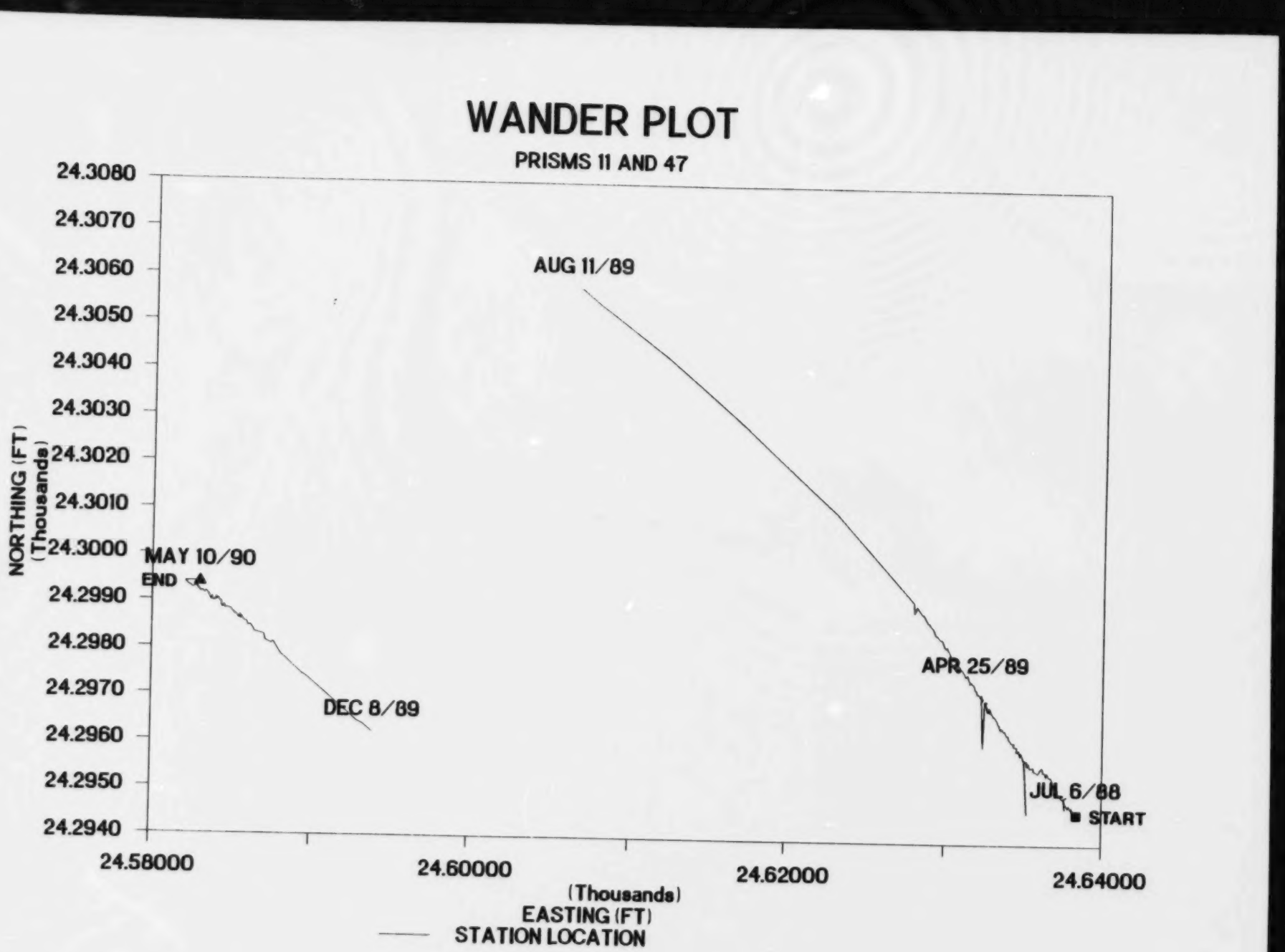
WANDER PLOT
PRISMS 11 AND 47
24.3080
24.3070
24.3060
24.3050
24.3040
24.3030
24.3020
24.3010
24.3000
24.2990
24.2980
24.2970
24.2960
24.2950
24.2940
NORTHING (FT)
(Thousands)
AUG 11/89
MAY 10/90
END
DEC 8/89
APR 25/89
JUL 6/88
START
24.58000
24.60000
24.62000
24.64000
(Thousands)
EASTING (FT)
STATION LOCATION

RELATIVE MOVEMENT VS TIME

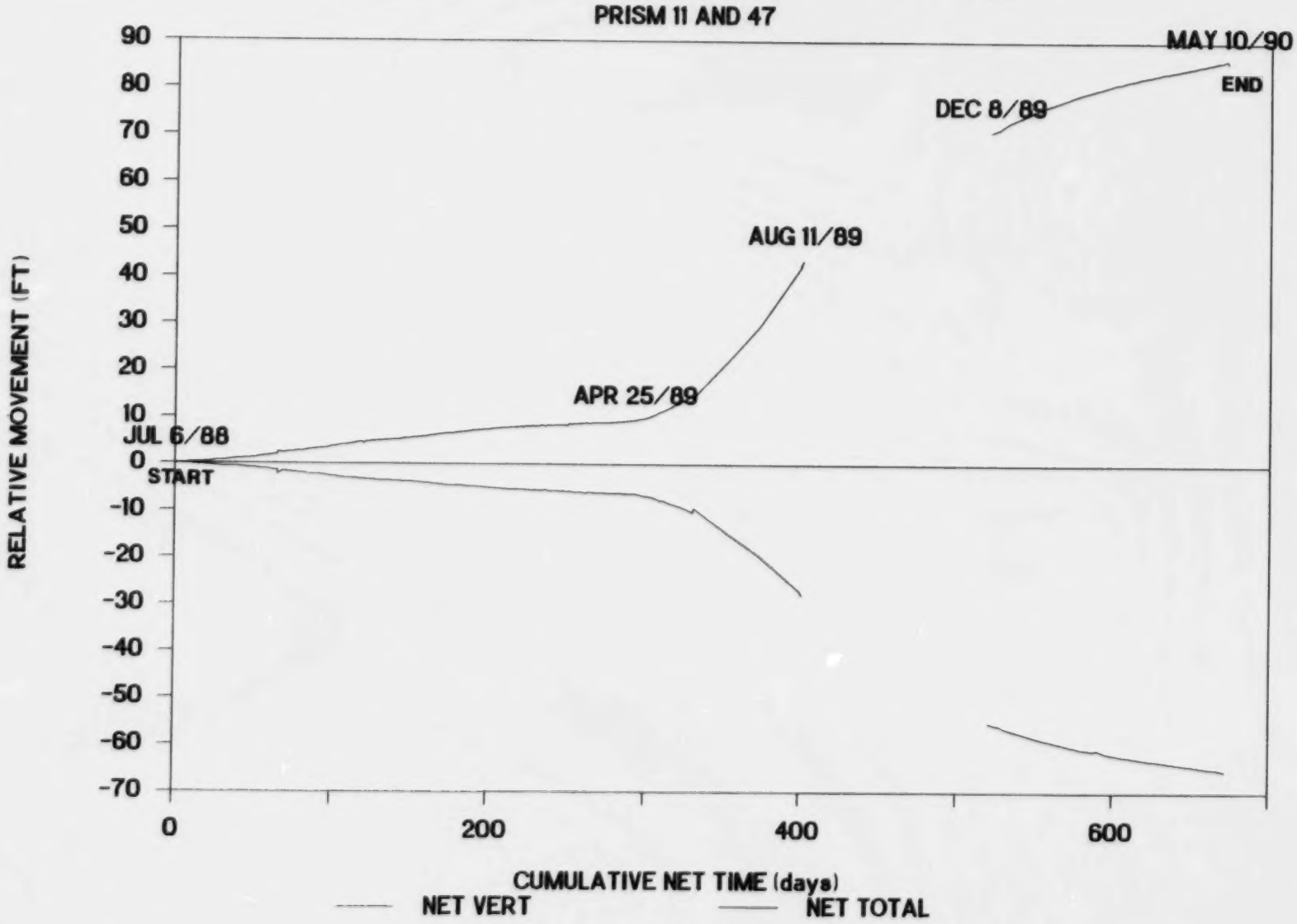

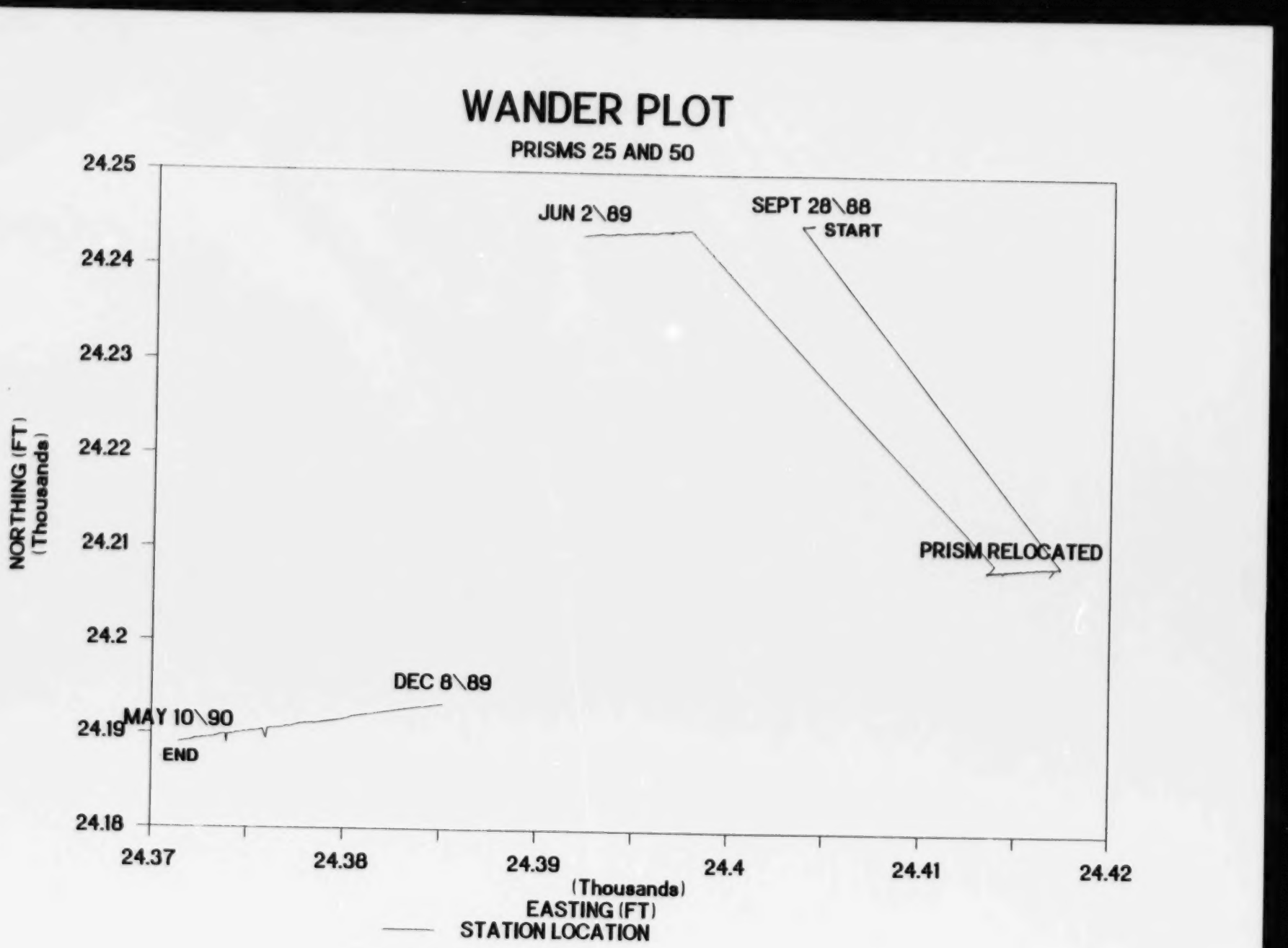
WANDER PLOT
PRISMS 25 AND 50
24.25
24.24
24.23
24.22
24.21
24.2
24.19
24.18
NORTHING (FT)
(Thousands)
JUN 2\89
SEPT 28\88
START
PRISM RELOCATED
DEC 8\89
MAY 10\90
END
24.37
24.38
24.39
24.4
24.41
24.42
(Thousands)
EASTING (FT)
STATION LOCATION

RELATIVE MOVEMENT VS TIME

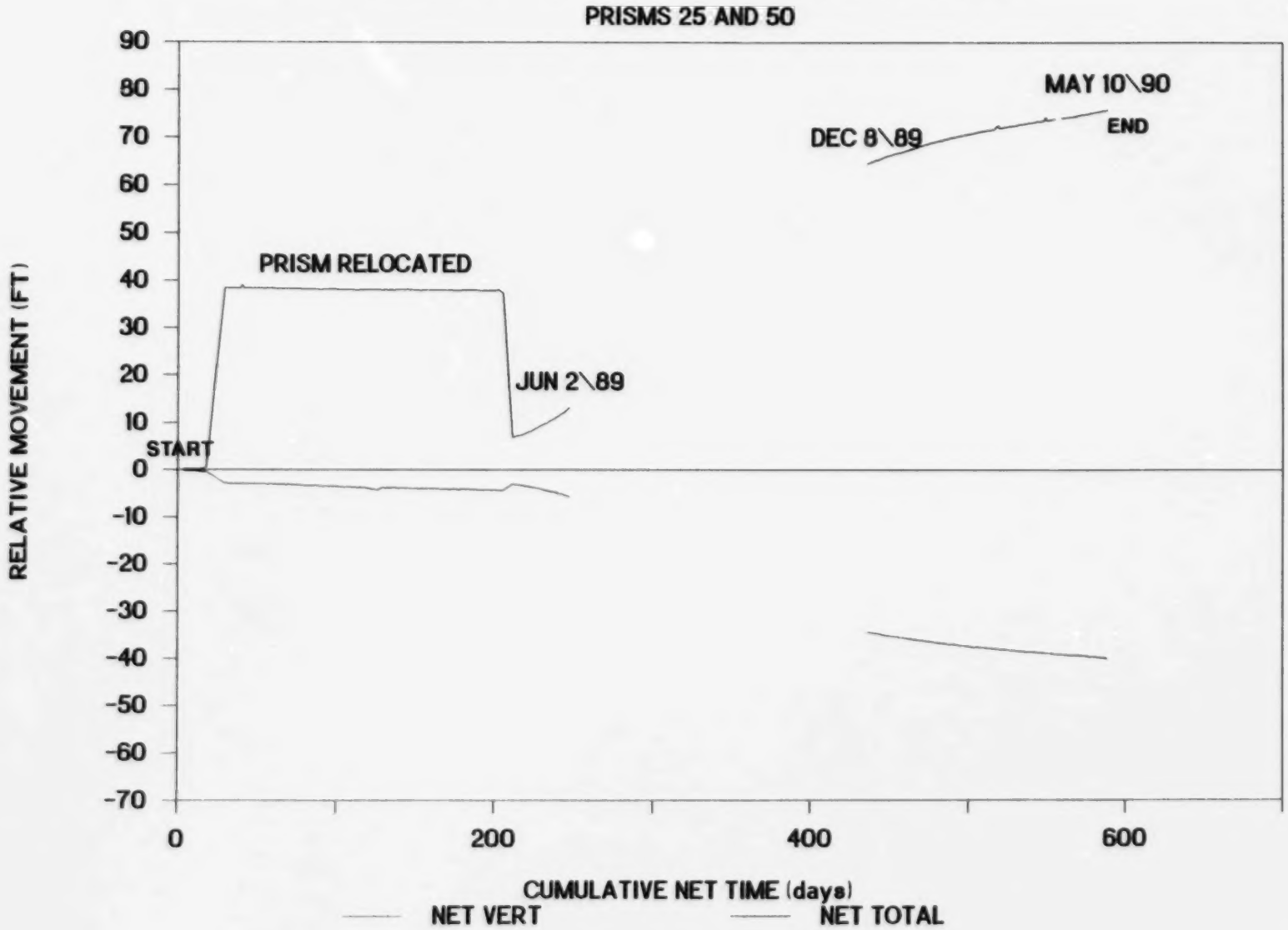

WANDER PLOT

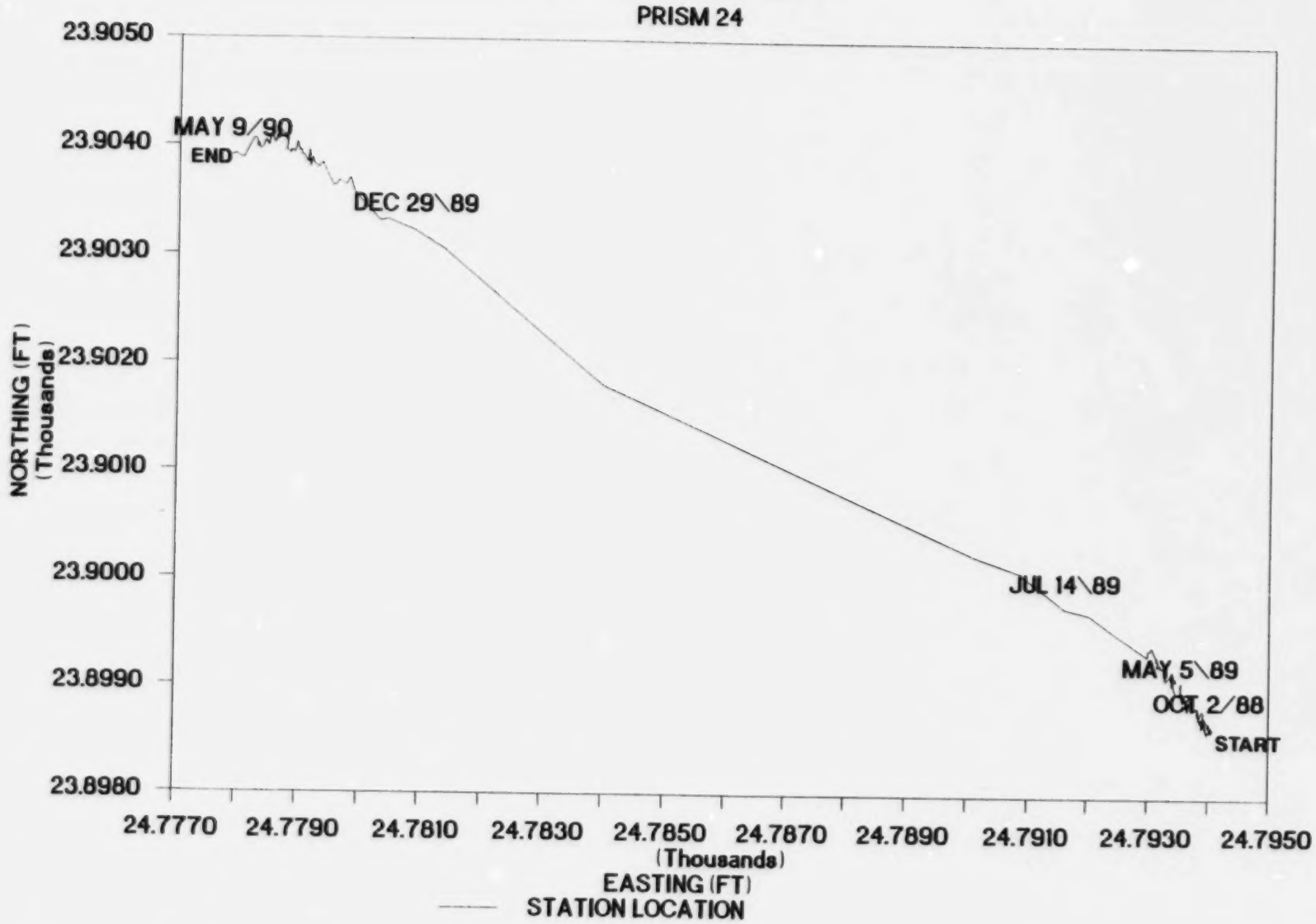
PRISM 24
23.9050
23.9040
23.9030
23.9020
23.9010
23.9000
23.8990
23.8980
NORTHING (FT)
(Thousands)
MAY 9/90
END
DEC 29\89
JUL 14\89
MAY 5\89
OCT 2/88
START
24.7770
24.7790
24.7810
24.7830
24.7850
24.7870
24.7890
24.7910
24.7930
24.7950
(Thousands)
EASTING (FT)
STATION LOCATION

RELATIVE MOVEMENT VS TIME

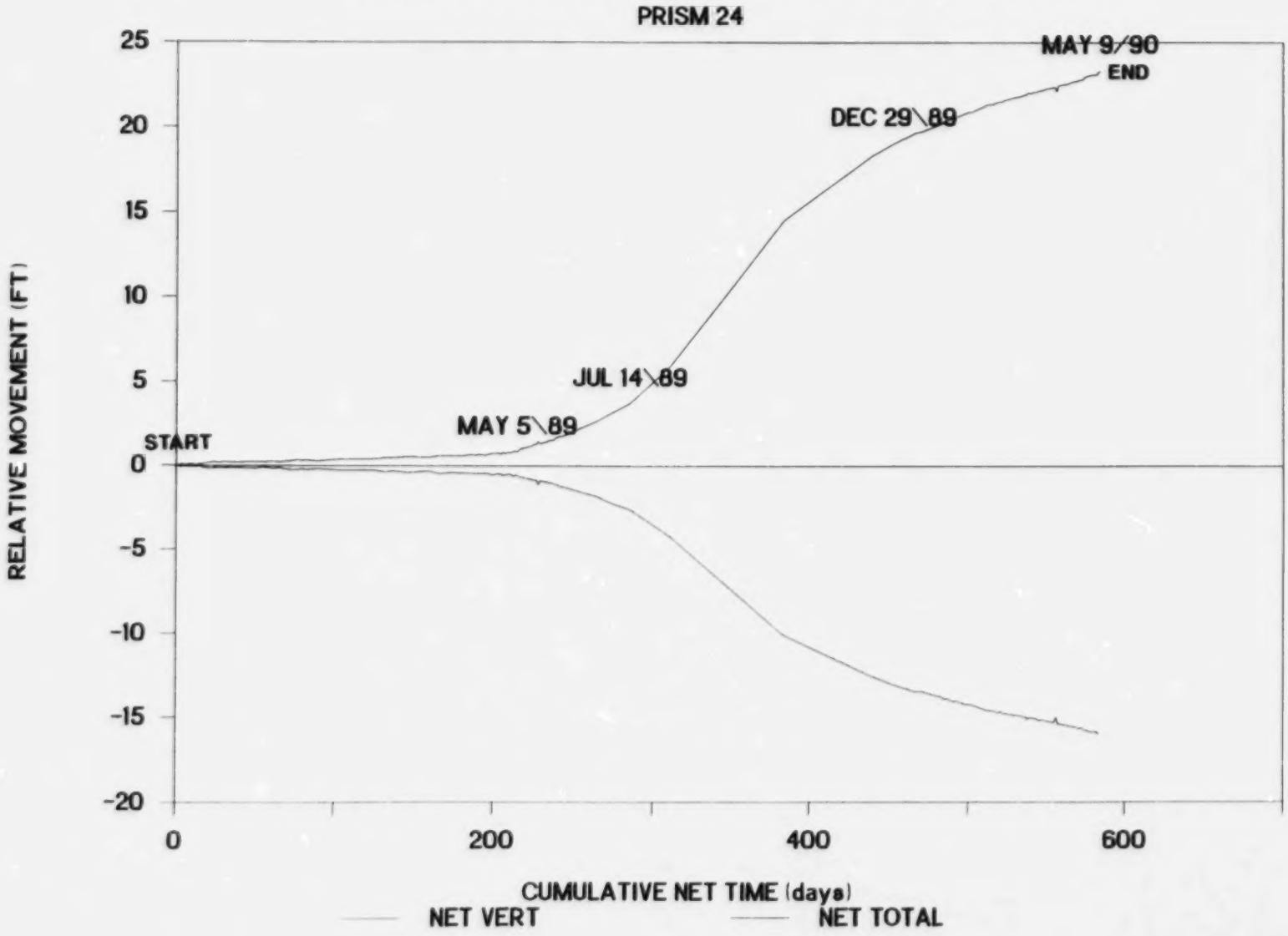

WANDER PLOT

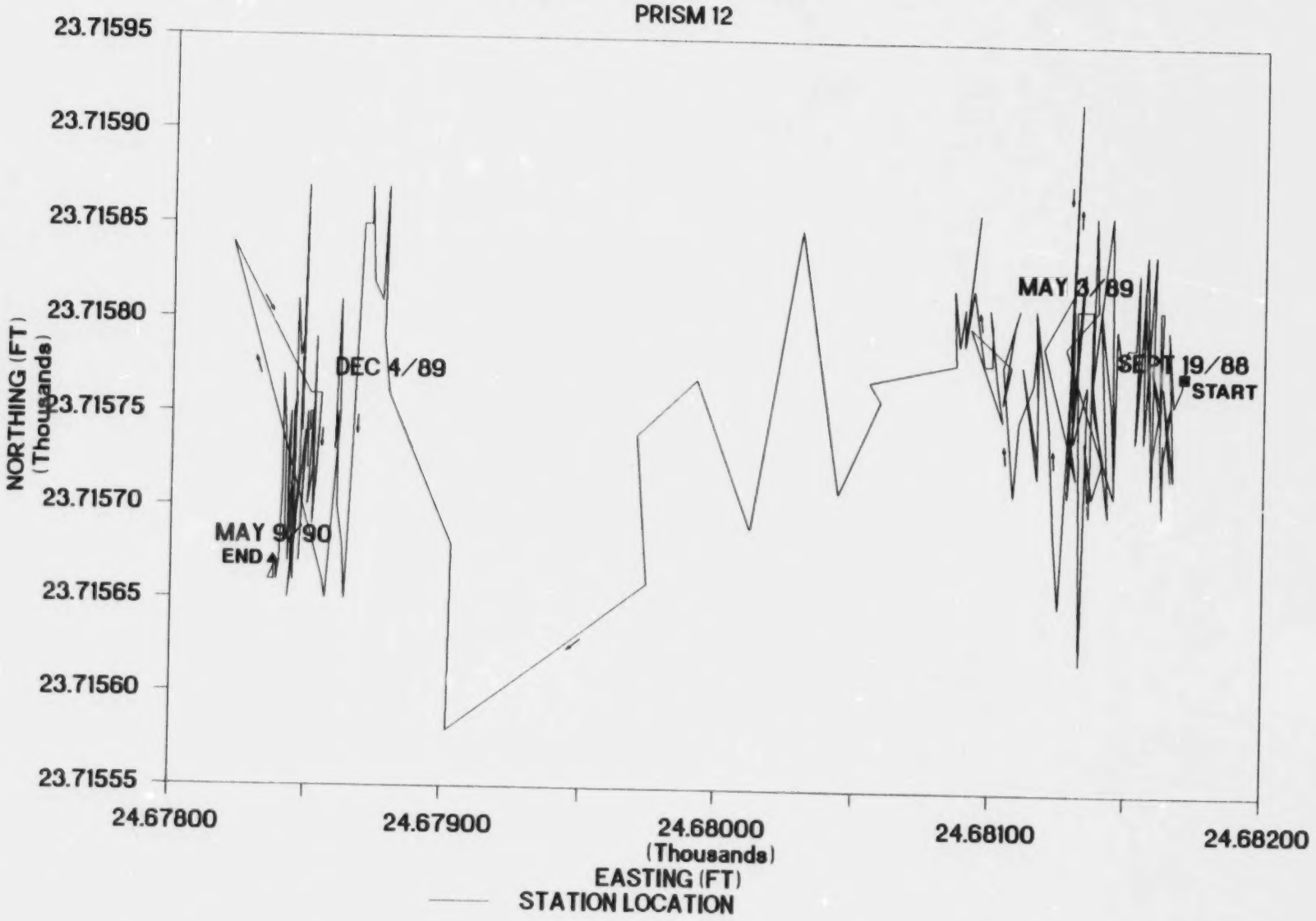
PRISM 12
23.71595
23.71590
23.71585
23.71580
23.71575
23.71570
23.71565
23.71560
23.71555
NORTHING (FT)
(Thousands)
DEC 4/89
MAY 3/89
SEPT 19/88
START
MAY 9/90
END
24.67800
24.67900
24.68000
24.68100
24.68200
(Thousands)
EASTING (FT)
STATION LOCATION

RELATIVE MOVEMENT VS TIME

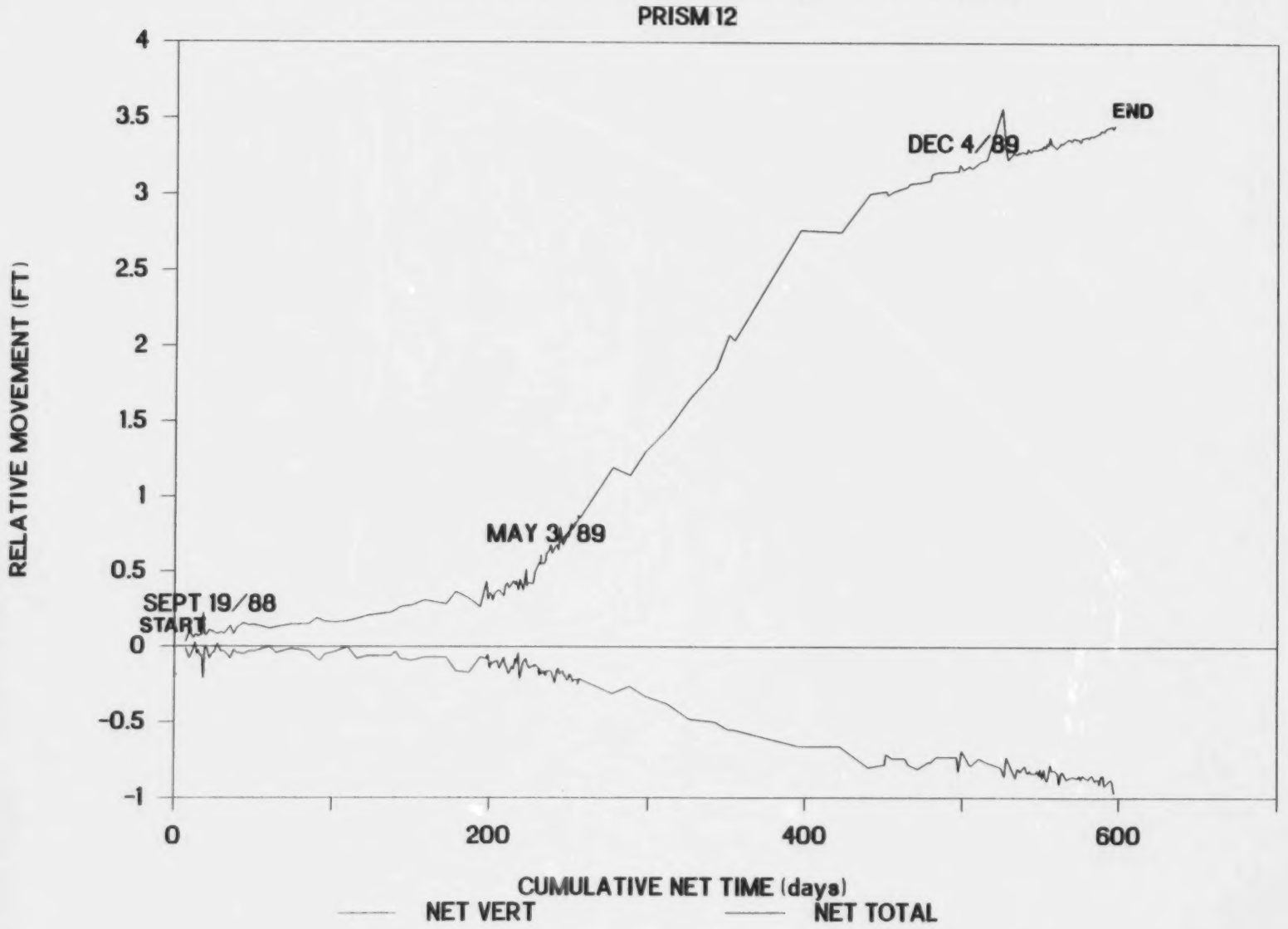

WANDER PLOT

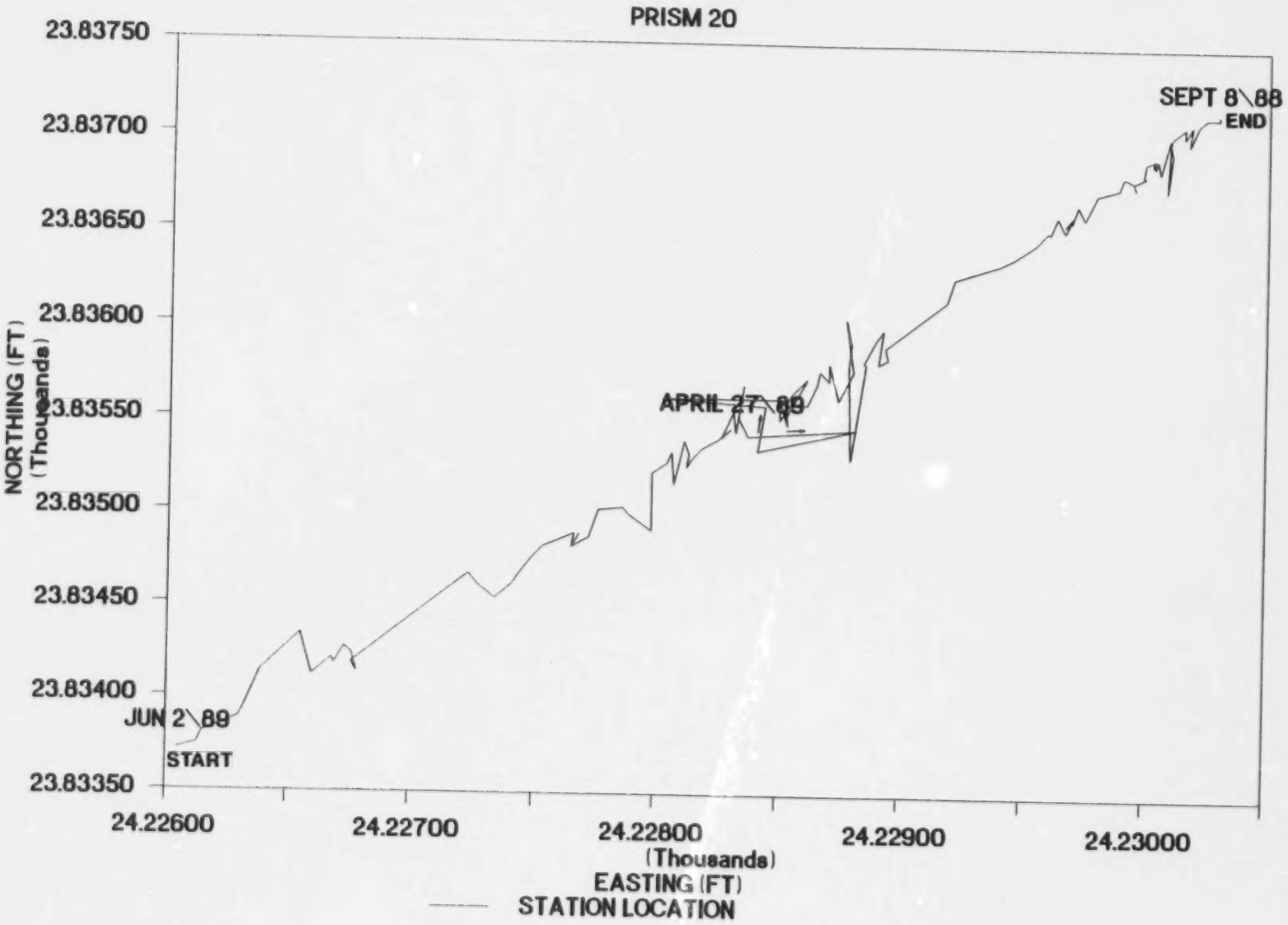
PRISM 20
23.83750
23.83700
23.83650
23.83600
23.83550
23.83500
23.83450
23.83400
23.83350
NORTHING (FT)
(Thousands)
SEPT 8\88
END
APRIL 27 89
JUN 2\89
START
24.22600
24.22700
24.22800
24.22900
24.23000
(Thousands)
EASTING (FT)
STATION LOCATION

RELATIVE MOVEMENT VS TIME

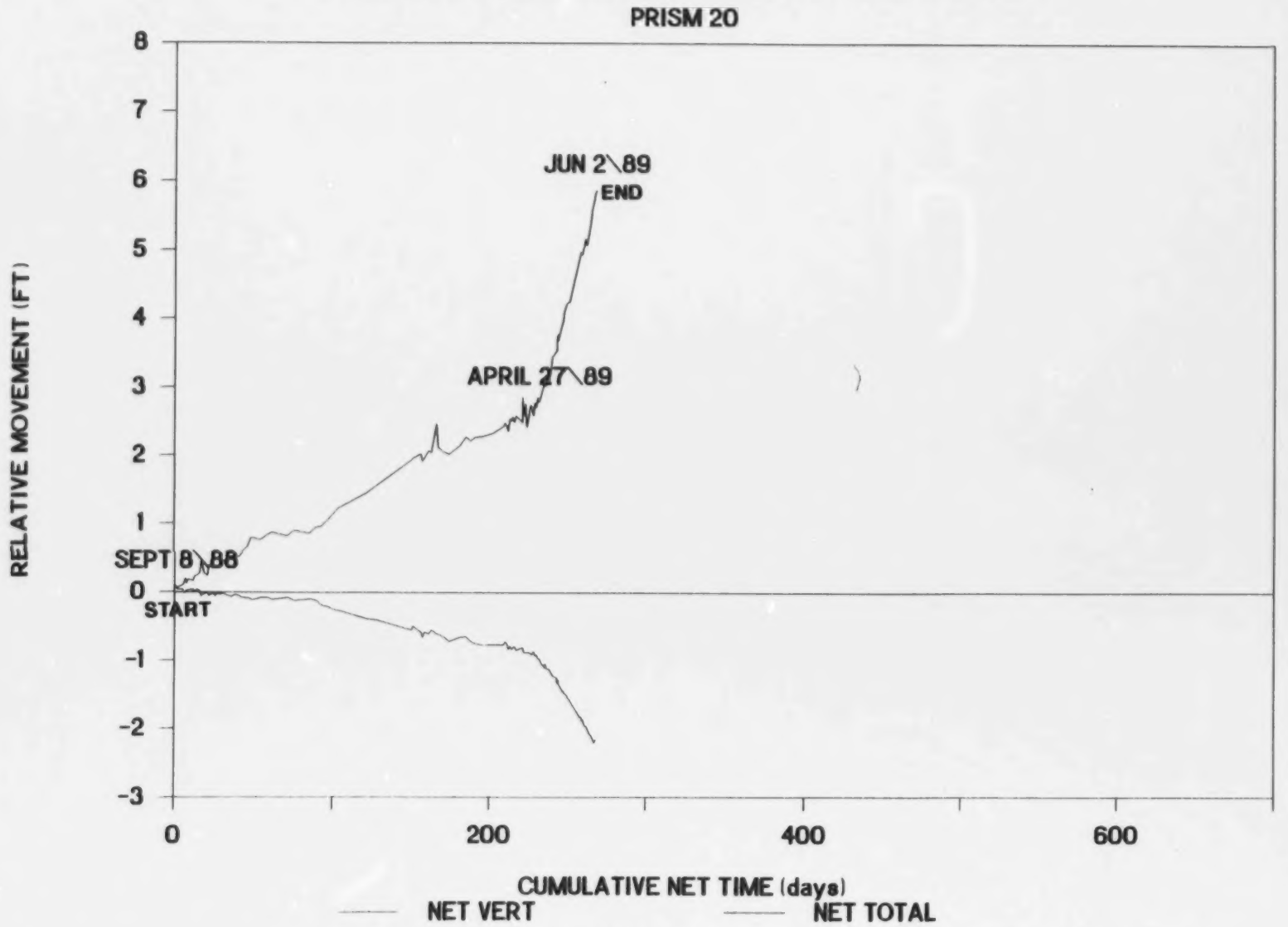

WANDER PLOT

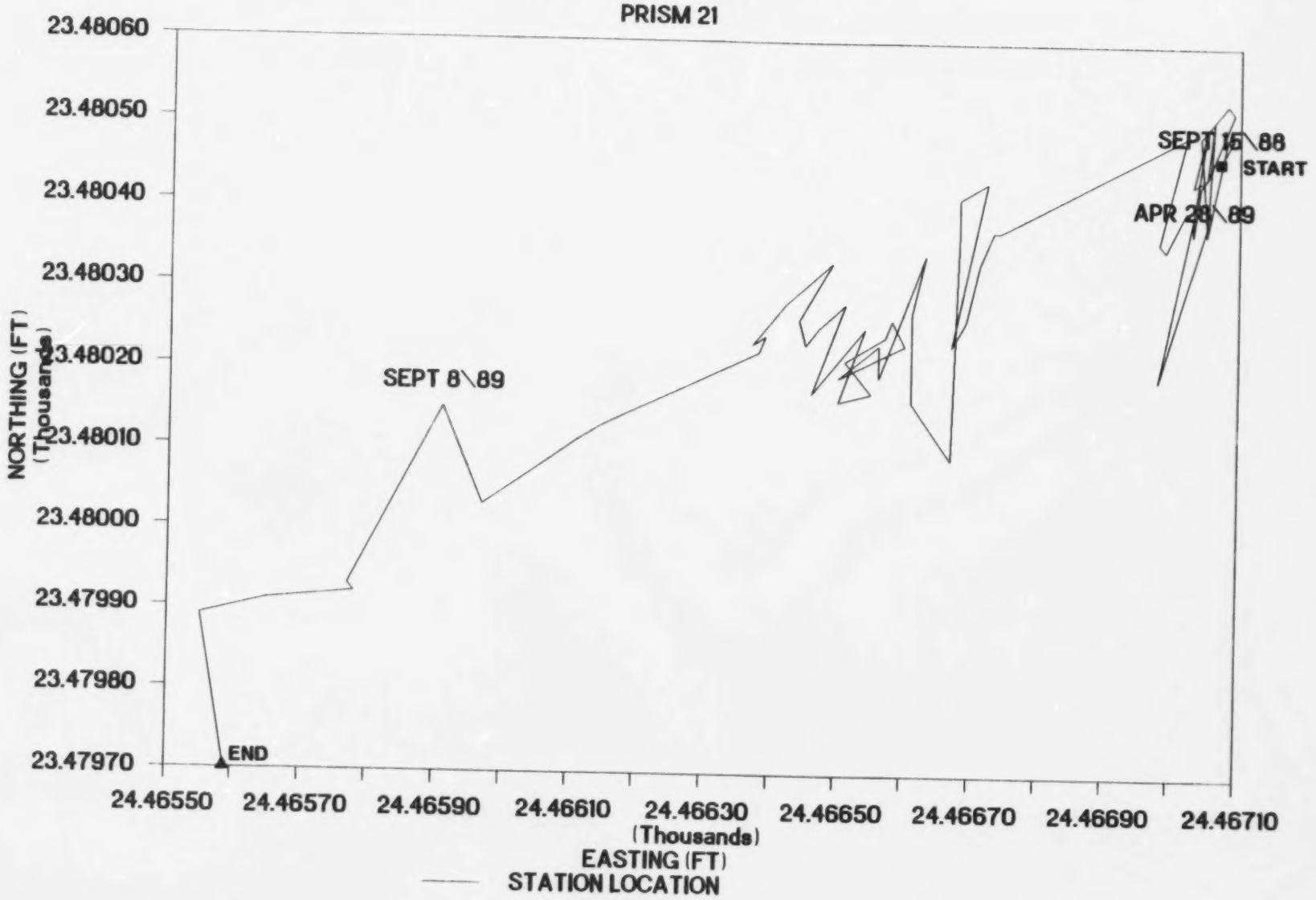
PRISM 21
23.48060
23.48050
23.48040
23.48030
23.48020
23.48010
23.48000
23.47990
23.47980
23.47970
NORTHING (FT)
(Thousands)
SEPT 15\88
START
APR 28\89
SEPT 8\89
END
24.46550
24.46570
24.46590
24.46610
24.46630
24.46650
24.46670
24.46690
24.46710
(Thousands)
EASTING (FT)
STATION LOCATION

RELATIVE MOVEMENT VS TIME

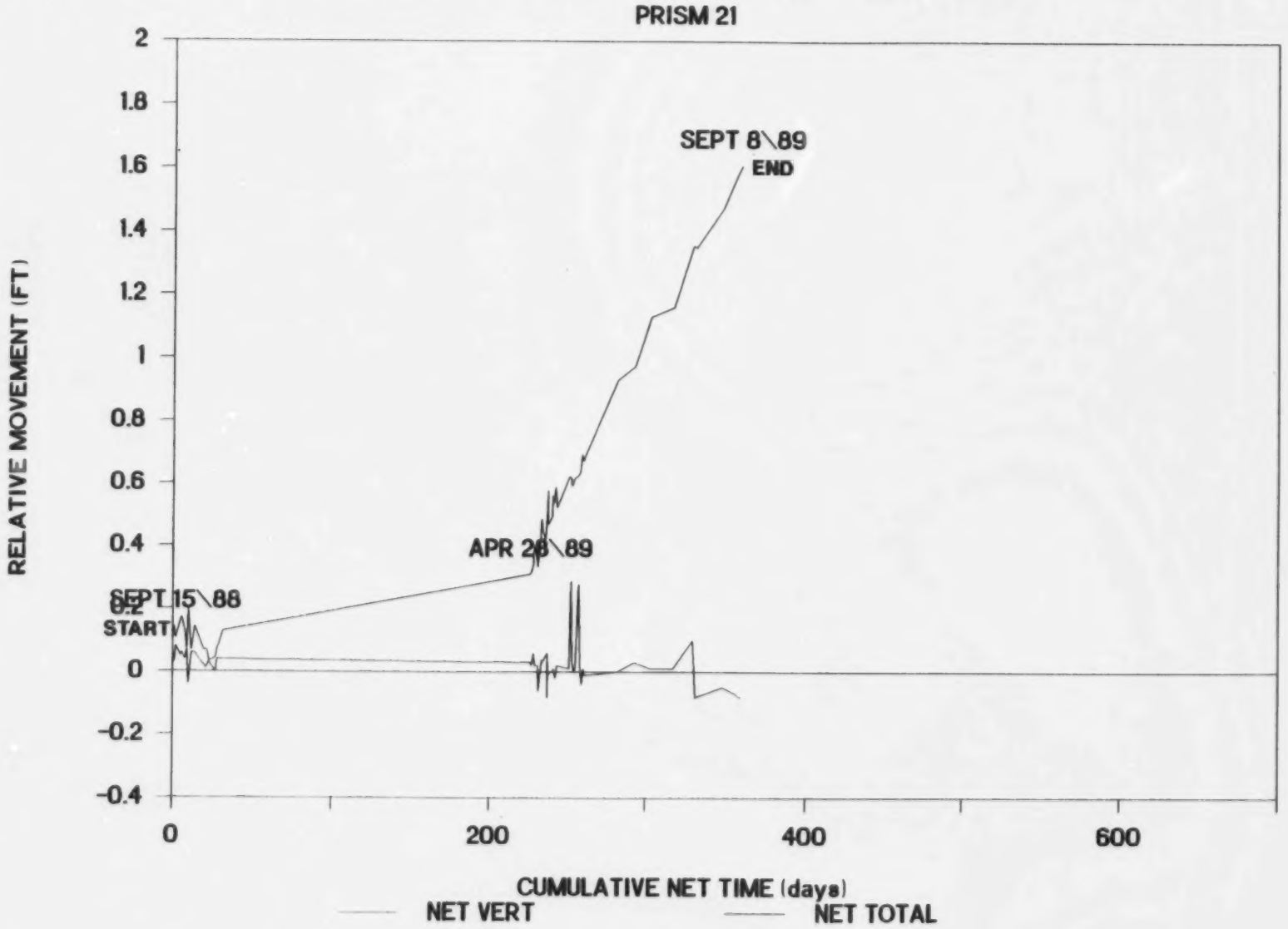

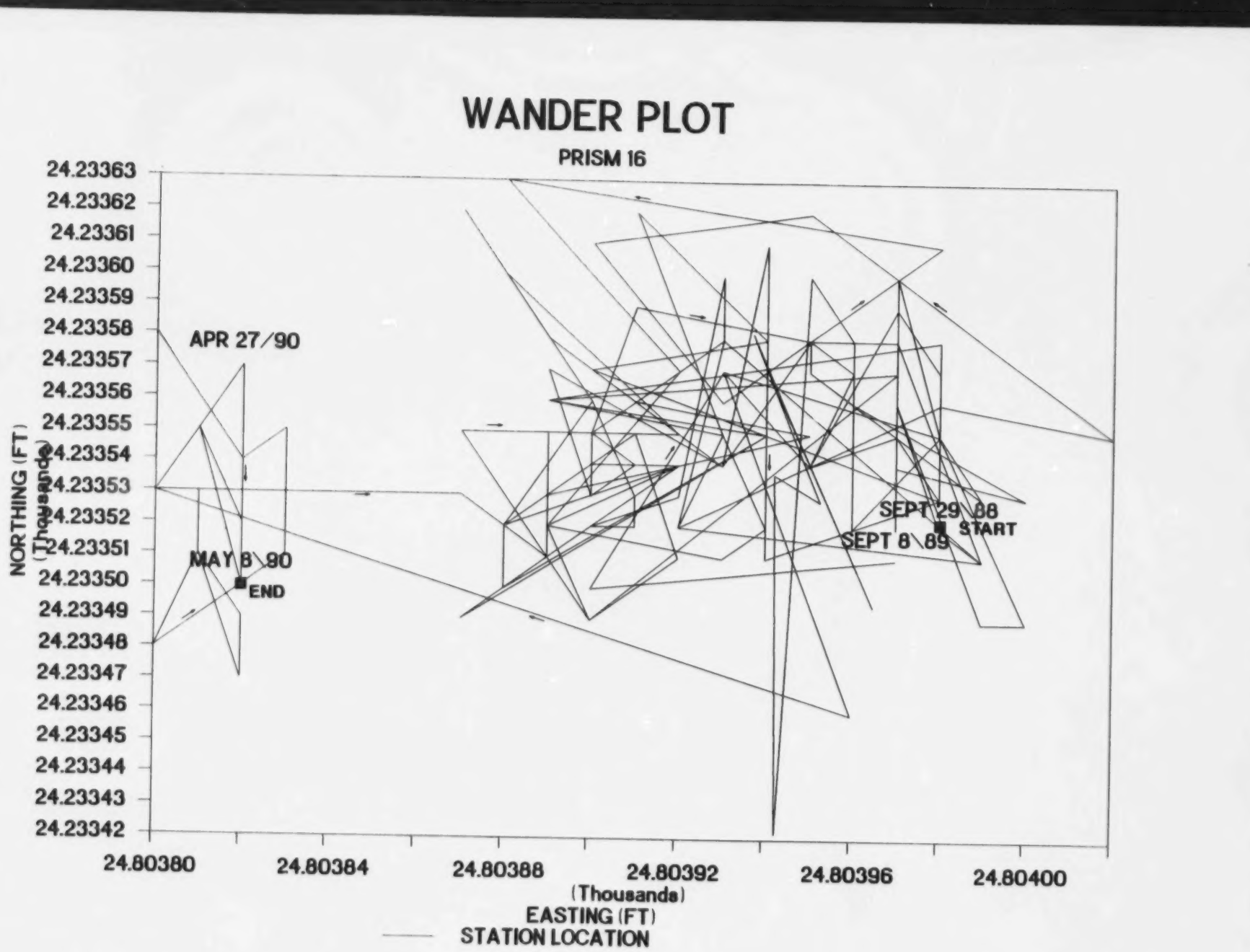
WANDER PLOT
PRISM 16
24.23363
24.23362
24.23361
24.23360
24.23359
24.23358
24.23357
24.23356
24.23355
24.23354
24.23353
24.23352
24.23351
24.23350
24.23349
24.23348
24.23347
24.23346
24.23345
24.23344
24.23343
24.23342
NORTHING (FT)
(Thousands)
APR 27/90
MAY 8\90
END
SEPT 29\88
START
SEPT 8\89
24.80380
24.80384
24.80388
24.80392
24.80396
24.80400
(Thousands)
EASTING (FT)
STATION LOCATION

RELATIVE MOVEMENT VS TIME

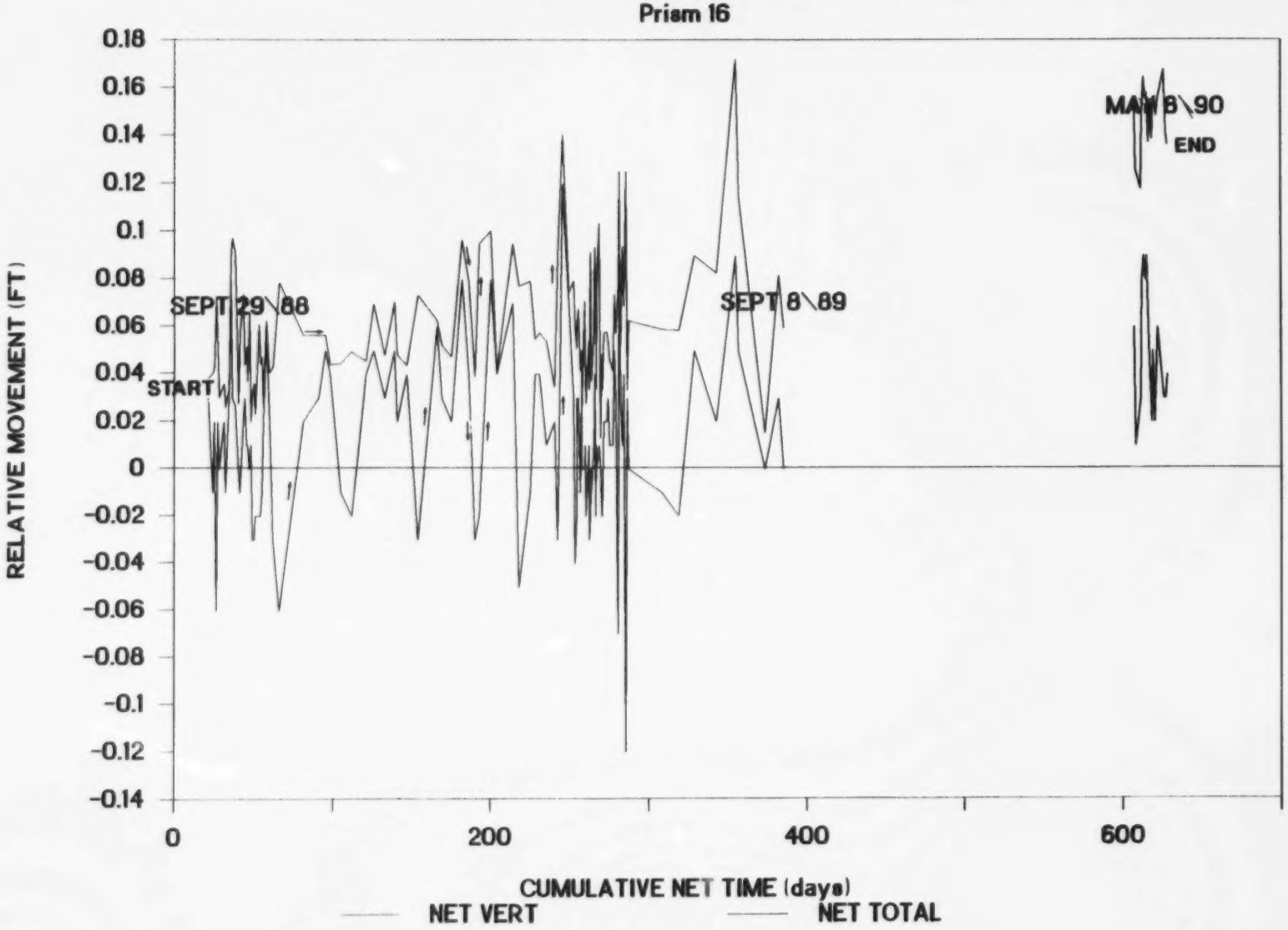

WANDER PLOT

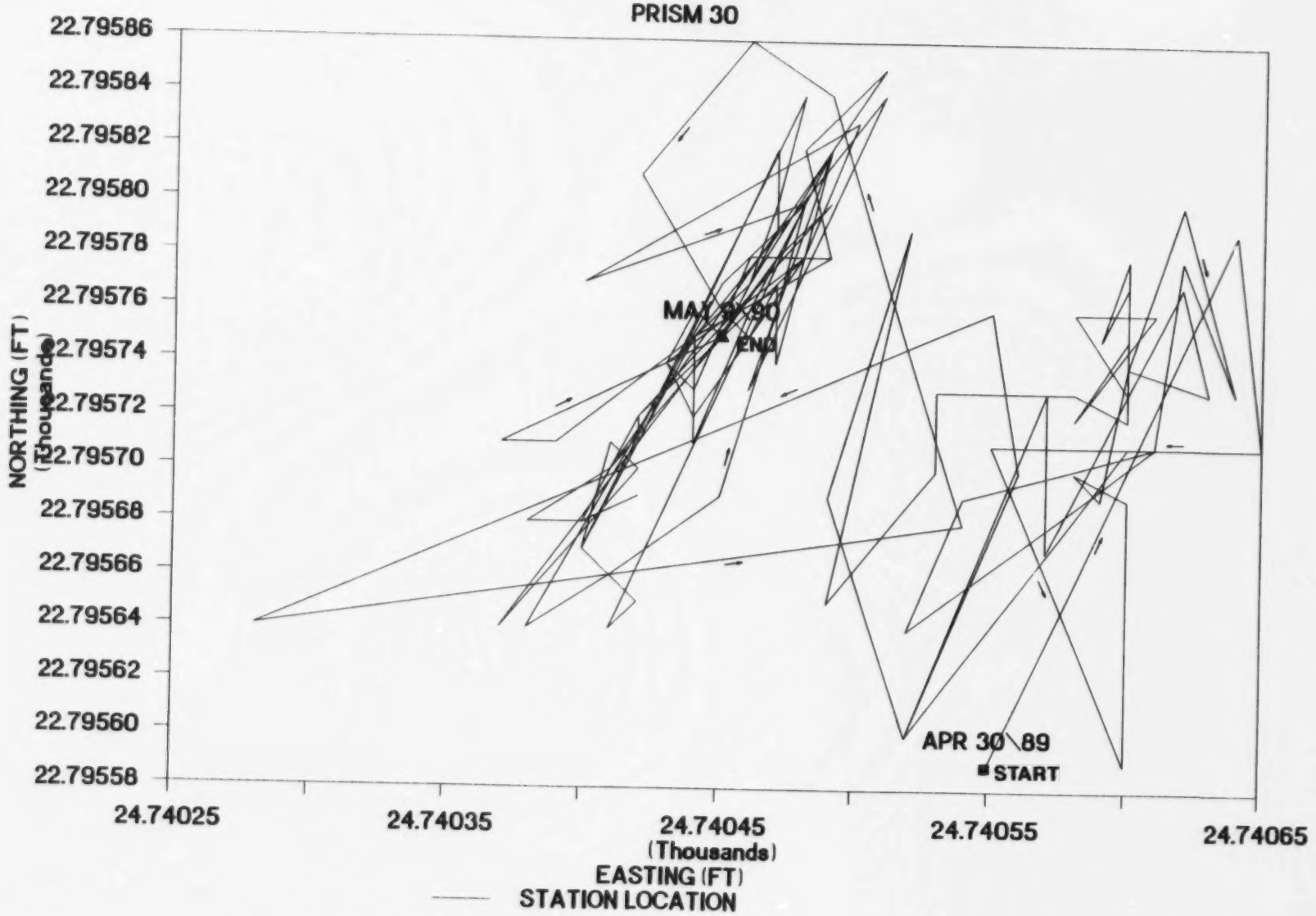
PRISM 30
22.79586
22.79584
22.79582
22.79580
22.79578
22.79576
22.79574
22.79572
22.79570
22.79568
22.79566
22.79564
22.79562
22.79560
22.79558
NORTHING (FT)
(Thousands)
MAY 1 '90
END
APR 30 '89
START
24.74025
24.74035
24.74045
24.74055
24.74065
(Thousands)
EASTING (FT)
STATION LOCATION

RELATIVE MOVEMENT VS TIME

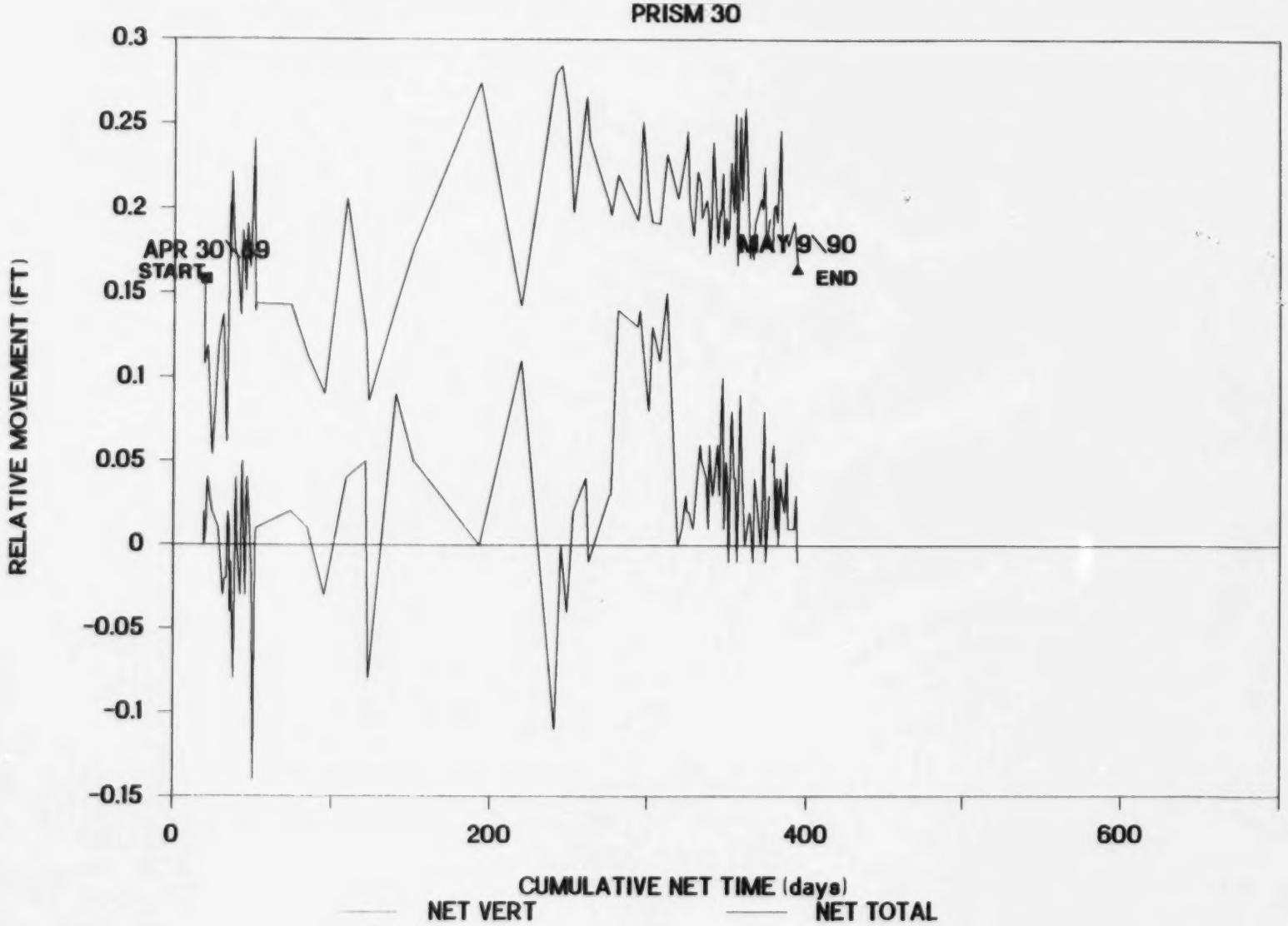

APPENDIX C

ANALYSIS METHOD AND RESULTS FOR THE THREE DIMENSIONAL LIMIT EQUILIBRIUM BACK ANALYSIS

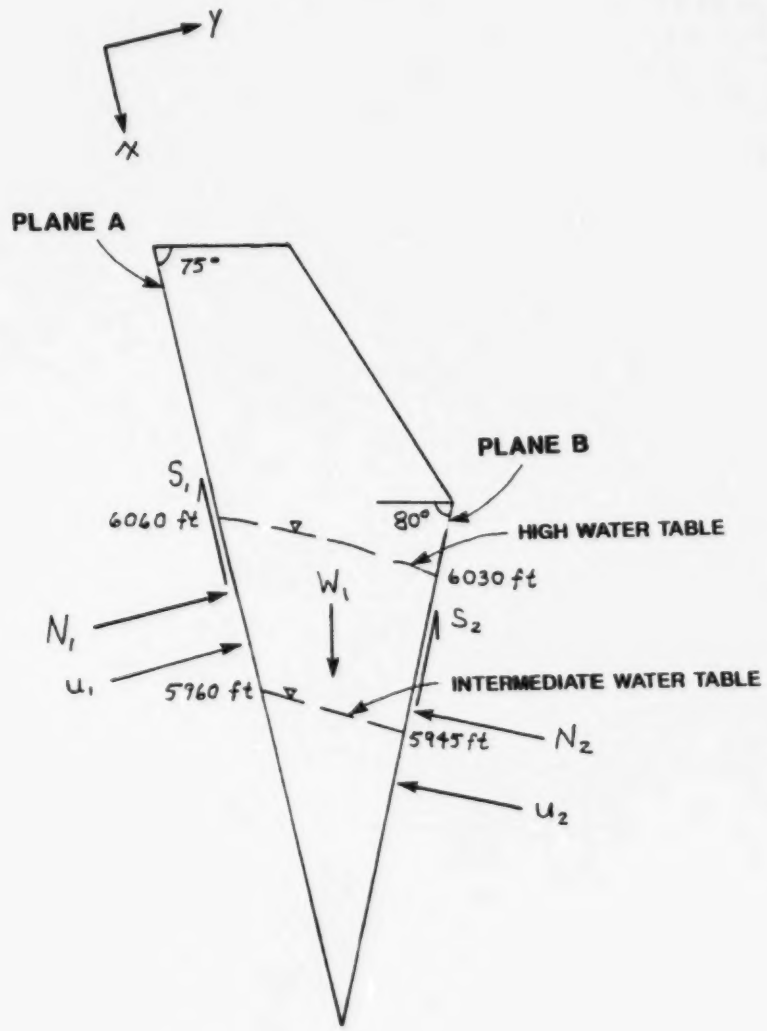

SCALE 1:100

NOTE: (-) RESTORING FORCES
(+) DRIVING FORCES

F BLOCK 1 N_1 (lb) = 1.14×10^9

AREA ft²

A = 2.05×10^5

B = $1.\_ \times 10^5$

...BEL... ...WATER ... (ft)

= $.23 \times 10$

= 2.1×10^5

...BEL... MED ... WATER ... = ... (ft)

A = 6.95 ...

B = 4.13 ...

...

...

...ABLE

...

26. ...

...ABLE

$$S_1 = (N_1 - u_1) \cdot \tan \phi_A \qquad S_2 = (N_2 - u_2) \tan \phi_B$$

$$u_1 = \frac{\gamma_w \cdot H_w \cdot A_{N(1)}}{3} \qquad u_2 = \frac{\gamma_w \cdot H_w \cdot A_{N(2)}}{3}$$

FOR LIMITING EQUILIBRIUM OF BLOCK 1

$$\Sigma F_x = 0 \qquad \Sigma F_y = 0$$

$$\Sigma F_x = N_1 \sin 75 - S_1 - N_2 \sin 25 - S_2 \cos 25$$

$$\Sigma F_y = -N_1 \cos 75 + N_1 - u_1 - S_2 \sin 25 - (N_2 - u_2) \cos 25$$

SUBSTITUTING FOR S_1 AND S_2 AND SOLVING FOR N_2 THE NORMAL COMPONENT OF FORCE TRANSFERRED TO BLOCK 2:

$$N_2 = \frac{N_1 (\cos 75 \cdot \tan \phi_A - \sin 75) - (-C_A A_1 + u_2 \tan \phi_B \cos 25 - C_B A_2 \cos 25 + C_B A_2 \sin 25 \tan \phi_A + u_2 \cos 25 \tan \phi_A)}{\tan \phi_A (\sin 25 \tan \phi_B - \cos 25) - (\sin 25 + \tan \phi_B \cos 25)}$$

FIG. C1

CANMET/SUPPLY AND SERVICES CANADA CASSIAR OPEN PIT SLOPE DEFORMATION STUDY	PITEAU ASSOCIATES GEOTECHNICAL CONSULTANTS VANCOUVER CALGARY		
THREE DIMENSIONAL LIMIT EQUILIBRIUM ANALYSIS	FREE BODY DIAGRAM OF BLOCK 1	BY: LAS	DATE: MAY 90
		APPROVED:	DWG:

JOB NUMBER

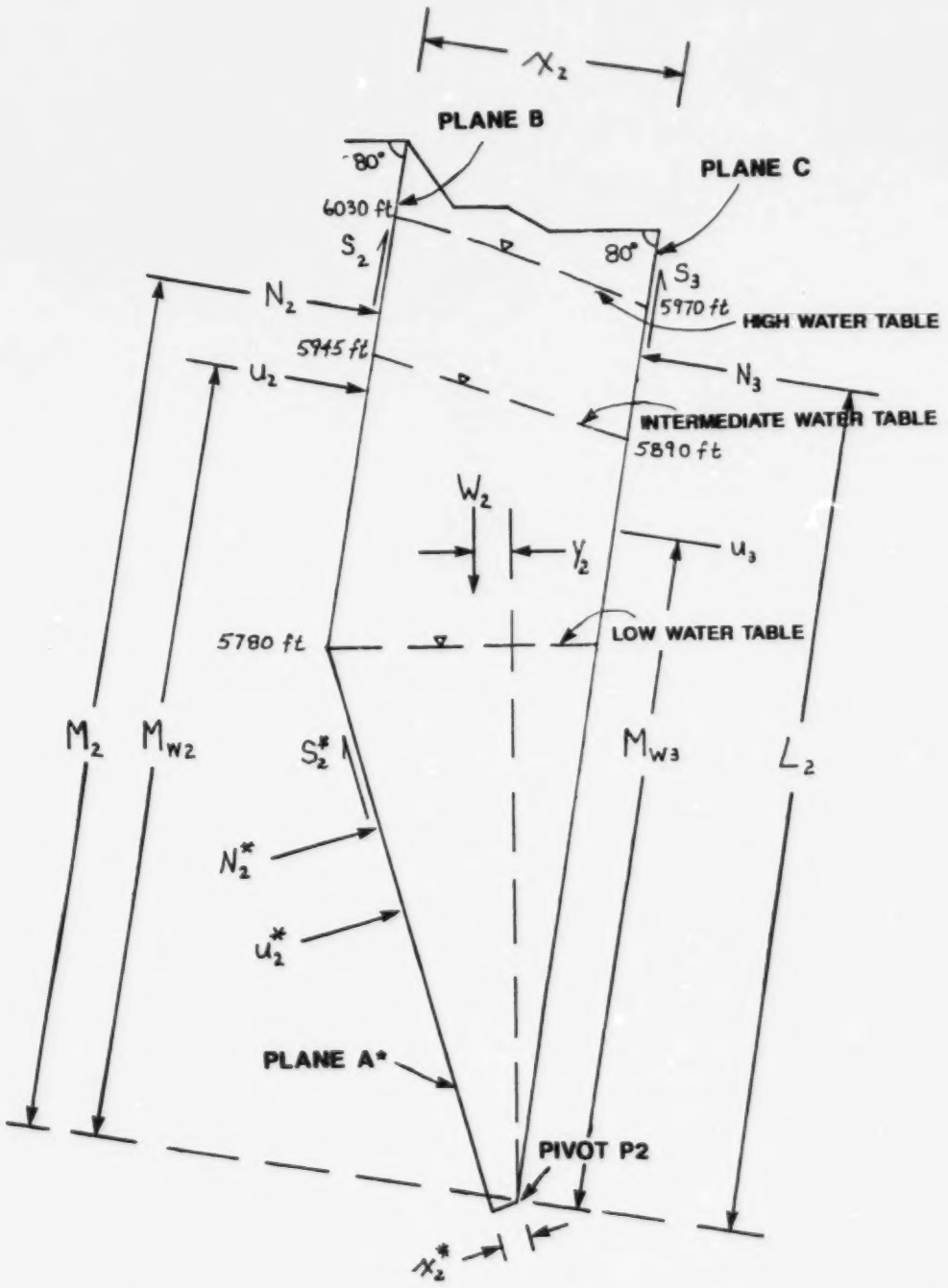

SCALE 1:100

WEIGHT OF BLOCK 2,

SURFACE AREA (ft

PLANE B = 9.20×

PLANE A* = 4.20×

PLANE C = 1.02×

SURFACE AREA BELOW

PLANE B = 6.27×

PLANE A* = 4.20×

PLANE C = 7.16×

SURFACE AREA BELOW

PLANE B = 4.13×

PLANE A* = 4.20×

PLANE C = 6.52×

SURFACE AREA BELOW

PLANE A* = 4.20×

PLANE C = 3.40

COHESION (psf)

C_A, C_B, C_C = VARIA

FRICTION ANGLE (deg

ϕ_A, ϕ_B, ϕ_C = VARIA

MOMENT ARM (ft)

$M_2 = 510$

$L_2 = 510$

$Y_2 = 20$

$X_2 = 150$

BLOCK 2, W_2 (lb) = $28^{9} \cdot 10^{7}$

AREA (ft^2)

$B = 9.20 \times 10^{4}$

$A^* = 4.20 \times 10^{4}$

$C = 1.02 \times 10^{5}$

REA BELOW HIGH WATER LEVEL (ft^2)

$B = 8.27 \times 10^{4}$

$A^* = 4.20 \times 10^{4}$

$C = 9.16 \times 10^{4}$

REA BELOW MEDIUM WATER LEVEL (ft^2)

$B = 7.13 \times 10^{4}$

$A^* = 4.20 \times 10^{4}$

$C = 6.52 \times 10^{4}$

AREA BELOW LOW WATER LEVEL (ft^2)

$A^* = 4.20 \times 10^{4}$

$C = 3.40 \cdot 10^{4}$

(psf)

c_c = VARIABLE

NGLE (deg)

, ϕ_c = VARIABLE

(ft)

$$S_2 = (N_2 - U_2) \tan \phi_B + C_B A_B$$

$$S_3 = (N_3 - u_3) \tan \phi_C + C_C A_C$$

$$S_2^* = (N_2^* - u_2^*) \tan \phi_A + C_A A_A^*$$

$$u_2 = \frac{\gamma_N \cdot H_N \cdot A_{N(B)}}{3} \qquad u_2^* = \gamma_N A_2^* \left(\frac{H_{w2}}{3} \right) + \gamma_N H_{w} A_2^*$$

$$u_3 = \frac{\gamma_N \cdot H_N \cdot A_{N(C)}}{3}$$

FOR MOMENT EQUILIBRIUM AROUND PIVOT POINT P_2

$$\Sigma M_{P_2} = 0$$

$$\Sigma M_{P_2} = N_2 \cdot M_2 + U_2 \cdot M_{W2} - S_2 \cdot x_2 + N_2^* \cdot H_2^* - S_2^* \cdot x_2^* + U_2^* \cdot M_{N2}^* - W_2 \cdot Y_2 - U_3 \cdot M_{W3} - N_3 \cdot L_3$$

ASSUMING $\Delta x^* \approx 0$ AND WE GET ONLY SEPARATION ON PLANE A THEN $N_2^* H_2^* - S_2^* x^* = 0$ AND

$$N_3 = \frac{N_2 \cdot M_2 + U_2 \cdot M_{W2} - x_2 \left[(N_2 - u_2) \tan \phi_B + C_B A_B \right] + U_2^* \cdot M_{W2}^* - W_2 \cdot l_2 - U_3 M_{W3}}{L_3}$$

FIG. C2

CANMET/SUPPLY AND SERVICES CANADA CASSIAR OPEN PIT SLOPE DEFORMATION STUDY	PITEAU ASSOCIATES GEOTECHNICAL CONSULTANTS VANCOUVER CALGARY		
THREE DIMENSIONAL LIMIT EQUILIBRIUM ANALYSIS	FREE BODY DIAGRAM OF BLOCK 2	BY: LAS	DATE: MAY 90
		APPROVED:	DWG:

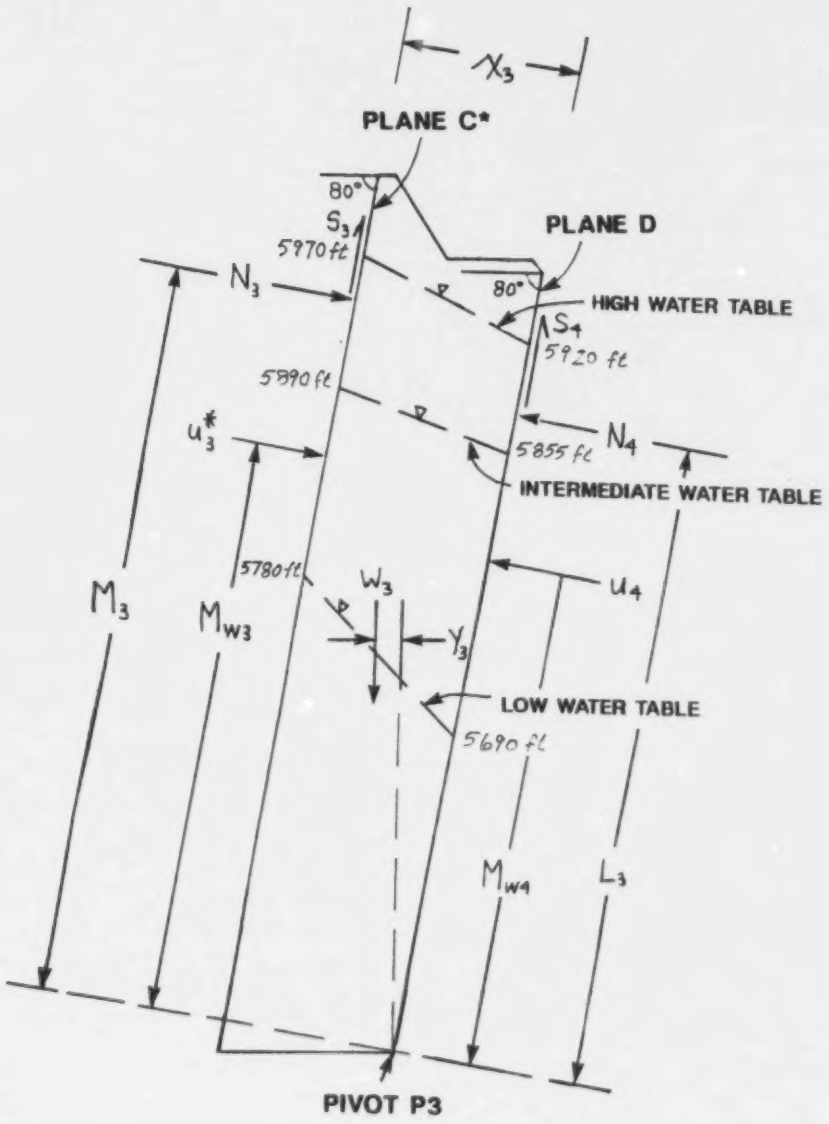

WEIGHT OF BLOCK 3 W_3 (lb)

SURFACE AREA (sq ft)

PLANE C = 9.3 × 10⁴

PLANE D = 6.28 × 10⁴

SURFACE AREA BELOW HIGH WATER

PLANE C* = 4.70 × 10⁴

PLANE D = 7.28 × 10⁴

SURFACE AREA BELOW INTERMEDIATE WATER

PLANE C* = 3.45 × 10⁴

PLANE D = 8.72 × 10⁴

SURFACE AREA BELOW LOW WATER

PLANE C* = 2.32 × 10⁴

PLANE D = 9.87 × 10⁴

CONSTANTS

C_0 = [illegible] lb/ft³

FRICTION ANGLE [illegible]°

D_s = [illegible] ft

MOMENT ARM (ft)

M_3 = 5

L_3 = 370

l_3 = 15

X_3 = 100

SCALE 1:100

$S_3 = (N_3 - U_3) \tan\phi_c + c_c \cdot A_c$ $S_4 = (N_4 - U_4) \tan\phi_c + c_c \cdot A_c$

$U_3 = \frac{\gamma_w \cdot h_w \cdot A_{w3}}{3}$ $U_4 = \frac{\gamma_w \cdot h_w \cdot A_{w4}}{3}$

WATER FORCE APPLIED AT HEIGHT h_w ABOVE BASE OF BLOCK

$$W = \frac{5 \cdot H_m \cdot \cos(\quad - 30)}{4}$$

FOR MOMENT EQUILIBRIUM AT PIVOT POINT P_2

$$\Sigma M_{P_2} = 0$$

$$\Sigma M_{P_2} = N_3 M_3 + U_3 - N_3 - S_3 \cdot x_3 - W_3 \quad - N_4 L_4 - U_4 -$$

$$N_4 = \frac{N_3 M_3 + U_3 - N_3 - x_3 \left[(N_3 - U_3) \tan\phi_c + c_c \cdot \right] - W_3 \quad - U_4 H_w}{L_4}$$

FIG. C3

CANMET/SUPPLY AND SERVICES CANADA CASSIAR OPEN PIT SLOPE DEFORMATION STUDY	PITEAU ASSOCIATES GEOTECHNICAL CONSULTANTS VANCOUVER CALGARY		
THREE DIMENSIONAL LIMIT EQUILIBRIUM ANALYSIS	FREE BODY DIAGRAM OF BLOCK 3	BY: LAS	DATE: MAY 90
		APPROVED:	DWG:

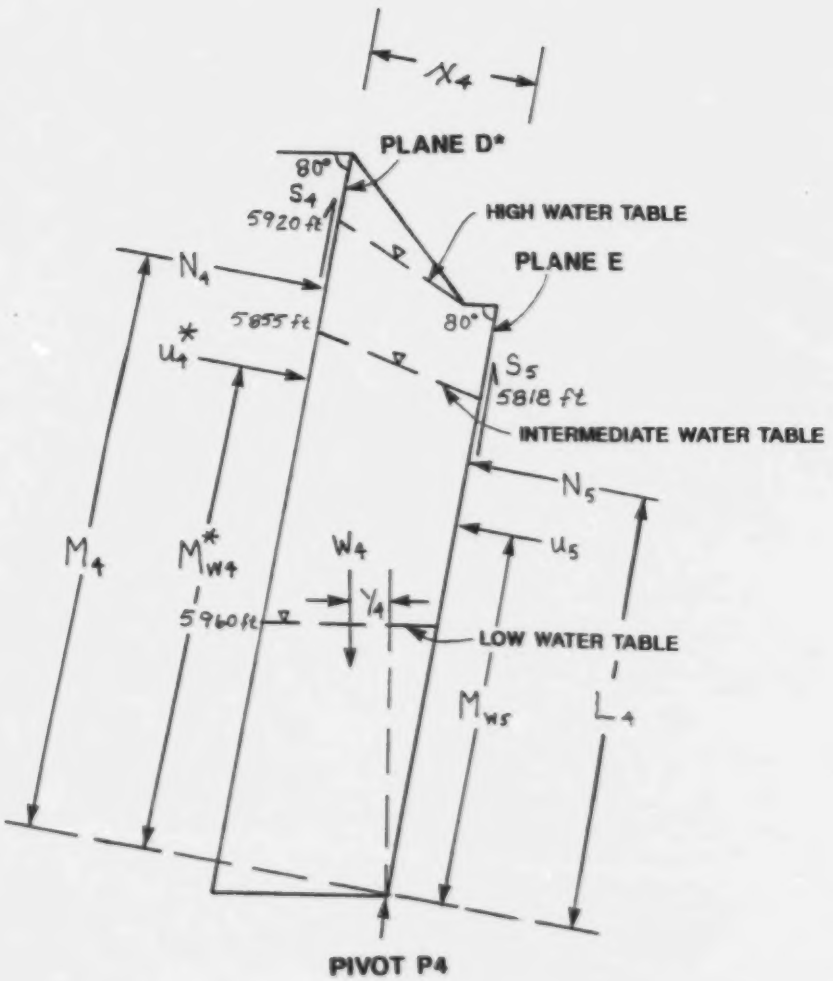

SCALE 1:100

WEIGHT OF BLOCK 4, N_4 (lb) =

SURFACE AREA (ft²)

PLANE D* = 6.20×10^{4}

PLANE E = 2.23×10^{5}

SURFACE AREA BELOW WATER

PLANE D* = 5.31×10^{4}

PLANE E = 2.20×10^{5}

SURFACE AREA ABOVE WATER

PLANE D* = 8.9×10^{3}

PLANE E = 1.57×10^{4}

CONTACT AREA BELOW WATER

PLANE D* = 7.35×10^{3}

PLANE E = 2.16×10^{4}

COHESION (psf)

C_4, C_5 = VARIABLE

FRICTION ANGLE (deg)

ϕ_4, ϕ_5 = VARIABLE

MOMENT ARM (ft)

$M_4 = 3.20$

$L_4 = 250$

$l_4 = 25$

$N_4 = 95$

$S_A = (N_A - U_A) \tan \phi_D - C_D \cdot A_D \qquad S_C = (N_C - U_C) \tan \phi_E - C_E \cdot A_E$

$J_A = \dfrac{\gamma_w \cdot H_w \cdot A_{N(3)}}{3} \qquad J_C = \dfrac{\gamma_w \cdot H_w \cdot A_{N(3)}}{3}$

WATER FORCE APPLIED AT HEIGHT N ABOVE BASE OF PLANE

$$N = \frac{\Sigma \cdot H_N \cdot \cos(90° - \Sigma)}{3}$$

FOR MOMENT EQUILIBRIUM AT PIVOT POINT P_A

$$\Sigma M_{PA} = 0$$

$$\Sigma M_{PA} = N_A \cdot M_A - U_A \cdot M_{NA} - S_A \cdot M_A - N_A \cdot L_A - N_C \cdot L_C - L_{NC} - M_C$$

$$N_C = \frac{N_A \cdot M_A - U_A \cdot M_{NA} - X \left[(N_A - U_A) \cdot \cos\phi_D + C_D \cdot A_D \right] - N_A \cdot L_A - L_C \cdot M_C}{L_C}$$

FIG. C4

CANMET/SUPPLY AND SERVICES CANADA CASSIAR OPEN PIT SLOPE DEFORMATION STUDY		PITEAU ASSOCIATES GEOTECHNICAL CONSULTANTS VANCOUVER CALGARY	
THREE DIMENSIONAL LIMIT EQUILIBRIUM ANALYSIS	FREE BODY DIAGRAM OF BLOCK 4	BY LAS	DATE MAY 90
		APPROVED	DWG

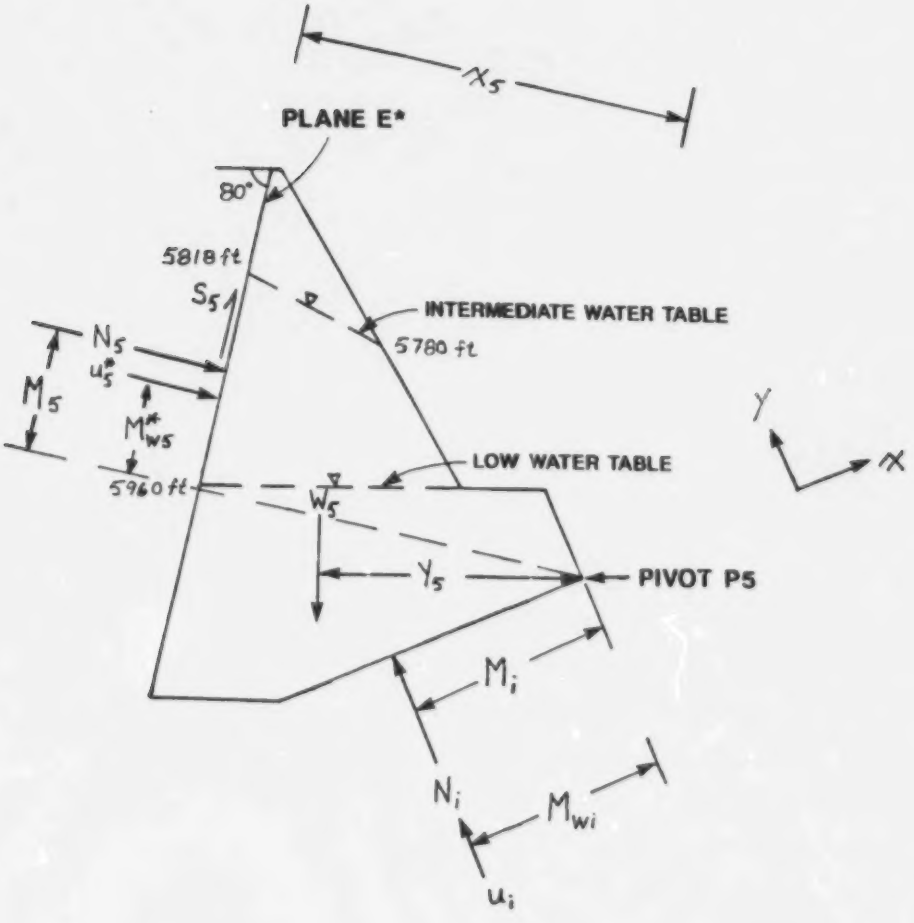
X_5
PLANE E*
80°
5818 ft
S_5
INTERMEDIATE WATER TABLE
5780 ft
N_5
u_5^*
M_5
M_{W5}^*
5960 ft
LOW WATER TABLE
W_5
Y_5
PIVOT P5
M_i
N_i
M_{wi}
u_i
y
x

SCALE 1:100

$C_E = (N_E - u_E)\tan\phi + C_E A_E$

$N_E = \dfrac{\sum N \cdot A_N + \sum N(E^*)}{3}$ $\quad u_i = \dfrac{\sum u \cdot A_{ni} \cdot \cos^2 \alpha}{3}$

WATER FORCE U_i APPLIED AT $\frac{1}{3}$ OF N ABOVE BASE OF PLANE

$N = \dfrac{\frac{1}{2} \cdot \gamma_w \cdot h_w \cdot \sin\alpha \cdot \sec\beta}{2}$

WATER FORCE U_i APPLIED 125 ft. ALONG BASE OF BLOCK FROM PIVOT POINT

SLIDING CASE

$\Sigma F_x = 0$

$\Sigma F_m = S_E \cdot \sin 35 - N_E \cdot \cos 35 - u_E \cos 35 + W_E \cdot \sin 35$
$+ 1.77\, W_E + (0.81\, W_E - U_i)\tan 26.5 + 6.5 A_E C_i$

TOPPLING CASE

$\Sigma M_{PS} = 0$

$\Sigma M_{PS} = N_S \cdot M_E + u_S \cdot M_{WS} - X_S[(N_S - u_S)\tan\phi_E + C_E \cdot A_E]$
$- W_S \cdot Y_E + u_i \cdot M_{wi} + N_i\, M_i$

FIG. C5

CANMET/SUPPLY SERVICES CANADA CASSIAR OPEN PIT SLOPE DEFORMATION STUDY		PITEAU ASSOCIATES GEOTECHNICAL CONSULTANTS VANCOUVER CALGARY	
THREE DIMENSIONAL LIMIT EQUILIBRIUM ANALYSIS	FREE BODY DIAGRAM OF BLOCK 5	BY LAS	DATE MAY 90
		APPROVED	DWG:

APPENDIX D

RESULTS OF TWO DIMENSIONAL NUMERICAL MODELLING USING THE UNIVERSAL DISTINCT ELEMENT CODE (UDEC)

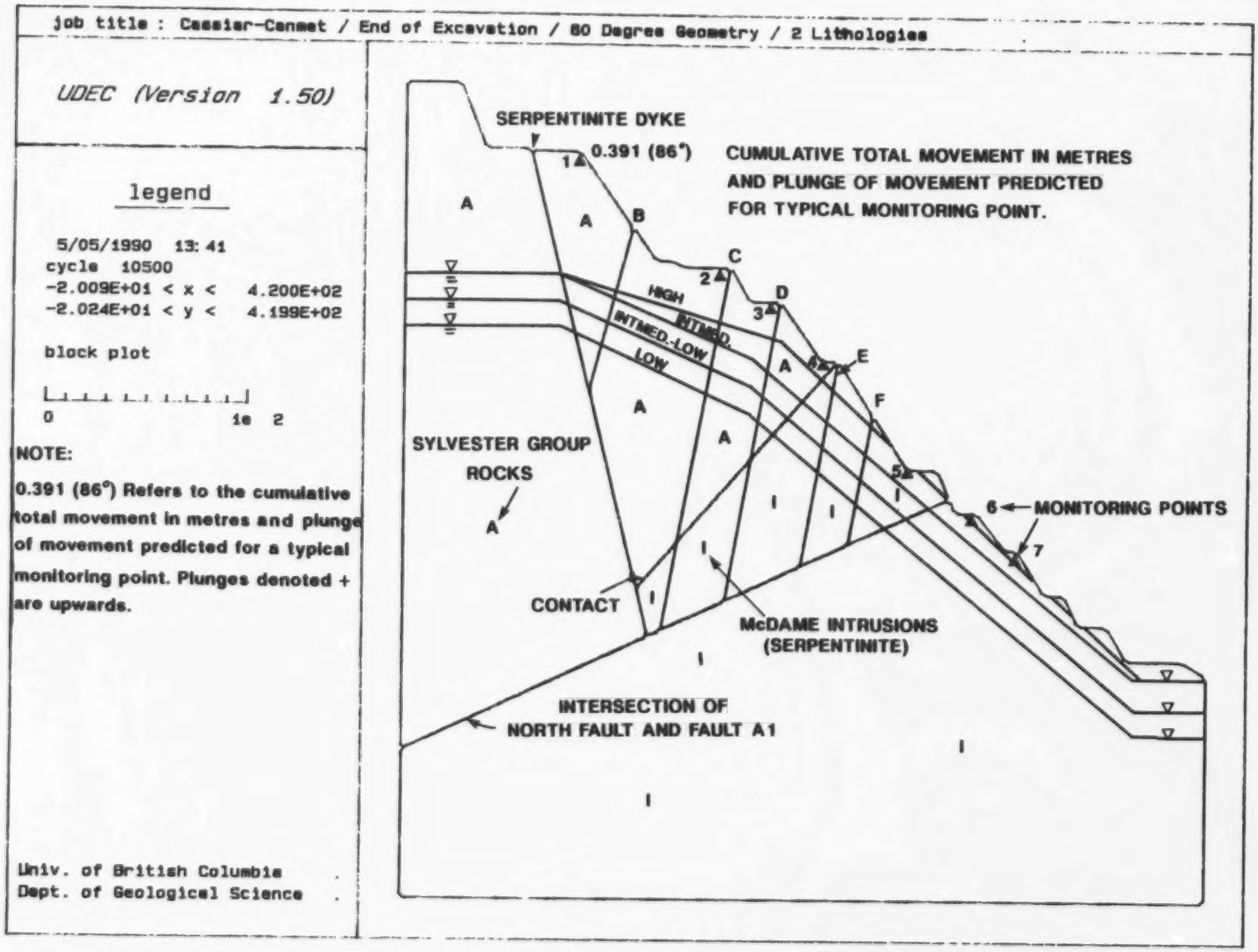
job title : Cassiar-Cemet / End of Excavation / 80 Degree Geometry / 2 Lithologies
UDEC (Version 1.50)
legend
5/05/1990 13:41
cycle 10500
-2.009E+01 < x < 4.200E+02
-2.024E+01 < y < 4.199E+02
block plot
0
1e 2
NOTE:
0.391 (86°) Refers to the cumulative total movement in metres and plunge of movement predicted for a typical monitoring point. Plunges denoted + are upwards.
Univ. of British Columbia
Dept. of Geological Science
SERPENTINITE DYKE
0.391 (86°)
CUMULATIVE TOTAL MOVEMENT IN METRES AND PLUNGE OF MOVEMENT PREDICTED FOR TYPICAL MONITORING POINT.
HIGH
INTMED.
INTMED.-LOW
LOW
SYLVESTER GROUP ROCKS
CONTACT
McDAME INTRUSIONS (SERPENTINITE)
INTERSECTION OF NORTH FAULT AND FAULT A1
MONITORING POINTS

Fig. D1 Slope model used for numerical modelling.

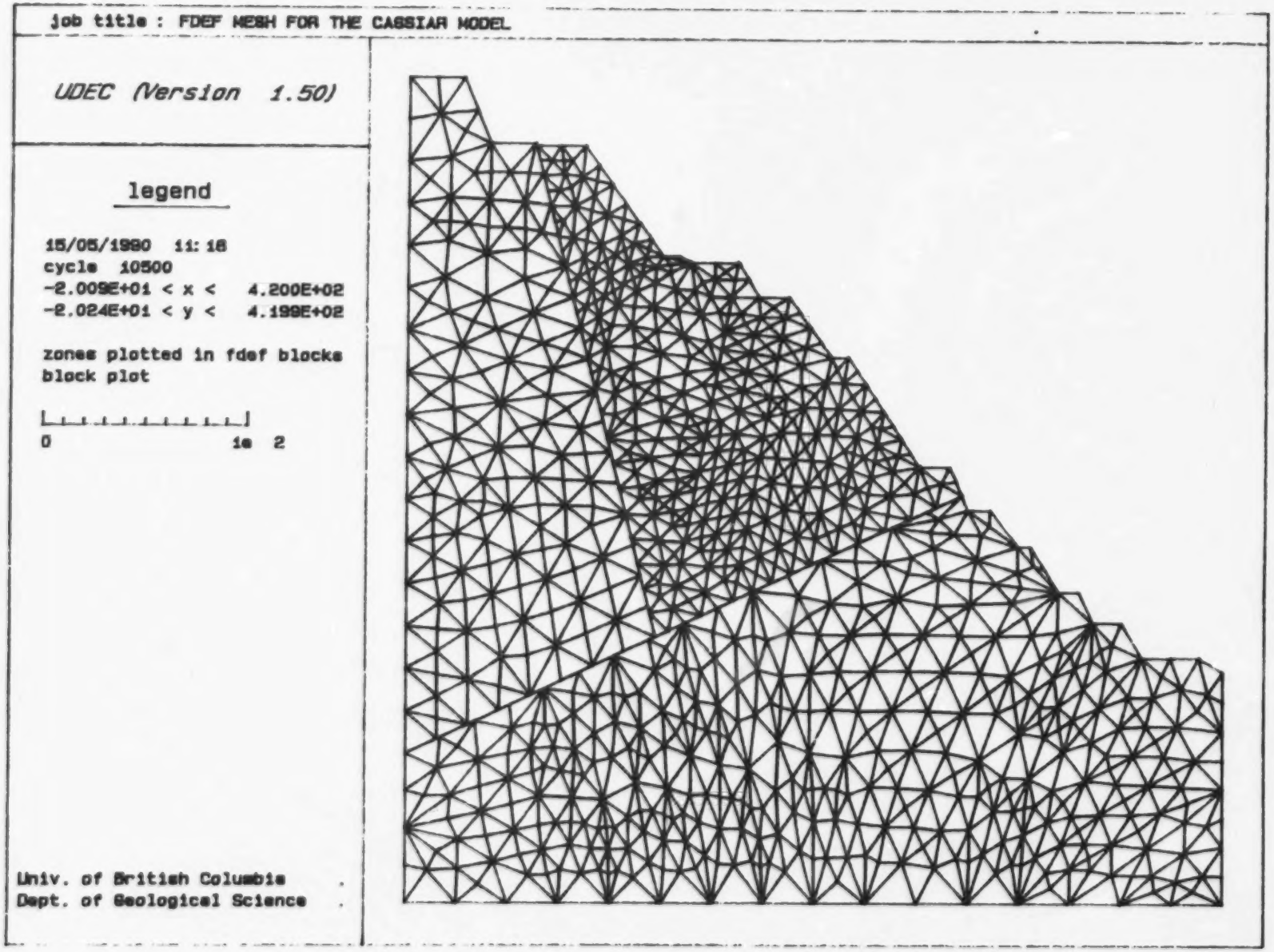

Fig. D2 Fully deformable mesh prepared for numerical modelling.

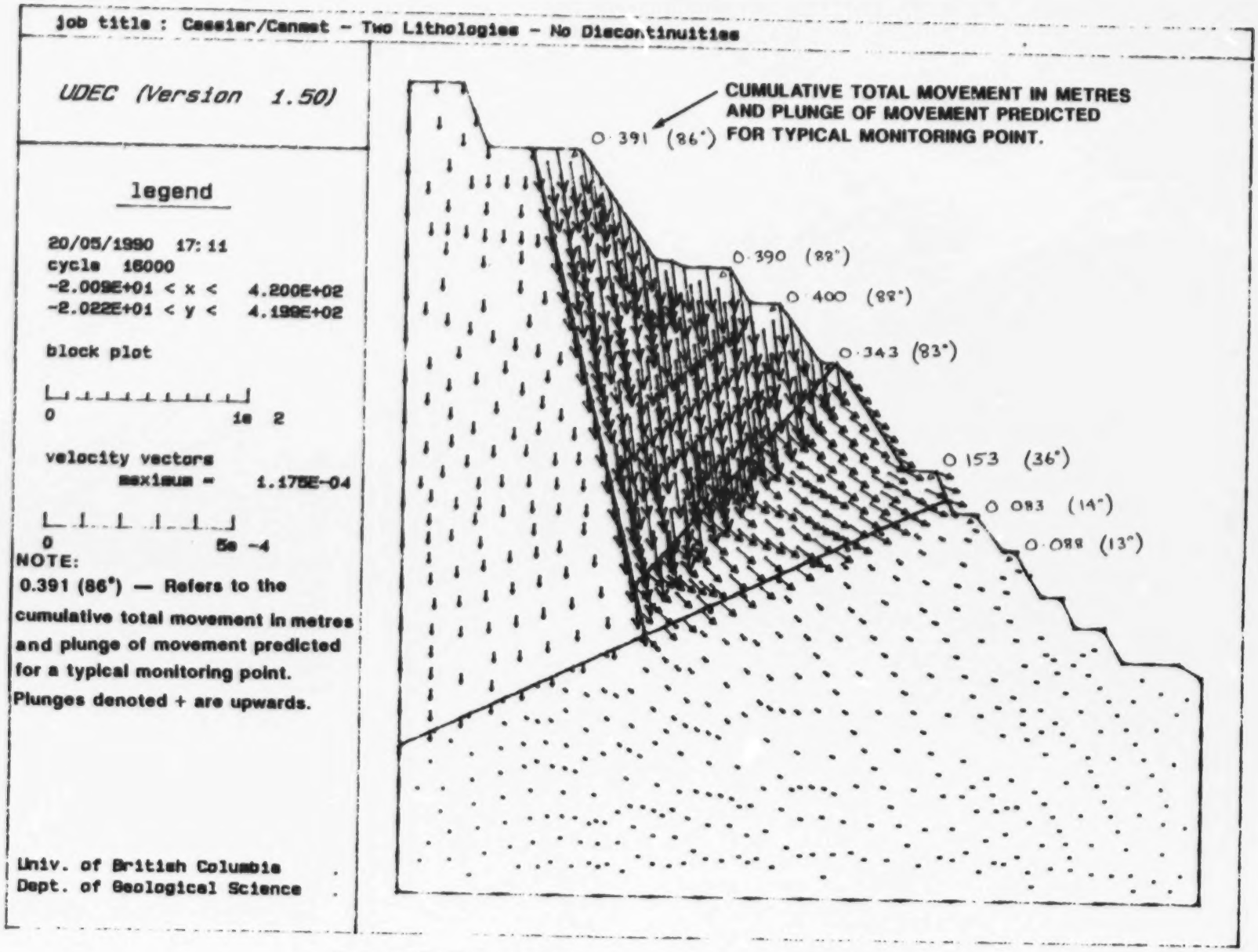

Fig. D3a Velocity vector plot for slope model consisting of two materials (argillite and serpentinite) without cracks assuming a high water table.

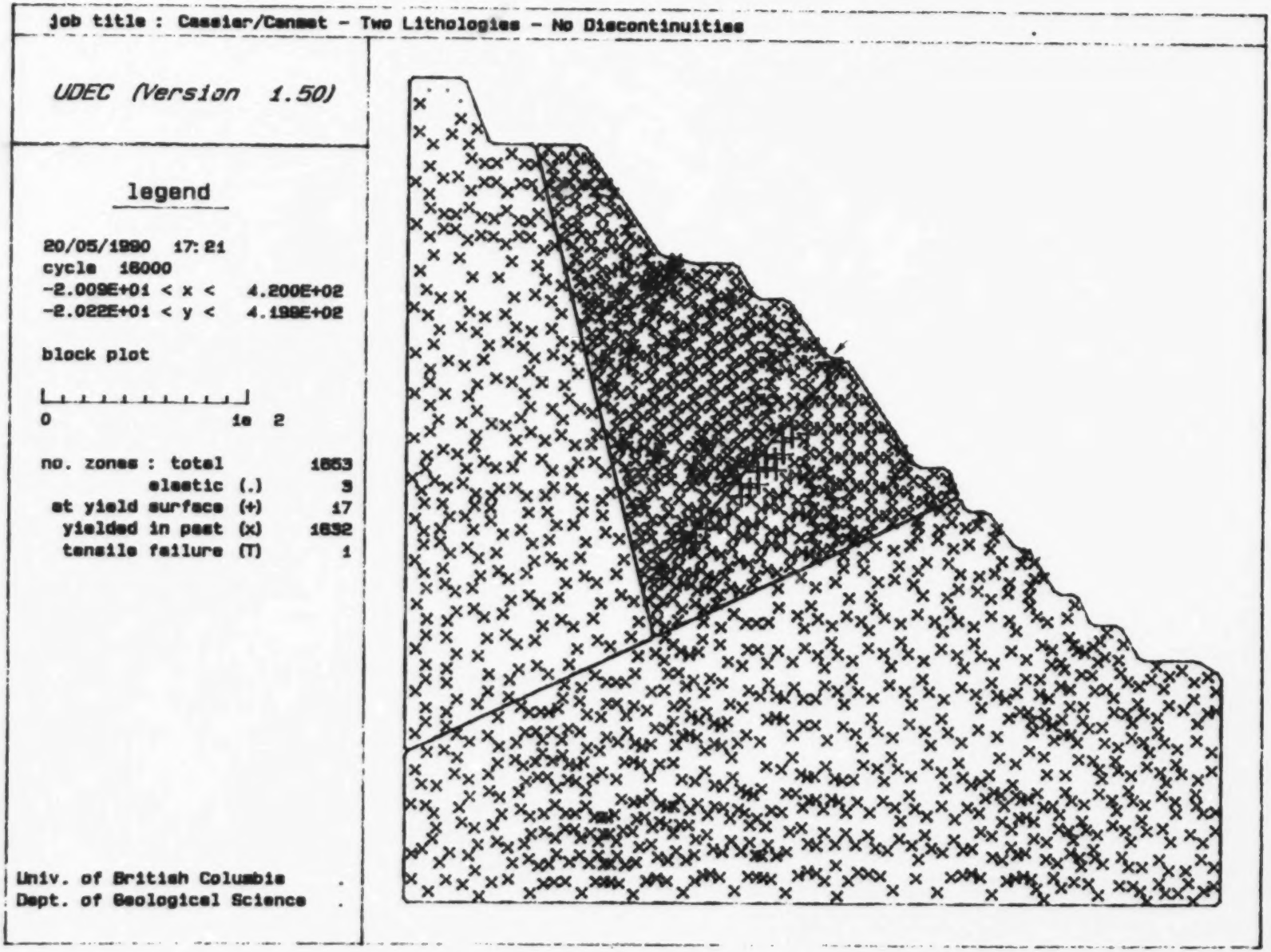

Fig. D3b Yield plot for slope model consisting of two materials without cracks assuming a high water table.

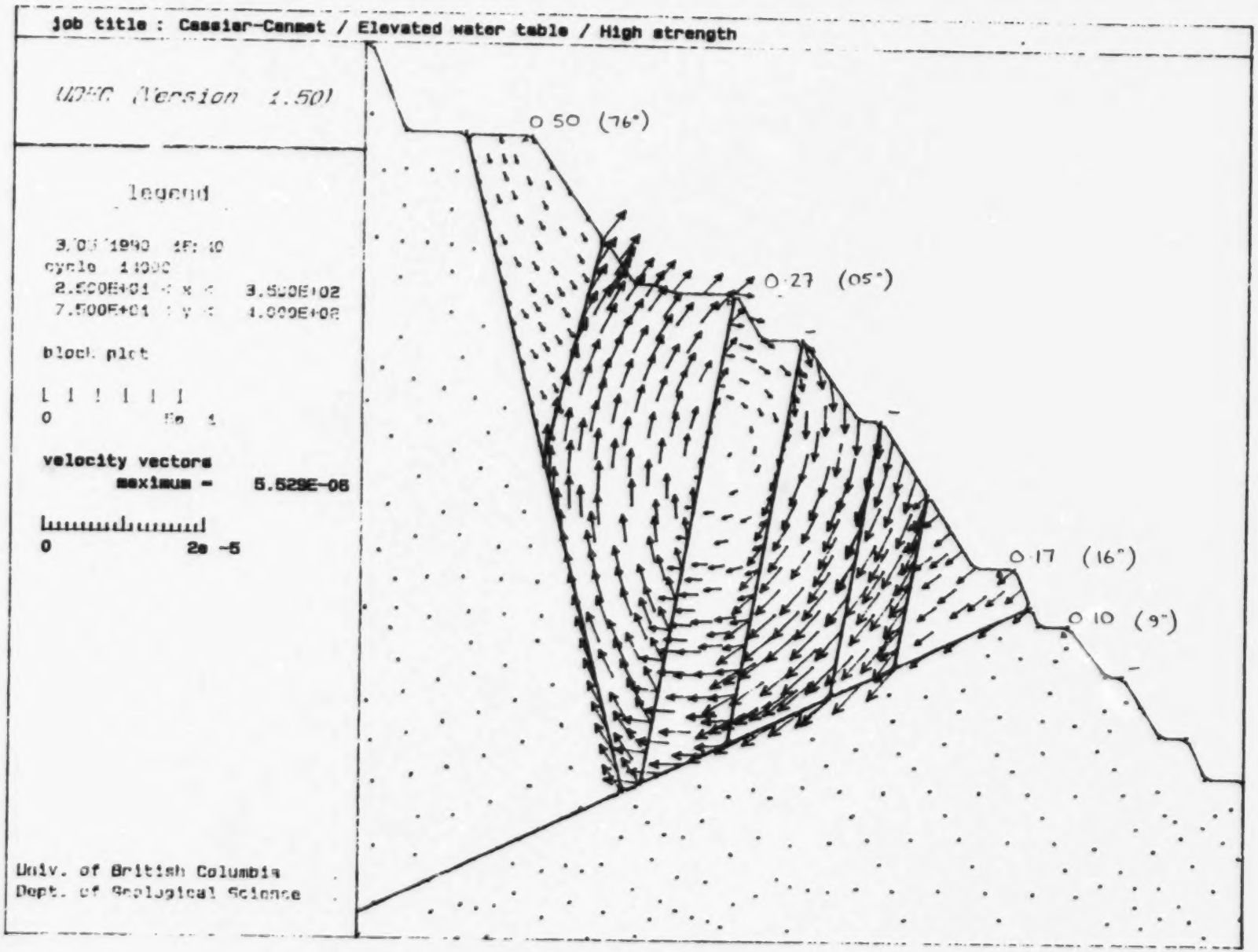

Fig. D4 Velocity vector plot for slope model assuming one material (argillite) with cracks in the active failure area, a high water table and a high discontinuity friction angle.

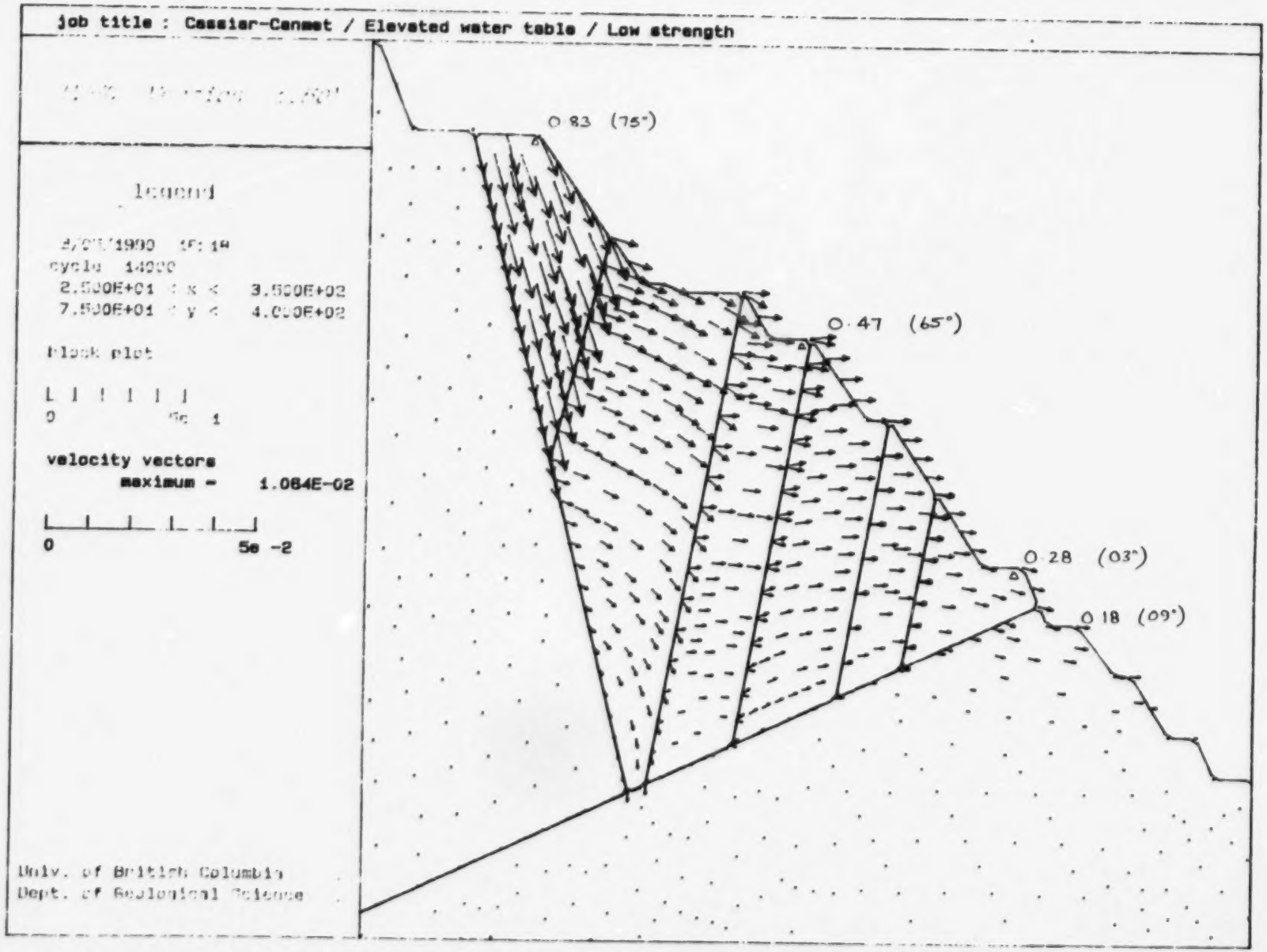

Fig. D5 Velocity vector plot for slope model assuming one material (argillite) with cracks in the active failure area, a high water table and a lower discontinuity friction angle.

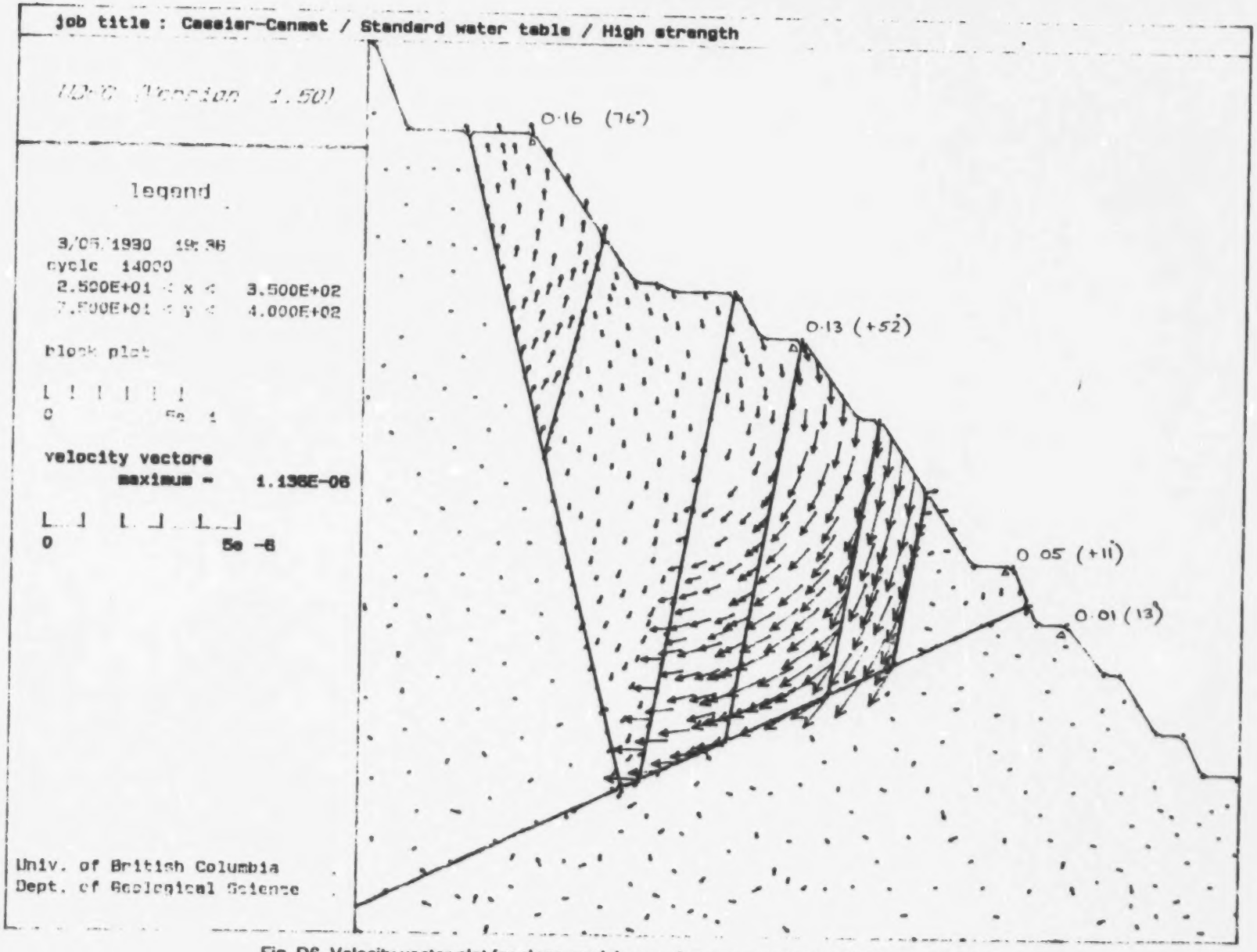

Fig. D6 Velocity vector plot for slope model assuming one material (argillite) with cracks in the active failure area, an intermediate water table and a high discontinuity friction angle.

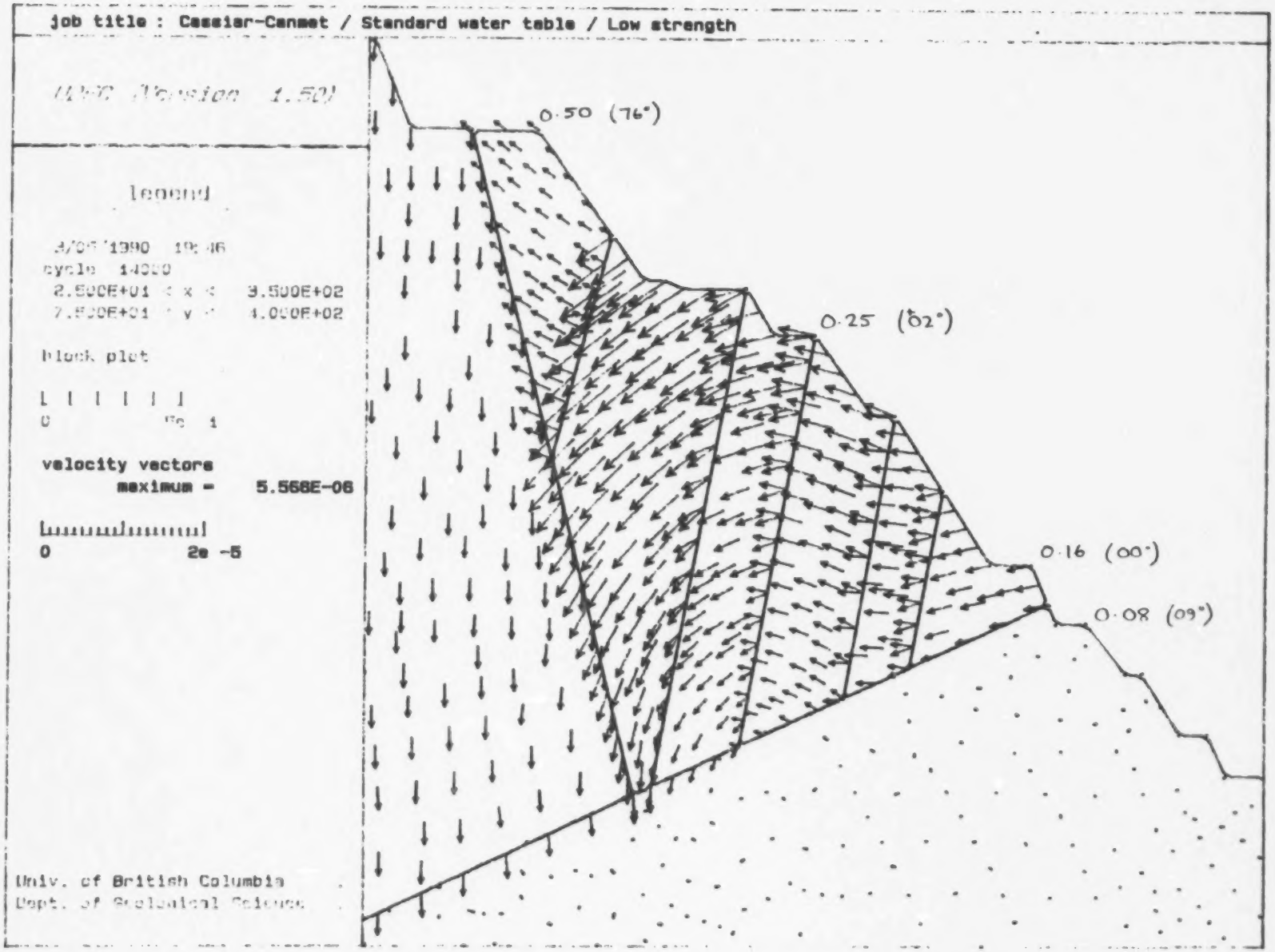

Fig. D7 Velocity vector plot for slope model assuming one material (argillite) with cracks in the active failure area, an intermediate water table and a lower discontinuity friction angle.

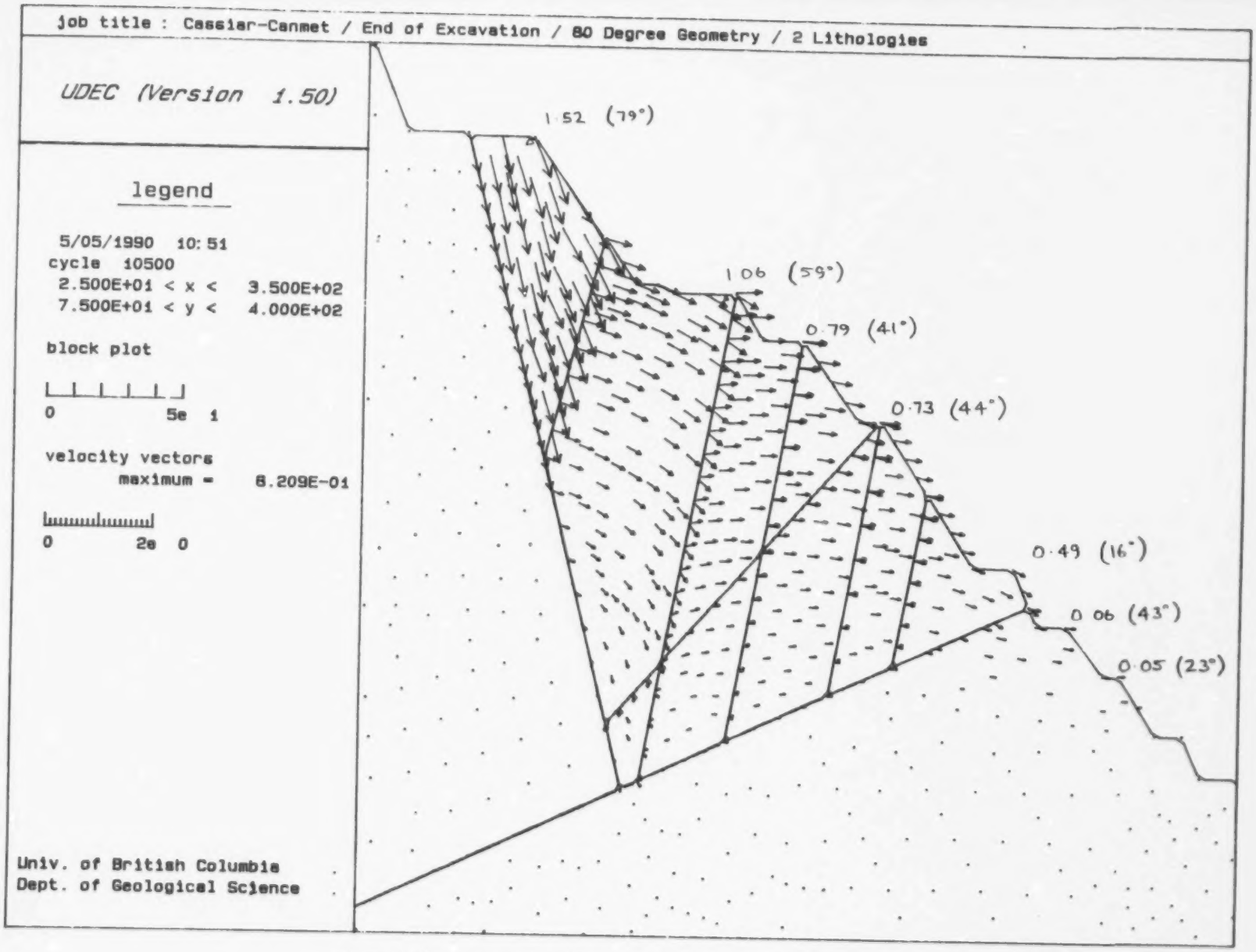

Fig. D8a Velocity vector plot for slope model assuming two materials, cracks in the active failure area, a high water table, and discontinuity strengths (cohesion, friction) of 700 kPa, 30° and 70 kPa, 24° for argillite and serpentinite respectively.

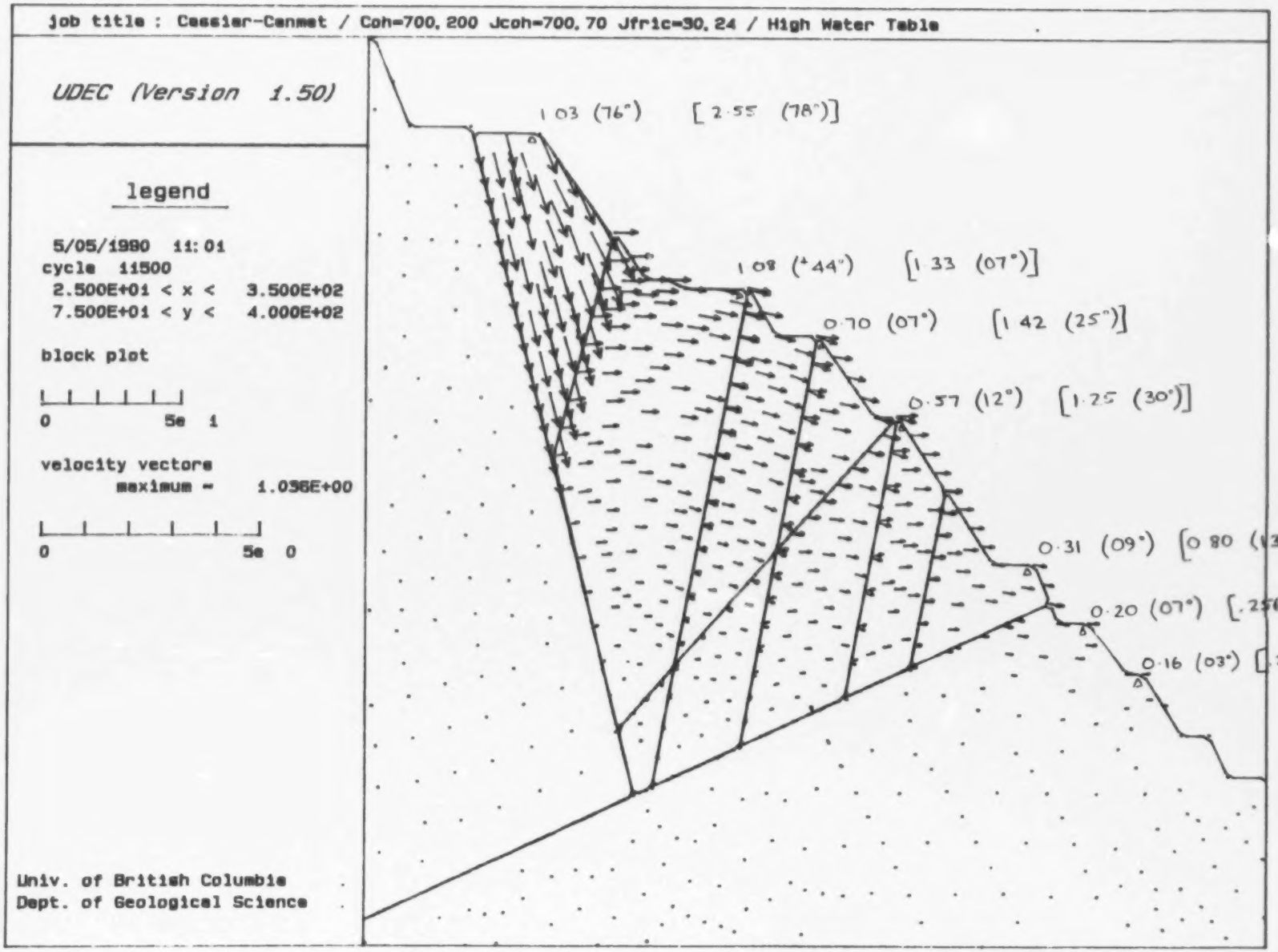

Fig. D8b Velocity vector plot for slope model assessed in Fig. 8a but after allowing a reduction of discontinuity strength of 20% to simulate strain softening of the discontinuities Argillite: C=595 kPa, Ø=30°; Serpentinite: C=59 kPa, Ø=24°

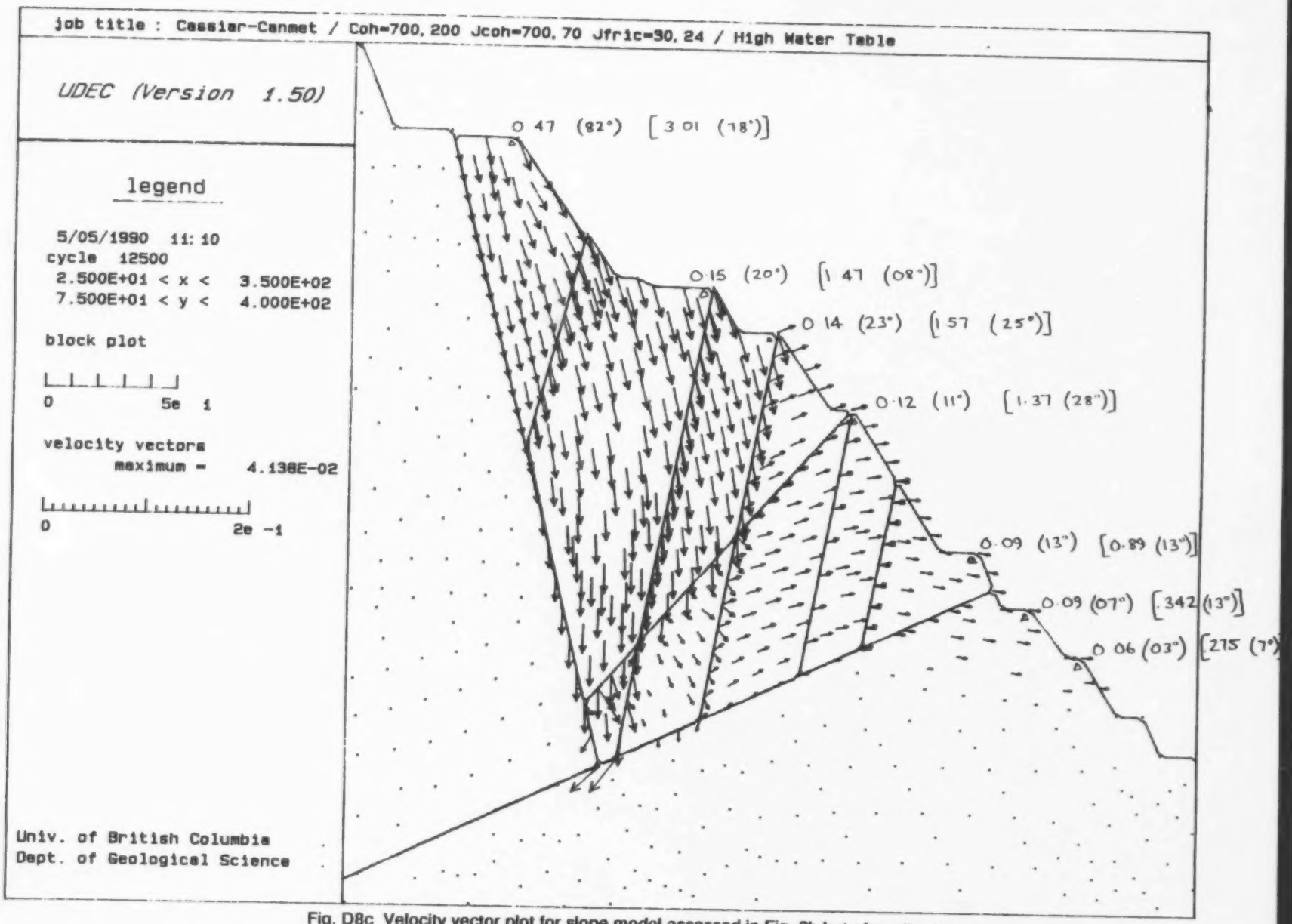
job title : Cassiar-Canmet / Coh=700. 200 Jcoh=700. 70 Jfric=30. 24 / High Water Table
UDEC (Version 1.50)
legend
5/05/1990 11: 10
cycle 12500
2.500E+01 < x < 3.500E+02
7.500E+01 < y < 4.000E+02
block plot
0 5e 1
velocity vectors
maximum = 4.138E-02
0 2e -1
Univ. of British Columbia
Dept. of Geological Science
0 47 (82°) [3 01 (78°)]
0 15 (20°) [1 47 (08°)]
0 14 (23°) [1 57 (25°)]
0 12 (11°) [1.37 (28°)]
0 09 (13°) [0.89 (13°)]
0 09 (07°) [.342 (13°)]
0 06 (03°) [.215 (7°)

Fig. D8c Velocity vector plot for slope model assessed in Fig. 8b but after allowing a reduction of discontinuity strength of 10% to simulate strain softening of the discontinuities Argillite: C=536 kPa, Ø=30°; Serpentinite: C=54 kPa, Ø=24°

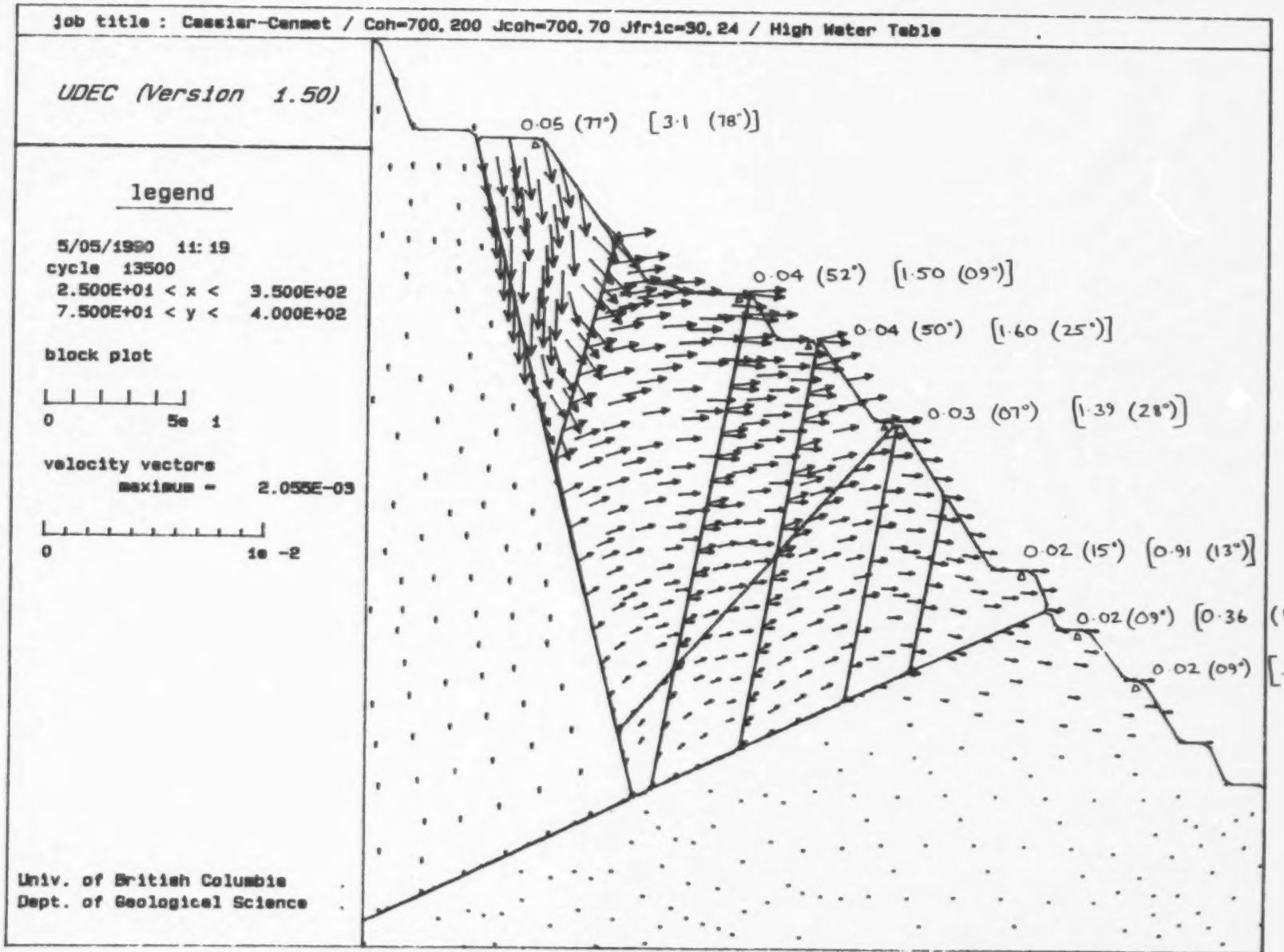

Fig. D8d Velocity vector plot for slope model assessed in Fig. 8c but after allowing a reduction of discontinuity strength of 5% to simulate strain softening of the discontinuities Argillite: C=509 kPa, Ø=30°; Serpentinite: C=51 kPa, Ø=24°

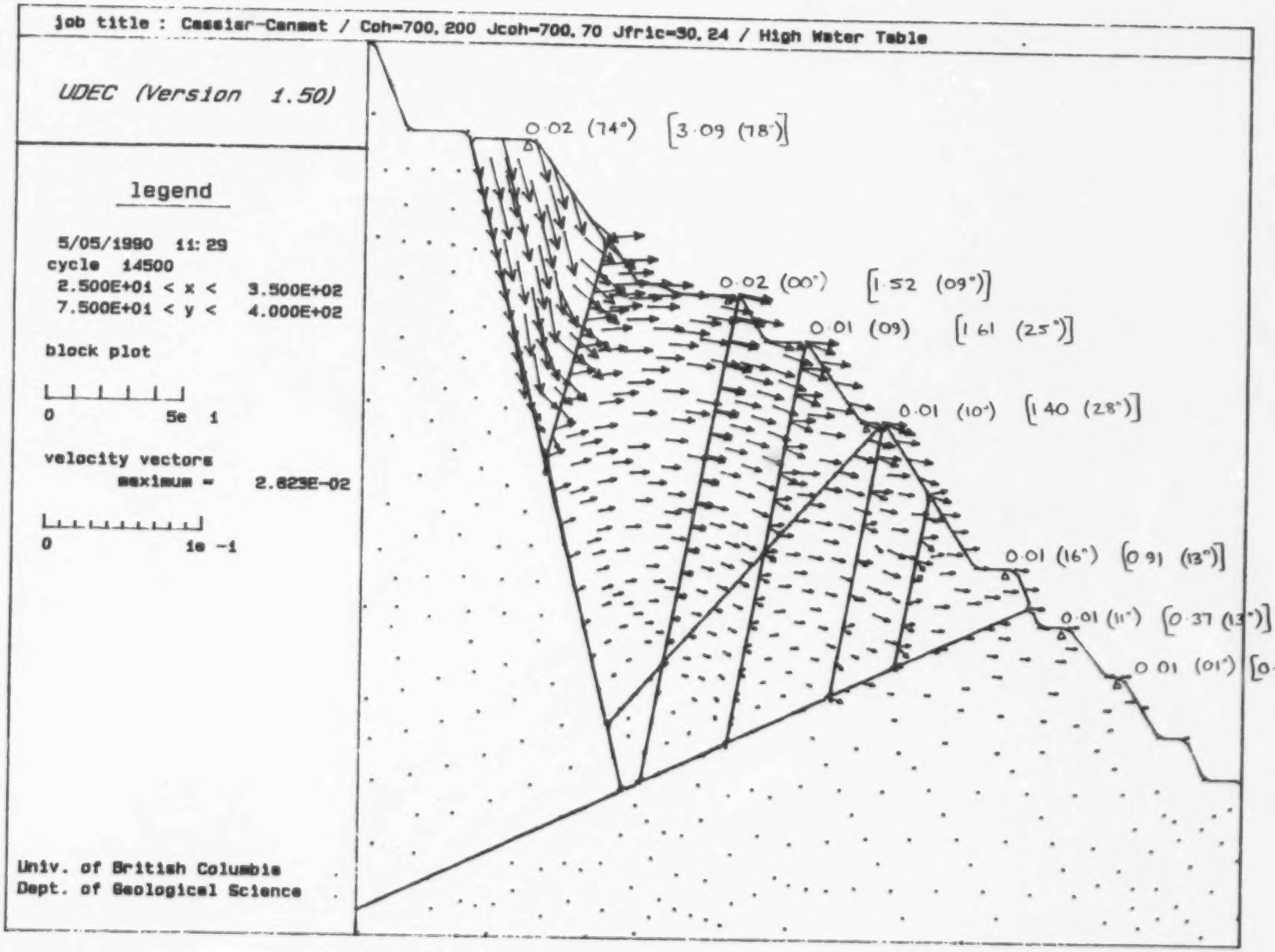

Fig. D8e Velocity vector plot for slope model assessed in Fig. 8d but after allowing a reduction of discontinuity strength of 5% to simulate strain softening of the discontinuities Argillite: C=483 kPa, Ø=30°; Serpentinite: C=48 kPa, Ø=24°

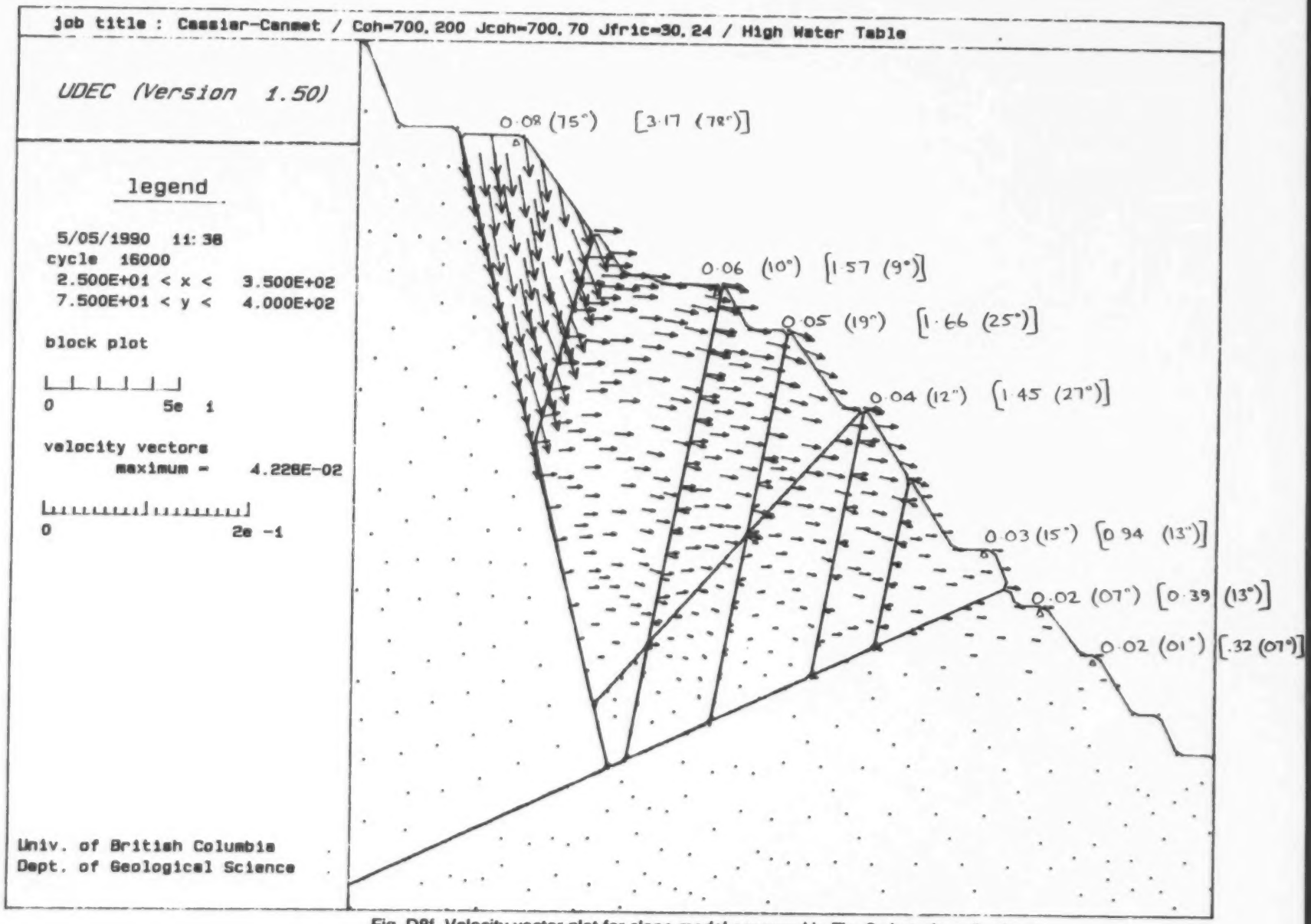

Fig. D8f Velocity vector plot for slope model assessed in Fig. 8e but after allowing a reduction of discontinuity strength of 5% to simulate strain softening of the discontinuities Argillite: C=459 kPa, Ø=30°; Serpentinite: C=46 kPa, Ø=24°

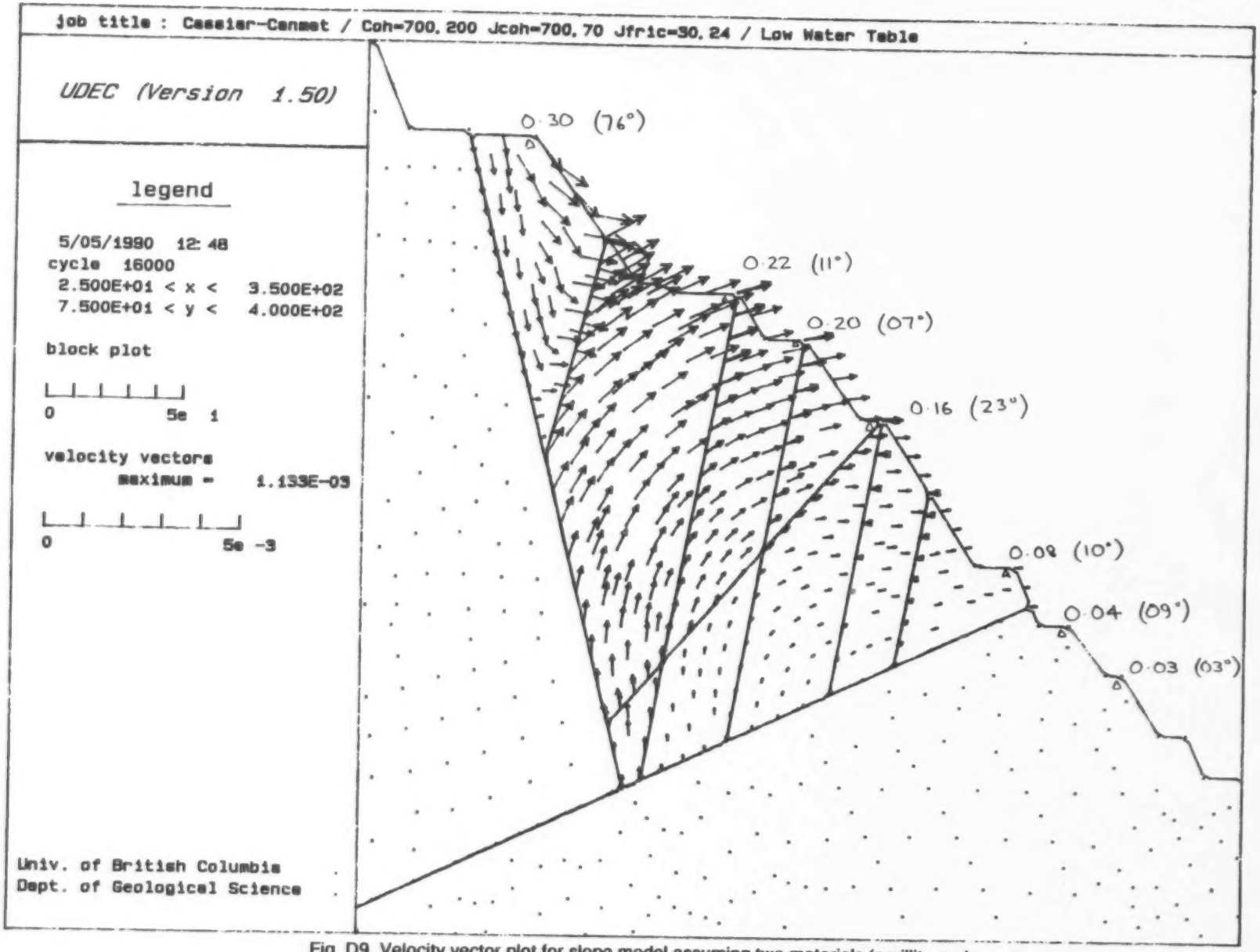

Fig. D9 Velocity vector plot for slope model assuming two materials (argillite and serpentinite), cracks in the active failure area, an intermediate water table and strain softening of discontinuities of 20%, 10%, 5%, 5%, and 5%.

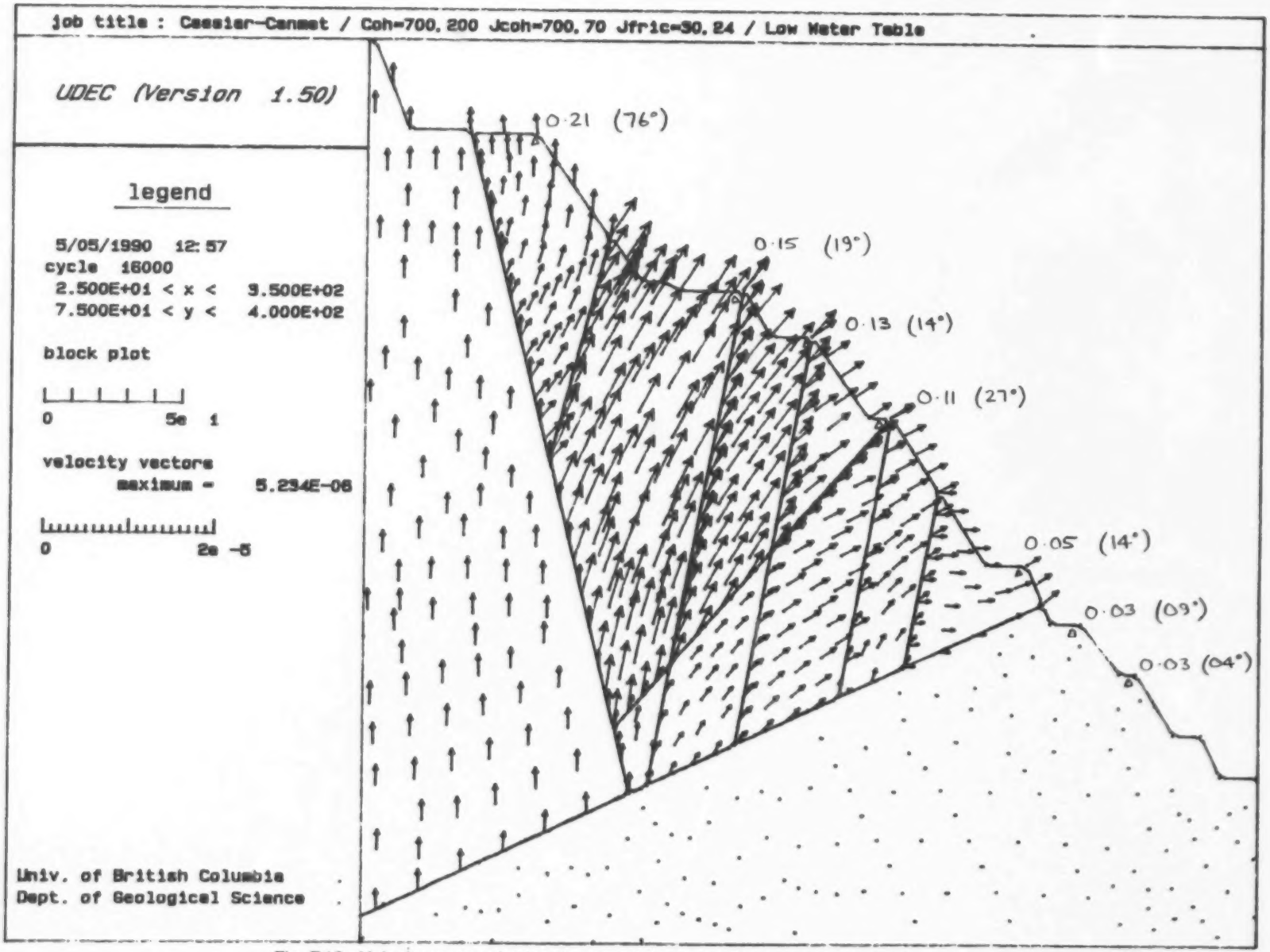

Fig. D10 Velocity vector plot for slope model assuming two materials (argillite and serpentinite), cracks in the active failure area, a low water table, Ø=30° and 24°, and strain softening of discontinuities of 20%, 10%, 5%, 5%, and 5%.

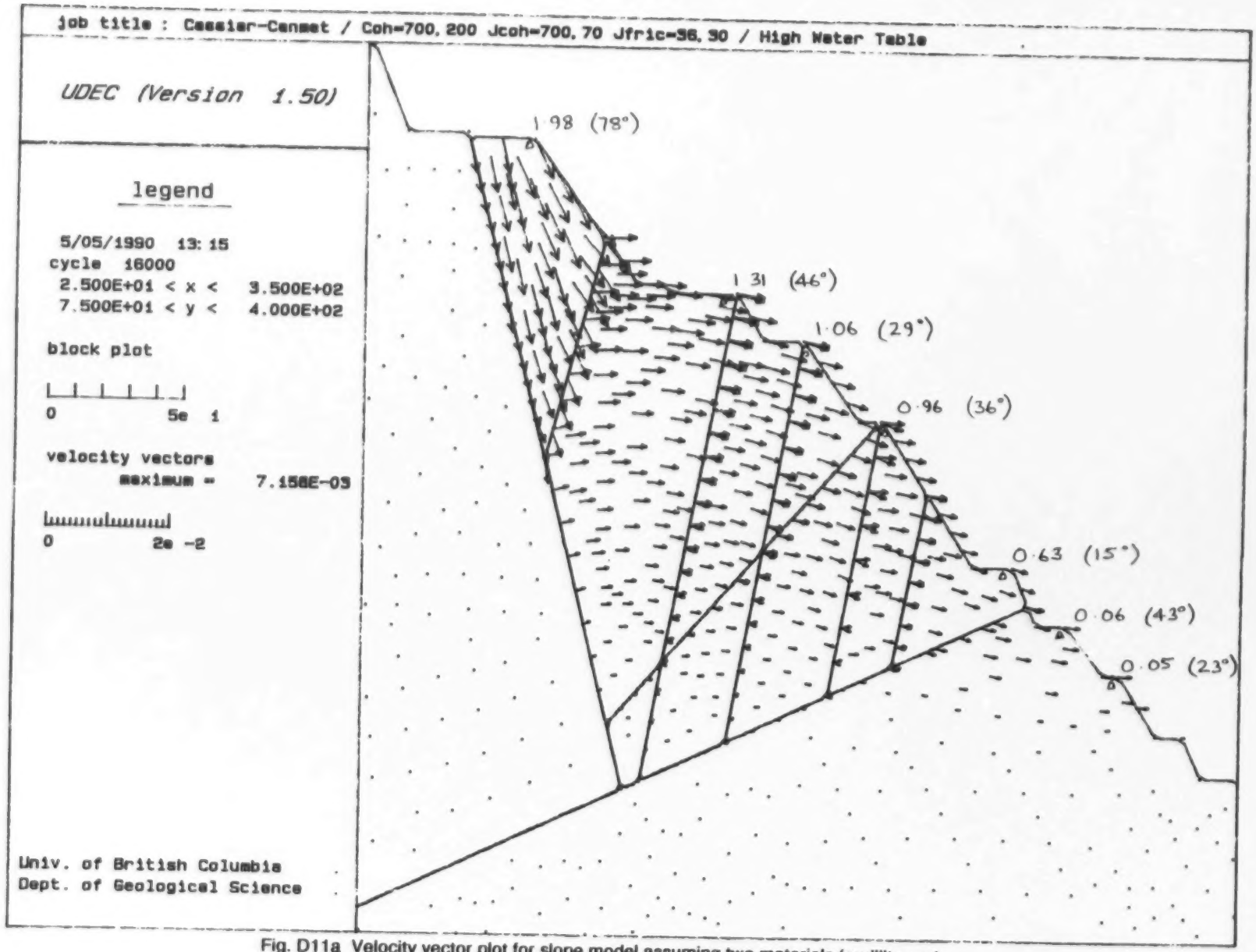

Fig. D11a Velocity vector plot for slope model assuming two materials (argillite and serpentinite), cracks in the active failure area, a high water table, high friction angles and strain softening of discontinuities of 20%, 10%, 5%, 5%, and 5%.

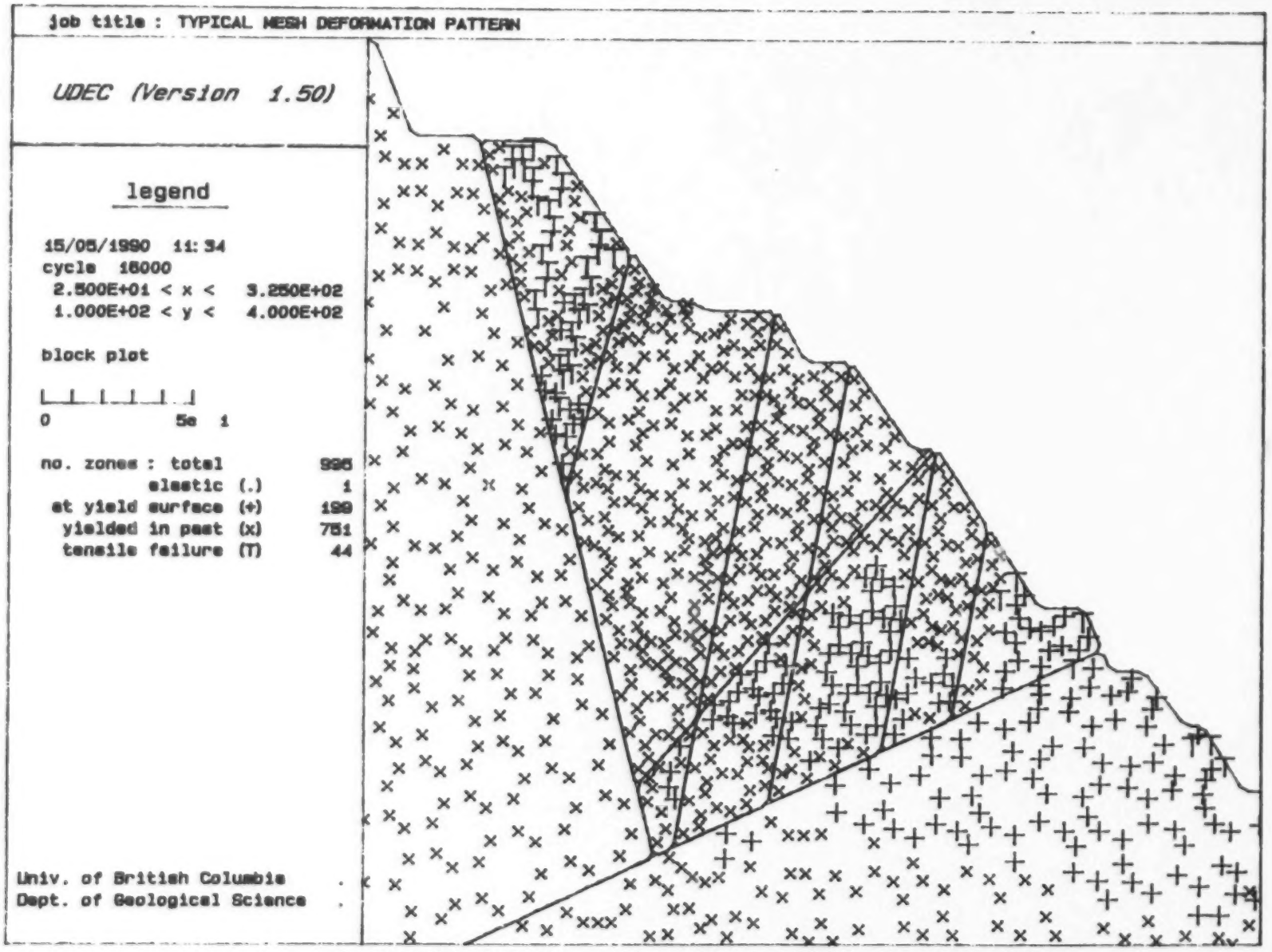

Fig. D11b Yield plot for slope model assuming two materials (argillite and serpentinite), cracks in the active failure area, a high water table, high friction angles, and strain softening of discontinuities of 20%, 10%, 5%, 5%, and 5%.

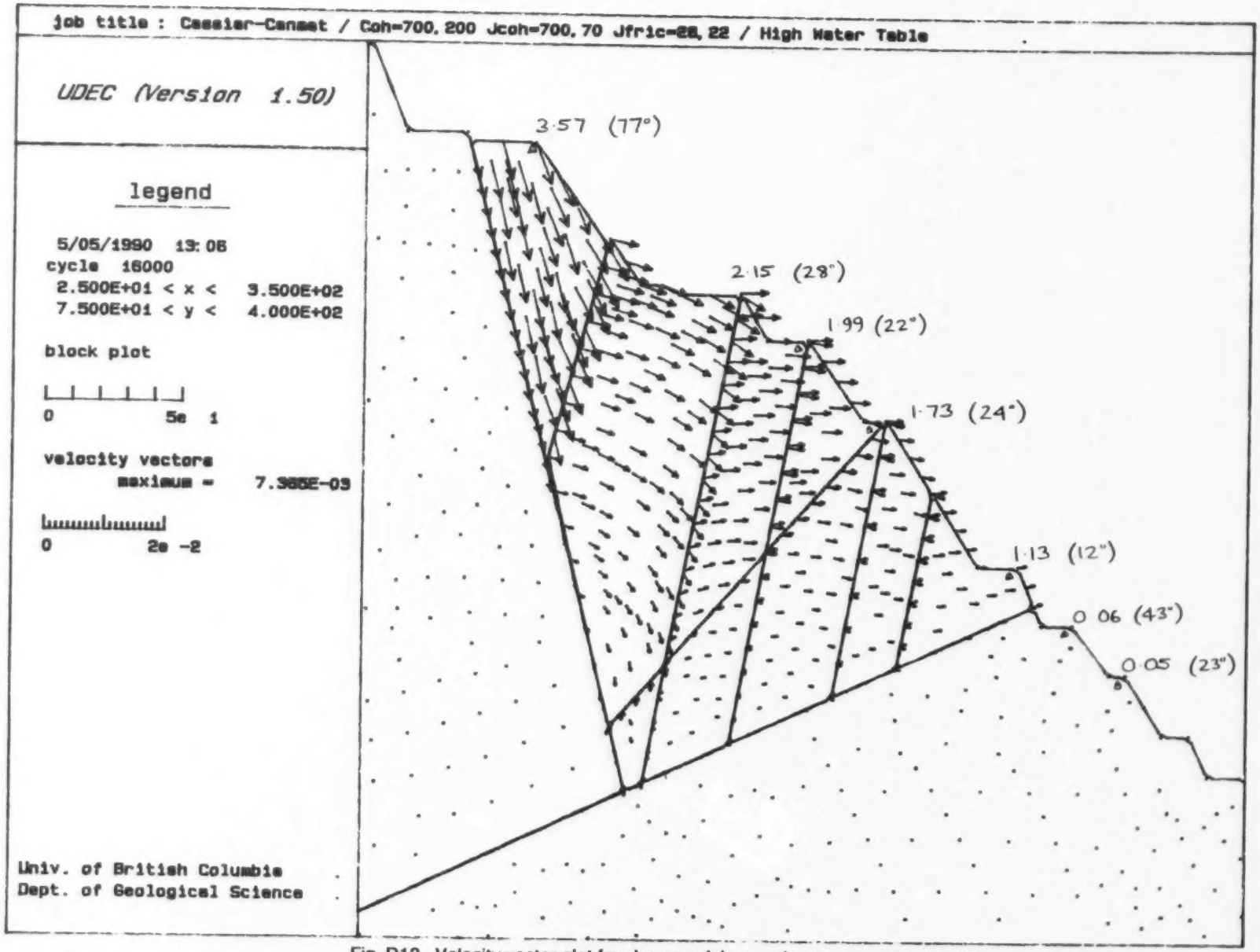

Fig. D12 Velocity vector plot for slope model assuming two materials (argillite and serpentinite), cracks in the active failure area, a high water table, low friction angles, and strain softening of discontinuities of 20%, 10%, 5%, 5%, and 5%.

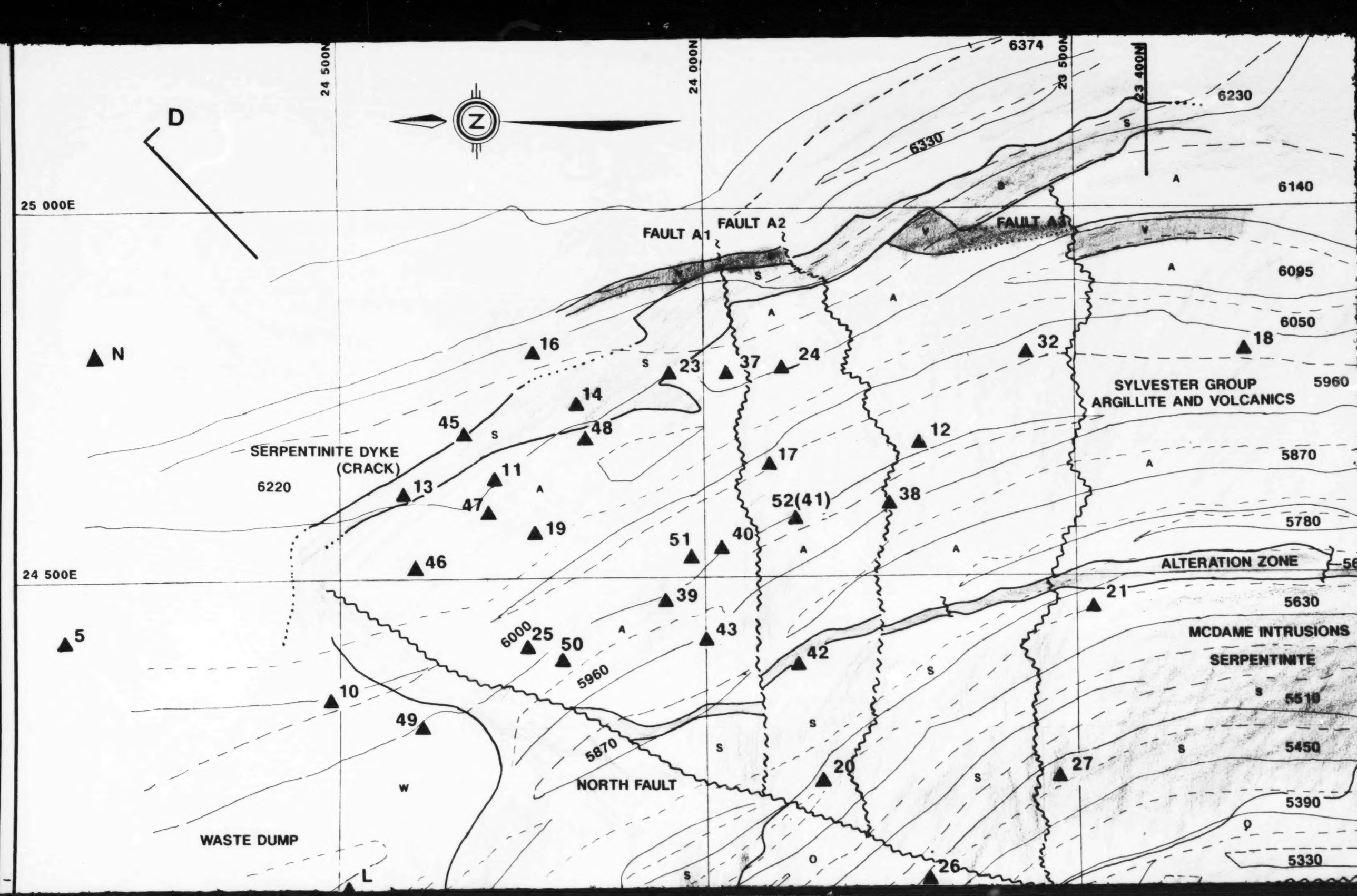
D
Z
24 500N
24 000N
23 500N
23 400N
25 000E
24 500E
6374
6330
6230
6140
6095
6050
5960
5870
5780
5630
5510
5450
5390
5330
6220
6000
FAULT A1
FAULT A2
FAULT A3
SYLVESTER GROUP
ARGILLITE AND VOLCANICS
SERPENTINITE DYKE
(CRACK)
ALTERATION ZONE
MCDAME INTRUSIONS
SERPENTINITE
NORTH FAULT
WASTE DUMP
N
L
A
S
W
O
16
23
37
24
32
18
14
45
48
12
11
13
47
17
52(41)
38
19
51
40
46
39
21
5
25
50
43
42
10
49
20
27
26

23 500N

23 400N

23 000N

22 500N

22 000N

25 000E

24 500E

6374

6230

6140

6095

6050

5960

5870

5780

5690

5630

5510

5450

5390

6410

6320

6230

6140

6050

5960

5870

5780

5690

5630

5570

5510

5450

FAULT A

SOUTH FAULT

ALTERATION ZONE

SYLVESTER GROUP
ARGILLITE AND VOLCANICS

MCDAME INTRUSIONS

SERPENTINITE

32

18

30

36

31

21

3

28

27

Z

Y

A

V

S

GS

H

O

22 500N

22 000N

25 000E

24 500E

SOUTH FAULT

30

36

31

3

Z

Y

6410

6320

6230

6140

6050

5960

5870

5780

5690

5570

5510

5450

5390

LEGEND

RECENT

W	TALUS AND WASTE DUMP MATERIAL

MCDAME INTRUSIONS-TRIASSIC

S O	SERPENTINITE(S), ORE BEARING SERPENTINITE(O) AND RELATED ULTRAMAFIC INTRUSIVE ROCKS
H, J	ALTERATION ZONE: HORNFELLS(H), JADE(J) AND RELATED CONTACT METAMORPHIC ROCKS

SYLVESTER GROUP-DEVONIAN

A	ARGILLITE(A), CHERTY ARGILLITE, MINOR ARENITE, PHYLLITE, SLATE AND ASSOCIATED ROCKS
V	GREENSTONE AND RELATED VOLCANIC ROCKS(V)
GS	GRAPHITIC SHIST(GS) AND RELATED ROCKS; GENERALLY ADJACENT TO MAJOR FAULTS IN FOOTWALL AREA

SYMBOLS

GEOLOGIC CONTACT : DEFINED, ASSUMED

FAULT: DEFINED, ASSUMED

FAULT ZONE/SHEAR ZONE

BENCH TOE, CREST AND ELEVATION — 5690

PRISM NUMBER LOCATION, TOTAL MOVEMENT AND DATE — 28 (2.1)

(movement rate in inches/day is given in brackets)

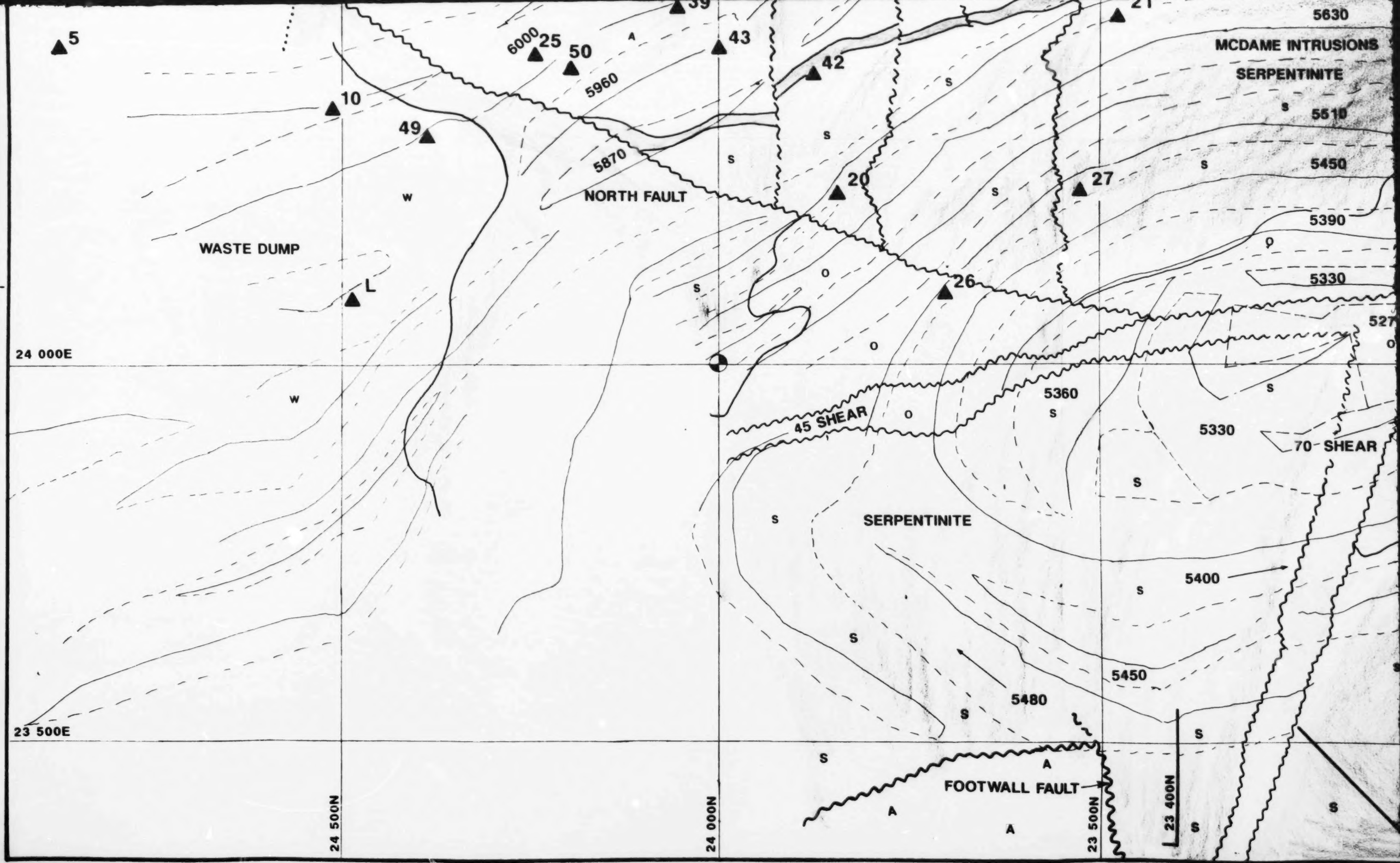
5
10
49
25
50
6000
5960
5870
43
42
39
21
5630
MCDAME INTRUSIONS
SERPENTINITE
5510
5450
27
20
NORTH FAULT
WASTE DUMP
L
26
5390
5330
527
24 000E
5360
45 SHEAR
5330
70 SHEAR
SERPENTINITE
5400
5450
5480
FOOTWALL FAULT
23 500E
24 500N
24 000N
23 500N
23 400N
S
A
O
W

MCDAME INTRUSIONS

SERPENTINITE

5630

5510

5450

5390

5330

5270

5360

5330

5400

5450

5480

70 SHEAR

45 SHEAR

ALL FAULT

23 500N

23 400N

23 000N

22 500N

22 000N

24 000E

23 500E

27

28

3

29

X

4

1

2

9

5780

5870

5960

6050

5570

5630

5680

5510

5450

5390

S

O

A

V

H

GS

D

CANMET/SUPP

CASSIAR OPEN

SLOPE DEFOR

ENGINEERI

GEOLOGY

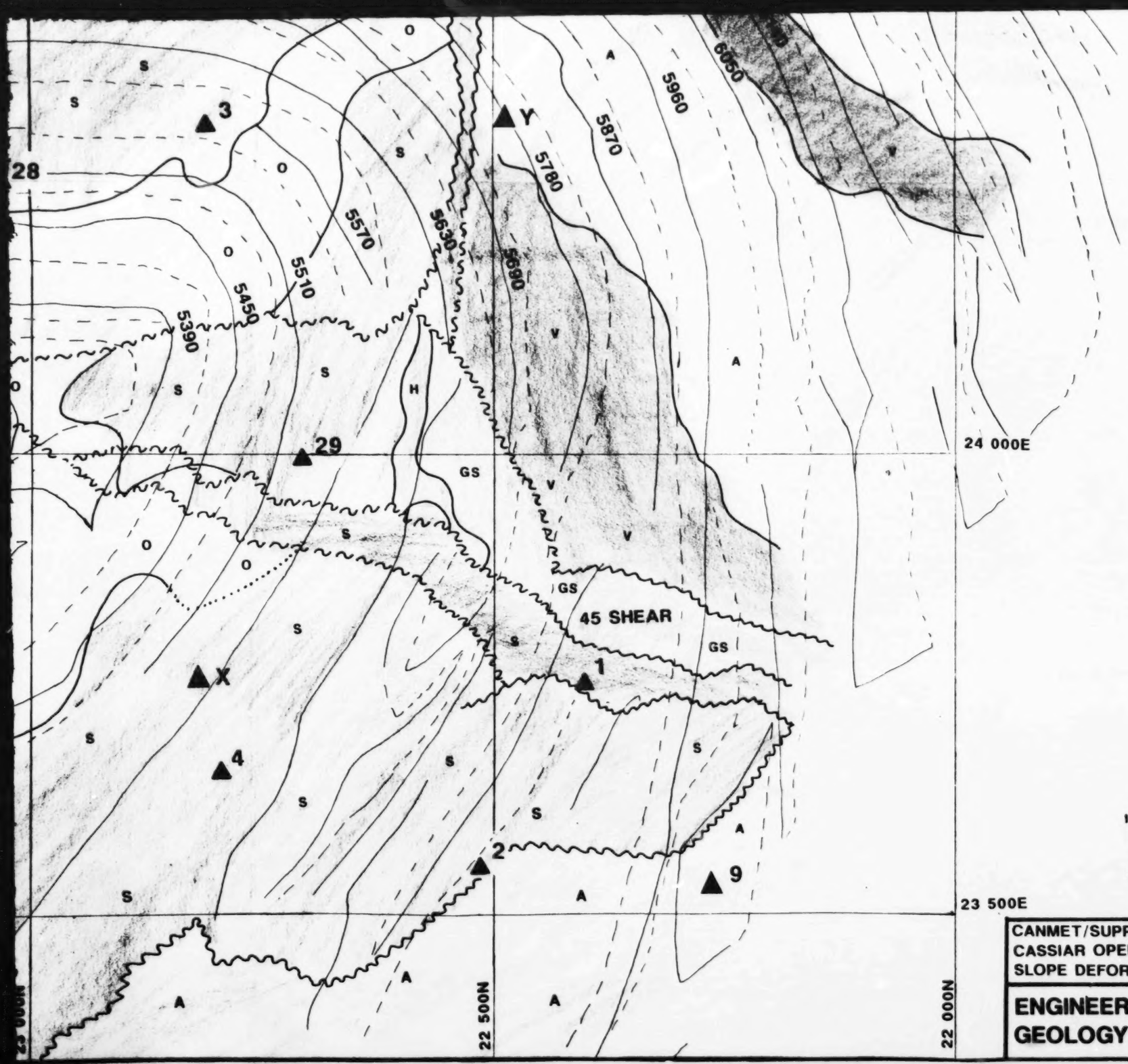

GEOLOGIC CONTACT : DEFINED, ASSUMED

FAULT: DEFINED, ASSUMED

FAULT ZONE/SHEAR ZONE

BENCH TOE, CREST AND ELEVATION 5690

PRISM NUMBER LOCATION, TOTAL MOVEMENT AND DATE (movement rate in inches/day is given in brackets) 28 (2.1)

0 1 2 3ft
0 0.5 1m
VECTOR SCALE

100 0 100 200 300 FEET
30 0 25 50 100 METRES
SCALE

FIG.2

CANMET/SUPPLY AND SERVICES CANADA
CASSIAR OPEN PIT
SLOPE DEFORMATION STUDY

PITEAU ASSOCIATES
GEOTECHNICAL CONSULTANTS
VANCOUVER CALGARY

ENGINEERING GEOLOGY AND STUCTURAL GEOLOGY OF THE CASSIAR OPEN PIT

DCM 7/4/90

718G-1